

Optical multi-stable operations of coupled lasers

Citation for published version (APA):

Zhang, S. (2006). *Optical multi-stable operations of coupled lasers*. [Phd Thesis 1 (Research TU/e / Graduation TU/e), Electrical Engineering]. Technische Universiteit Eindhoven. <https://doi.org/10.6100/IR613180>

DOI:

[10.6100/IR613180](https://doi.org/10.6100/IR613180)

Document status and date:

Published: 01/01/2006

Document Version:

Publisher's PDF, also known as Version of Record (includes final page, issue and volume numbers)

Please check the document version of this publication:

- A submitted manuscript is the version of the article upon submission and before peer-review. There can be important differences between the submitted version and the official published version of record. People interested in the research are advised to contact the author for the final version of the publication, or visit the DOI to the publisher's website.
- The final author version and the galley proof are versions of the publication after peer review.
- The final published version features the final layout of the paper including the volume, issue and page numbers.

[Link to publication](#)

General rights

Copyright and moral rights for the publications made accessible in the public portal are retained by the authors and/or other copyright owners and it is a condition of accessing publications that users recognise and abide by the legal requirements associated with these rights.

- Users may download and print one copy of any publication from the public portal for the purpose of private study or research.
- You may not further distribute the material or use it for any profit-making activity or commercial gain
- You may freely distribute the URL identifying the publication in the public portal.

If the publication is distributed under the terms of Article 25fa of the Dutch Copyright Act, indicated by the "Taverne" license above, please follow below link for the End User Agreement:

www.tue.nl/taverne

Take down policy

If you believe that this document breaches copyright please contact us at:

openaccess@tue.nl

providing details and we will investigate your claim.

Optical Multi-stable Operations of Coupled Lasers

PROEFSCHRIFT

ter verkrijging van de graad van doctor aan de
Technische Universiteit Eindhoven, op gezag van de
Rector Magnificus, prof.dr.ir. C.J. van Duijn, voor een
commissie aangewezen door het College voor
Promoties in het openbaar te verdedigen
op donderdag 05 oktober 2006 om 16.00 uur

door

Shaoxian Zhang

geboren te Lingyuan, China

Dit proefschrift is goedgekeurd door de promotoren:

prof.ir. G.D. Khoe
en
prof.dr. D. Lenstra

Copromotor:
dr. H.J.S. Dorren

CIP-DATA LIBRARY TECHNISCHE UNIVERSITEIT EINDHOVEN

Zhang, Shaoxian

Optical multi-stable operations of coupled lasers / by Shaoxian Zhang. –
Eindhoven : Technische Universiteit Eindhoven, 2006.

Proefschrift. – ISBN-10: 90-386-1873-5

ISBN-13: 978-90-386-1873-9

NUR 959

Trefw.: optische bistabiliteit / lasertoepassingen / optische signaalverwerking
/ optische telecommunicatie.

Subject headings: optical bistability / laser feedback / optical information
processing / optical fibre communication.

Copyright © 2006 by Shaoxian Zhang

All rights reserved. No part of this publication may be reproduced, stored in a retrieval
system, or transmitted in any form or by any means without the prior written consent
of the author.

Typeset using Microsoft Word, printed in the Netherlands.

Review Committee:

Prof.dr. T. Erneux:	Faculty of Science, Free University of Brussels
Prof.dr. P.M. Koenraad:	Department of Applied Physics, Eindhoven University of Technology
Prof.dr. I.H. White:	Department of Engineering, University of Cambridge



This research is supported by the Dutch Technology Foundation STW, applied science division of NWO and the Technology Program of the Ministry of Economic Affairs.

Summary

Optical memories are optical bi(multi-)stable systems whose states can be switched all optically. Acting as a fundamental building block for digital optical signal processing, they have received considerable attention. Many types of optical memories have been explored, which all have in common that they are optical storage elements with two states. Multi-stable optical logic building blocks are interesting for applications in telecommunication systems, since they have potential to process a large number of wavelength channels in parallel.

In this thesis, we present two types of multi-stable operation of coupled lasers. The first one is based on coupled ring lasers, which share a single active element and a feedback arm. A single ring laser with feedback can be regarded as an oscillator, since the intensity of the lasing light in the lasing cavity is periodically oscillating. When two such oscillators are coupled together, sharing the same active element and the same feedback arm, they synchronize in a common oscillation frequency if their individual oscillation periodicities are close to each other; otherwise they show bistability between the two oscillators. Switching between different stable states can be realized by injecting external light, in this sense, the system act as an optical memory. Moreover, this concept can easily realize multi-state operation, since only one active element is required. An eight-state optical memory is demonstrated.

The second type of multi-stable operation of coupled lasers is based on serially interconnected lasers using the principle of gain quenching. The light from the dominant laser suppresses its neighboring lasers through gain saturation, but still receives amplification by the active element of the suppressed lasers, compensating for coupling losses. This light passes through each of the successive lasers, simultaneously suppressing and being amplified. By this mechanism all the other lasers are suppressed. Only one of the lasers can lase at a time, thus the state of the optical memory is determined by the wavelength of the dominant laser, as same as the first type. A five-state optical memory based on this concept is experimentally demonstrated.

Moreover, we use the optical memories as a fundamental logic unit to realize sophisticated optical logic. We present an optical shift register that consists of two serially connected optical memories driven by common clock pulses. The concept is demonstrated at an operation speed of 20 kHz, which is limited by the laser cavities implemented by 10 meter long fiber pigtailed components. Furthermore, we cascade

Summary

the optical shift register and an optical XOR gate to realize an optical pseudorandom number generator based on optical memories.

Contents

1 General introduction	1
1.1 Introduction to optical bistability	1
1.2.1 Absorptive and dispersive bistability	3
1.2.2 Two-mode and two-active-element bistability	6
1.2.3 Research trend	8
1.2 Motivation of investigating optical multi-stable system	9
1.3 Contribution of this thesis	11
1.4 Outline of this thesis	12
 2 Laser dynamics of a unidirectional ring laser with optical incoherent feedback	 15
2.1 Introduction to dynamics of semiconductor laser with optical feedback	15
2.2 Model of unidirectional ring laser with incoherent feedback	18
2.2.1 General model	19
2.2.2 Model with optical filter	23
2.3 Simulation and experimental results	26
2.3.1 Origin of oscillation	26
2.3.2 Control parameter k	30
2.3.3 Control parameter K_f	32
2.4 Conclusion	35
 3 Synchronization and bistability of two coupled oscillators based on ring lasers with incoherent feedback	 37
3.1 Introduction to dynamics of coupled oscillators	38
3.2 Model of two coupled ring lasers sharing the same nonlinear gain medium as well as the same feedback arm	39
3.3 Experimental results on synchronization and bistability	42
3.3.1 Synchronization	43

3.3.2 Bistability	44
3.4 Dynamic investigation on synchronization and bistability.....	45
3.4.1 Evolution process of synchronization	46
3.4.2 Wavelength dependence of the bistability	50
3.4.2 Switching methods	51
3.5 Conclusion	54
4 Multi-stable operation of coupled oscillators	55
4.1 Multi-fold stability of coupled oscillators	56
4.1.1 Demonstration of four-fold stability of coupled oscillators	56
4.1.2 Experimental realization of an eight-state optical memory	58
4.2 Sixteen-state optical memory based on two connected four-state optical memories	60
4.3 Discussion	62
5 Multi-stable operation of serially interconnected lasers	65
5.1 Optical memories based on gain quenching	65
5.2 Operation principle.....	68
5.3 Experiment and results	70
5.3.1 Five-state optical memory	70
5.3.2 Two switching methods using external light injection	71
5.4 Conclusion	75
6 Optical shift register based on optical memories	77
6.1 Introduction to shift registers	77
6.2 Operation principle.....	79
6.3 Experiment and results	80
6.4 Shift more data.....	85
6.5 Conclusion	86
7 Optical pseudorandom number generator based on optical memories	89
7.1 Introduction to pseudorandom number generators	89
7.2 Operation principle	90
7.3 Experiment and results	94

7.4 Conclusion	97
8 Conclusion	99
References	103
Appendix A: List of abbreviations	115
Appendix B: List of publications	117
Samenvatting in het Nederlands	121
Acknowledgements	123
Curriculum Vitae	125

Chapter 1

General introduction

In Section 1, we firstly introduce the concept of bistability and the origin of research on optical bistability, afterwards we explain the physical mechanism behind the main types of optical bistability in combination with a concise historical review on each of them, and finally we summarize the current trends in this field.

1.1 Introduction to optical bistability¹

A *bistable* system is a system that has two possible stable states for a given set of parameters. The state, into which the system evolves, depends on the operation history of the system. If we treat a bistable system as a black box, a typical response curve is shown in Figure 1.1, where the same value of the input I_{in} accounts for two output states I_{out} over the range between input values I_{\downarrow} and I_{\uparrow} (such a region is called *bistable range*). In the bistable region, it is necessary to know both I_{in} and the operation history to reveal I_{out} [1].

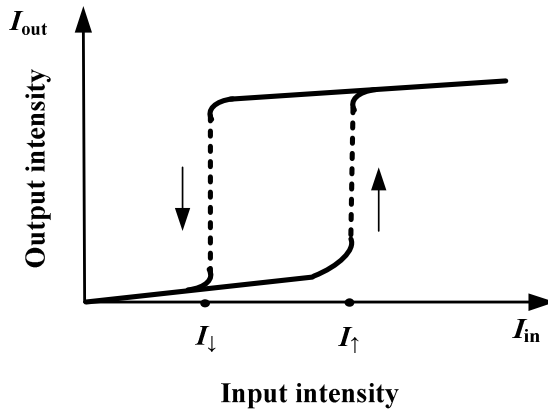


Figure 1.1: characteristic curve for a bistable system

¹ The term *optical multi-stability* is used to describe the circumstance in which more than two stable states are possible.

The phenomenon of bistability has already been known for a long time in mechanics and electromagnetics [2], and is also observed in various disciplines, such as in chemistry [3] and in biology [4]. Bistabilities have been extensively studied in fundamental research [5, 6] and engineering, because they have important applications in signal processing and storage.

The origin of research on optical bistability can be traced back to the birth of the laser in 1960 [7], which could provide the high intensity light to explore the nonlinear response of a material system to an applied optical field [8]. After the discovery of nonlinear optical phenomena, the question arose as to the conditions under which bistabilities may occur in optical systems. Soon the absorptive bistability was discovered [9, 10], followed by dispersive bistability [11, 12]. They attracted tremendous research interests in 1970s and 1980s, since they were believed to have potential applications as all optical logics toward optical computing [1]. In early 1990s, due to the rapid progress of electronic computers and the difficulties of realizing applicable optical logics, researches on optical computing based on optical bistable devices waned. However, the dramatic booming of the Internet since the middle of 1990s led to a rapidly evolving optical telecommunication network, where all optical technologies are now considered to be necessary to overcome the “electronic bottleneck” [13]. New optical bistable devices, acting as logic units and storage devices, have received great attention again for their potential applications in optical signal processing in optical telecommunication network [14]. But the research efforts have been devoted into a new category of optical bistability: two-mode [15] and two-active-element bistabilities [16], which promise easier control of switching operation and higher operation speed.

In the remaining part of this Section, we will introduce the physical mechanisms of main types of optical bistability in combination with a concise historical review on each of them, and summarize the trend of this field in terms of technology.

1.1.1 Absorptive and dispersive bistability

Absorptive active bistability is the first observed optical bistability, and was proposed in a laser system by Lasher in 1964 [9] and soon experimentally demonstrated by Nathan in 1965 [10]. In 1960s and 1970s, tremendous research efforts were devoted to Lasher’s absorptive bistable laser, since it can potentially be used for all optical logics.

A switching time of 1 ns was achieved in early 1980s [17], while the switching time of the electronic logic circuit at that time was in the order of ms.

A schematic configuration of an absorptive bistable laser diode is shown in Figure 1.2a, where two regions are indicated, an absorptive and an active one. The absorption region is basically a saturable absorber, whose absorption coefficient drops dramatically at high levels of incident radiation (this phenomenon is often called *bleaching*). Therefore, the combination of laser facet and the absorption region acts as an intensity-dependent “mirror” [18]. The reflection of that “mirror” is weak at low incident intensity, whereas it is strong when the absorber is bleached by high intensity.

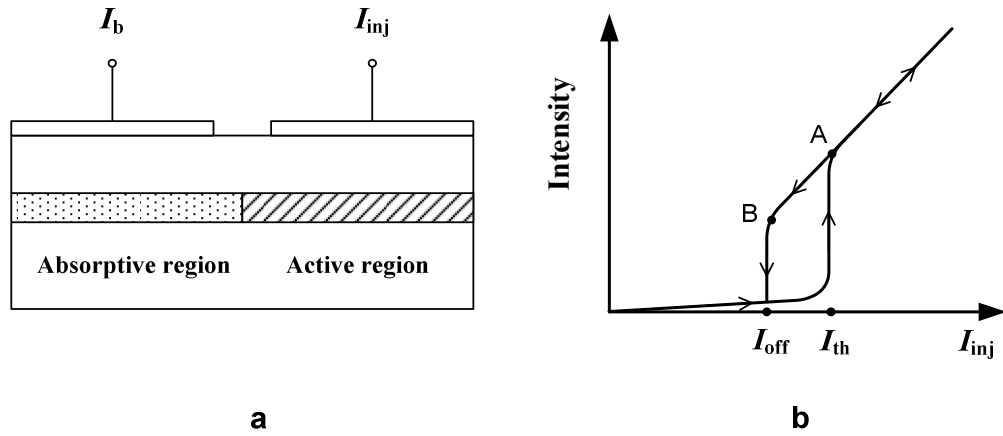


Figure 1.2: Panel a: Schematic configuration of absorptive bistable laser diode. Panel b: the hysteretic curve showing bistability.

The laser starts lasing when the injection current I_{inj} exceeds the threshold current I_{th} , at which the gain in the active region overcomes the loss in the absorptive region. The lasing light initially saturates both the active region and the absorptive region, which leads to a decrease of the gain as well as the cavity loss. The intensity of the lasing light continues to increase until the net gain (the gain minus the cavity loss) of the cavity reaches zero. This state refers to the point ‘A’ in Figure 1.2b. During this process, the lasing light bleaches the absorptive region. After the intensity of the lasing light has jumped to the upper level, it won’t trace the same curve back with decreasing of I_{inj} , because the saturable absorber has been bleached. When I_{inj} is decreased lower than I_{off} , at which the intensity of the lasing light is at the threshold of maintaining the absorptive region bleached, a small decrease of the intensity of the

lasing light leads an increase of the loss in the absorptive region, which in turn makes the intensity of the lasing light decrease further, the lasing operation eventually stops. The intensity-versus- I_{inj} curve is called *hysteretic* curve, referring to the fact that the output intensity depends on the operation history of the system. The system is thus bistable in the hysteretic region, defined by I_{th} and I_{off} .

Note that this is an intuitive explanation on the concept of absorptive bistability. The actual phenomena are far more complicated. For example, in the absorptive bistable laser diode, self-pulsation occurs when the carrier lifetime of the absorptive region is shorter than the active region [19]. Further more, mode-locking [20, 21], chaos [22], have been found in this type of laser. In general, complex dynamic behaviors are strongly connected with bistability [23], which will be exemplified by our work in Chapter 2 and 3.

Optical absorptive bistability was also observed in passive optical devices (containing no gain medium), which were performed by several researchers studying independently in 1969 [24, 25]. The ideas were to inject light into a Fabry-Perot cavity containing absorptive material. Various nonlinear absorptive materials such as dyes [26], cryptocyanine in methanol [27], were soon studied in this frame.

Unaware of the earlier work on absorptive bistability, McCall pointed out in 1974 that a nonlinear Fabry-Perot cavity could be bistable [11], and conducted the experiment using Na vapor between the mirrors of a plane Fabry-Perot interferometer in 1975 [12]. However, the observed optical bistability was due to nonlinear refractive index effects, not to the anticipated nonlinear absorptive effects.

Optical dispersive bistability is based on the fact that the refractive index n is a function of the optical intensity. The mechanism of optical dispersive bistability can be intuitively explained using a Fabry-Perot interferometer shown in Figure 1.3a. A semiconductor element acts as the nonlinear gain medium [28, 29]. For a semiconductor medium, n is related to the optical gain g . Saturation of g , which means the carrier number N is decreased, occurs when the optical intensity (P_{in}) injected into the semiconductor active medium is increased. n is thus depended on N . The ratio of dn/dN and dg/dN is denoted as α -parameter [30] and defined as

$$\alpha = -4 \frac{\pi}{\lambda} \frac{dn/dN}{dg/dN} \quad (1.1)$$

Where λ is the wavelength.

It is well known [31] that the transmittance T of the Fabry-Perot cavity depends on the frequency ω_{in} of the injected light. T increases significantly if ω_{in} gets close to the resonant frequency ω_r of the Fabry-Perot cavity, and reaches maximum value when $\omega_{in} = \omega_r$, as shown in Figure 1.3b.

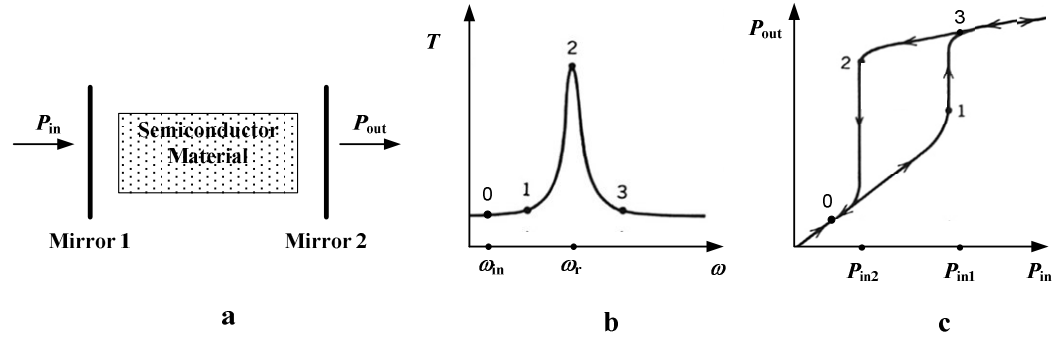


Figure 1.3: Optical dispersive bistability. Panel a: Schematic of a Fabry-Perot interferometer. Panel b: The transmittance T of the Fabry-Perot as a function of the frequency of the input light. Panel c: the injected power P_{in} versus output power P_{out} , showing hysteric curve.

Suppose the injected light has a slightly negatively detuned frequency ω_{in} ($\Delta\omega = \omega_{in} - \omega_r < 0$) and intensity P_{in} . The injected light decreases the carrier density N in the nonlinear element, which increases the refractive index n according to Equation 1.1. The increase in refractive index causes the resonant frequency ω_r of the cavity to decrease (towards ω_{in}). With small value of P_{in} , this effect is weak, T keeps almost constant, the output intensity P_{out} increase linearly with P_{in} , as shown in Points '0' in Figure 1.3b and 1.3c, respectively.

Increasing P_{in} leads ω_r to decrease further. The transmittance T increases significantly when P_{in} exceeds P_{in1} , as shown in points '1' in Figure 1.3b and 1.3c, respectively (Note that it is equivalent and convenient to increase ω_{in} towards ω_r in order to show the change of T). As a result, the intensity inside the cavity increases, which in turn drives ω_r to shift further. The process repeats until the system reaches a new balance, where ω_r is decreased to become smaller than ω_{in} , T decreases with further decreased

ω_t . The new balanced state refers to Points ‘3’ in Figure 1.3b and 1.3c, restively. P_{out} jumps to the upper level.

However, from point ‘3’, P_{out} won’t trace the old path back when P_{in} is reduced. Decreasing P_{in} leads ω_t to increase according to Equation 1.1. The increased ω_t leads a larger T . As a result P_{out} only decreases slightly. P_{out} decreases significantly when P_{in} is reduced beyond a certain value $P_{\text{in}2}$. A hysteretic curve thus exists, as shown in Figure 1.3c. A dispersive bistability is thus realized in the hysteretic region, defined by $P_{\text{in}1}$ and $P_{\text{in}2}$.

It is shown in the two examples that both absorptive and dispersive bistable systems contain nonlinear elements in Fabry-Perot cavities. A system is absorptive or dispersive depending on whether the nonlinear element responses by way of an intensity-dependent absorption or refractive index change. However there is not a sharp distinction between this two. The refractive index in the absorptive bistable system also changes with gain or absorption, but this effect on the operation of the absorptive system is rather small compared to the change of the net gain of the cavity. However, the change of the refractive index is crucial for the dispersive bistable system, since the transmittance of the cavity is so sensitive on it.

1.1.2 Two-mode and two-active-element bistability

Optical bistability can also be obtained by two modes or two optical active elements competing with each other. Any of the two modes (elements) has a equally possibility to be active. However, if one mode (element) becomes active firstly, it destroys the condition under which the other mode (element) can be active. The system is thus bistable.

Two-mode bistability was demonstrated in semiconductor lasers in 1980s [15, 32], using the Transverse Electric (TE) and Transverse Magnetic (TM) modes of a laser diode. Hence two-mode bistability is often called polarization bistability, which has also been demonstrated in vertical-cavity surface-emitting lasers (VCSELs) [33]. Two-mode bistability at two different wavelengths is also demonstrated [34].

Two-mode bistability based on cross-saturation effects is explained as follows: It is well known that, to the lowest order in the nonlinearity, the saturated gain $g(P)$ of a particular model of an idealized laser is related to the unsaturated gain g_0 through the mode intensity P and saturation parameter ε as follows: $g(P) = g_0(P - \varepsilon P)$. In the case of two modes, the gain g 's for each mode are expressed as:

$$g_1 = g_0(P_1 - \varepsilon_{11}P_1 - \varepsilon_{12}P_2) \quad (1.2a)$$

$$g_2 = g_0(P_2 - \varepsilon_{22}P_2 - \varepsilon_{21}P_1) \quad (1.2b)$$

Where ε_{11} and ε_{22} are self-saturation coefficients, ε_{12} and ε_{21} are cross-saturation coefficients, and g_1 and g_2 are the net gain for each mode, respectively. The two modes are assumed to have a same unsaturated gain g_0 . Such a system is a gain-coupled two-mode laser system.

For simplicity, assume that the system is symmetric so that $\varepsilon_{11} = \varepsilon_{22} = \varepsilon_s$ $\varepsilon_{12} = \varepsilon_{21} = \varepsilon_c$. Suppose $\varepsilon_c > \varepsilon_s$, which means the intensity of each mode saturates the gain of the other mode deeper than that of its own. If the initial intensity of mode '1' is set to be larger than that of mode '2', g_1 is larger than g_2 (due to $\varepsilon_c > \varepsilon_s$). The larger g_1 leads to a stronger mode 1, which in turn saturates g_2 further. The process repeats until g_1 becomes zero, whereas g_2 is saturated to be negative, mode '2' is thus quenched by the cross gain saturation. Mode '1' can be quenched as well if the initial intensity of mode '2' is set to be larger. The system is therefore bistable with one of the two modes being active. Note that the state that two modes are active with same intensity is not stable, for any perturbation will kick the system to evolve into one of the two stable states.

The cross-saturation effect in semiconductor material is not strong. However, the idea that two modes are competing for being active through gain saturation can be adapted in other formats. Figure 1.4 shows a schematic of two coupled lasers. A semiconductor optical amplifier (SOA) acts as the gain medium in each laser cavity, which is formed by two wavelength dependent mirrors. Laser 1 and Laser 2 have lasing wavelengths of λ_1 and λ_2 , respectively. A portion of the lasing light in each cavity is coupled to the other cavity via two optical couplers, and saturates the corresponding SOA.

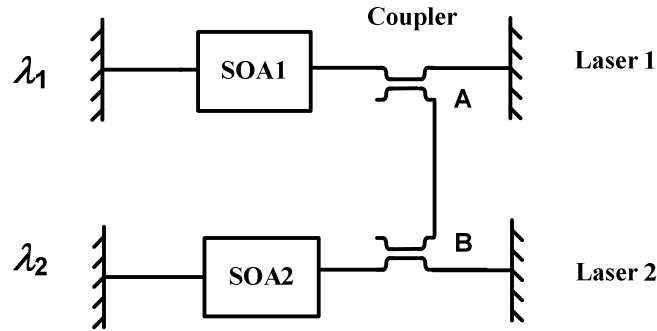


Figure 1.4: Two-active-element bistability based on gain quenching.
SOA: Semiconductor Optical Amplifier

If the coupling of the two lasers is strong enough, the system is bistable in the sense that only one of the lasers is lasing. For example, if the initial intensity of laser 1 is set to be larger, SOA2 in cavity ‘2’ is saturated deeper than SOA1 in cavity ‘1’. Therefore, the light in cavity ‘1’ receives more amplification becomes stronger, which in turn leads that SOA2 is further saturated. As a result, less light from Laser ‘2’ is injected into Laser ‘1’, this makes the intensity of the light in Laser ‘1’ further increase. The process repeats until the lasing operation of Laser ‘2’ is quenched. It is same for Laser ‘2’ to become dominant if its initial intensity is set to be larger. The key of this type of bistability is that the lasing operation of the slave laser is ceased because its gain medium is deeply saturated by the injected light from the master laser (this phenomenon is called *gain quenching*).

The concept of a bistable laser system based on gain quenching was first proposed in [35]. However, it was only experimentally demonstrated two decades later with dye lasers [36], and nearly four decades later with semiconductor devices [16]. This general principle can be applied to achieve other optical bistabilities through other means, like phase [37], or polarization rotation [38].

1.1.3 Research trend

Optical bistabilities have been well explored for more than four decades in several passive optical bistable setups [39], hybrid optical bistable systems [1], and in various types of lasers, such as gas lasers [40], solid-state lasers [14], dye lasers [26] and

semiconductor lasers (laser diodes) [41]. In the last ten years, in order to do optical signal processing in high speed optical telecommunication network, great research efforts have been devoted to improve the operation quality of optical bistable systems in various aspects: integration, switching speed, power consumption, and reliability. Optical bistable systems based on semiconductor material are particular interesting for optical signal processing, since they can be potentially made very small with fast response and low power consumption. Following the trend of technical innovation, new engineering terminologies, *optical memory or optical flip-flop*², are named to optical bistable systems, whose bistable states can be optically set and reset.

Recently, a remarkable device with two-coupled micro-ring lasers shows bistability based on gain quenching and injection locking [42]. Such a device has a size of $18 \times 40 \mu\text{m}^2$ on an InP/InGaAsP photonic integrated circuit, and switches within 20 ps. Today, it is a still ongoing effort to make a small, lower power consumption, fast switching and robust optical memory. A trend emerging from today's efforts is to make use of the integrable optical memories to realize complex optical logic function for optical signal processing in optical telecommunication network. Another trend is to investigate multi-stable optical systems also for optical signal processing in optical telecommunication network, which operates intrinsically in parallel optical wavelength channels. This will be elaborated further in the following section.

1.2 Motivation of investigating optical multi-stable systems

Optical memories have been extensively investigated for applications in various fields, especially in optical telecommunication network, which adapts optical fiber as the transmission medium. Comparing with other transmission means like copper wires, coaxial cables, Microwaves, optical fiber has vast transmission capability. It has been demonstrated [43] that one wavelength channel in a single optical fiber can transmit information at a data-rate 2.5 Tbit/s, which means 39 million conventional telephone calls can be transmitted simultaneously. Furthermore, the transmission capacity can be increased further by multiplexing wavelength channels in a single optical fiber. In wavelength division multiplexing (WDM) network, a transmission rate of 10.92 Tbit/s has been reached by employing 273 wavelength channels at a bit-rate of 40

² In this thesis, the terminology, *optical bi(multi-)stability*, is used in the context of describing the physical principles, while the terminology, *(multi-state) optical memory*, is used in the context of explaining the technical operations.

Gbit/s per channel [44]. The theoretical bandwidth of an optical fiber is even twenty times larger.

Along with the trend that the transmission speed in optical networks is rapidly increasing, the control of the optical network needs to be more flexible. All optical technologies play essential roles to deal with vast amount of information in a complex network. As a basic logic unit and a fundamental storage element, optical memories are promising in the fields like optical packet switching, optical buffering, and so on.

In optical packet switching technologies [45], which are triggered by the large-scale penetration of the Internet which is supported by data-packets [46], Optical memories serve as one of the key building blocks to rout optical packets. Despite of many technical challenges like optical header processing, optical packet buffering, optical packet scheduling, the optical memories should operate in multiple states in order to rout multiple optical packets. Multi-state operation can be achieved by cascading memories which have two states, but this increases the complexity, power consumption, and decreases operation speed. Therefore a single optical memory operating in multiple states is essential to rout multiple optical packets.

Optical memories have also been shown to be one of the candidates to realize optical buffering [47, 48] in situations where optical data should be stored temporally in optical telecommunication network. Optical memories in multi-state operation provide the opportunity to increase the buffering efficiency.

Furthermore, a multi-state optical memory has potential to be generalized to process a large number of wavelength channels in parallel. It should be noted, that in contrast to electronics, optical signal processing could exploit the inherent parallelism of photonics, i.e. in photonics many wavelength channels can propagate in parallel through optical fibers and waveguides. By utilizing a form of parallelism in photonic devices one could enhance the integration density, since the same chip-area could be used to process a larger number of channels in parallel.

In short, as a basic logic unit and a fundamental storage element, optical memories in multi-state operation are appealing in the fields where multiple optical units have to be processed or stored.

1.3 The contribution of this thesis

Although multi-state optical memories are important and interesting, very few of the existing optical memory concepts can be extended to operate in multiple states. It is shown in Ref. [49] that the stability of more than three states is impossible in the two-mode laser systems. In Ref. [50] a three-state optical memory based on gain quenching is presented. This concept requires that each laser be connected with all the other lasers in the memory, making the number of inter-connections large and the operating power high.

In the thesis, two types of multi-state optical memory are presented. The first one is based on coupled ring lasers with feedback. A single ring laser with feedback can be regarded as an oscillator, since the intensity of the lasing light in the lasing cavity is periodically oscillating. When two such oscillators are coupled together sharing the active element and the same feedback arm, they synchronize together in a common oscillation frequency if their individual oscillation periodicities are close to each other. Otherwise they show bistability between the two oscillators. Switching between different stable states can be realized by injecting external light. Moreover, this concept can easily realize a multi-state optical memory, since only one active element is required. An eight-state optical memory has been demonstrated.

A significant feature of this type of optical memory is that an optical memory with a large number of states can be realized by using only one active element. However two characteristics of this type of optical memory prevent its application in optical packet-switching scenario: The output of the optical memory is oscillating in intensity; the device can not be made shorter than several millimeters, since a necessary component, namely an optical isolator, can not be integrated in small scale, which limits the switching speed up to several hundreds MHz.

Therefore, we continue to investigate a second type of multi-state optical memory, which is based on serially interconnected lasers using the principle of gain quenching. The light from the dominant laser suppresses its neighboring lasers through gain quenching, but still receives amplification by the active element of the suppressed lasers, compensating for coupling losses. This light passes through each of the successive lasers, simultaneously suppressing and being amplified. By this mechanism all the other lasers are suppressed. Only one of the lasers can lase at a time, thus the state of the optical memory is determined by the wavelength of the

dominant laser, as same as the first type. A five-state optical memory based on this concept is experimentally demonstrated.

Although this type of optical memory requires an equal number of active elements to realize a certain states, the output of the device is a CW light, and the device can be integrated in a photonic chip, which leads to an operation speed at GHz. These features make this type of optical memory suitable for applications in optical packet switching network.

Moreover, we use the optical memories as a fundamental logic unit to realize more sophisticated optical logics. An optical shift register and an optical pseudorandom number generator based on cascaded optical memories are demonstrated.

In short, we present in this thesis two types of multi-state optical memory, investigate the underlying laser dynamics, and show optical digital systems based optical memories are feasible.

1.4 Outline of this thesis

The contribution of this thesis is outlined as follows.

In Chapter 2, after giving a brief review of dynamics of semiconductor laser with optical feedback, we present a model to describe the dynamical behavior of the unidirectional ring laser with optical incoherent feedback. Both experimental and numerical results confirm that the system behaves as an oscillator in some regimes.

In Chapter 3, we present dynamical behavior of two coupled unidirectional ring lasers sharing a single active element and one feedback arm. The two coupled oscillators either synchronize together if their individual oscillation periodicities are close to each other; or show bistability between the two oscillators. The principle of the bistability is investigated both numerically and experimentally. The feedback light makes it impossible for the two oscillators to co-exist if their oscillation periodicities are not close to each other. The synchronization behavior is investigated experimentally by recording the evolution process of two coupled oscillators. Moreover, features of the bistability, like wavelength dependency, switching method and switching speed, are further investigated in this Chapter.

In Chapter 4, the multi-stability of coupled oscillators is investigated. An eight-state optical memory is demonstrated. Moreover, a sixteen-state optical memory is achieved by cascading two sets of four-coupled oscillators. A further discussion on optical multiple-state memory is given.

In Chapter 5, we present a multi-state optical memory that consists of a large number of serially interconnected lasers. The principle of the multi-stability is based on gain quenching. A five-state optical memory is demonstrated. Two switching methods are realized.

In Chapter 6, optical digital systems based on optical memories are investigated. We present an optical shift register that consists of two serially connected optical memories driven by common clock pulses.

In Chapter 7, the optical shift register and an optical XOR gate are cascaded to realize an optical pseudorandom number generator based on cascaded optical memories.

In Chapter 8, this thesis is concluded with a summary and recommendations for further investigation.

Chapter 2

Laser dynamics of a unidirectional ring laser with optical incoherent feedback

As introduced in Chapter 1, the first type of multi-state optical memory is based on coupled ring lasers sharing a single active element and one feedback arm. The dynamics of a single ring laser with optical feedback is discussed in this chapter¹, which is organized as follows. Section 2.1 presents a brief introduction to dynamics of semiconductor laser with optical feedback. A model for the unidirectional ring laser with optical incoherent feedback is given in Section 2.2. Both experimental and numerical investigation on the dynamics of such a system is shown in Section 2.3. A short summary of this Chapter is shown in Section 2.4

2.1 Introduction to dynamics of semiconductor laser with optical feedback

Semiconductor lasers have been applied intensively in many areas such as optical telecommunication and optical disks, due to their small size, reliability and volume productivity. Huge research efforts have been devoted to their fundamental and applied physical properties over the last three decades. Semiconductor lasers differ from conventional lasers not only in size but also in ‘openness’: while conventional lasers let through only a small fraction of the light intensity to the outside world (1-5%) and are therefore considered ‘closed’, semiconductor lasers are wide open, as they allow ~70% of the light intensity to escape. Combining the low facet reflectivity and high gain of the active medium, semiconductor lasers are hence extremely

¹ This chapter is based on the following paper:

S. Zhang, D. Lenstra, Y. Liu, H. Ju, Z. Li, G.D. Khoe and H.J.S. Dorren, Multi-state optical flip-flop memory based on ring lasers coupled through the same gain medium, *Optics Communications*, accepted.

sensitive to external perturbations like optical feedback, external light injection, etc. (For an overview, see Refs.[51, 52]). On one hand external perturbations deteriorate semiconductor lasers in most cases; on the other hand an extra freedom is given to modify the properties of semiconductor lasers by controlling the external perturbations. For example, narrow-linewidth operation can be achieved by controlling optical feedback [53].

Moreover, the corresponding dynamics is also very interesting from a fundamental physics point of view, since nonlinear dynamics and chaos is one of the still growing fields in physics. The use of laser in nonlinear dynamics was initiated by Haken in 1975 [54], who showed that there is a strong mathematical resemblance between the dynamics of some types of lasers and the turbulent Raleigh_Benard convective fluid dynamics, used by Lorenz 1963 in his classical paper on the unpredictability of atmospheric dynamics ('chaos') [55]. Since the mid 1970s numerous types of lasers (including diode lasers) have been used to investigate nonlinear dynamics [56]. A milestone in the research on semiconductor laser dynamics is the paper by Lang and Kobayashi in 1980, who reported on some aspects of the dynamics of a semiconductor laser exposed to optical feedback [57]. They showed that its dynamical properties are significantly affected by external feedback from a distant reflector as shown in Figure 2.1. The light out of the diode laser is reflected back to the diode laser after a certain delay, and propagates in the laser cavity with lasing light.

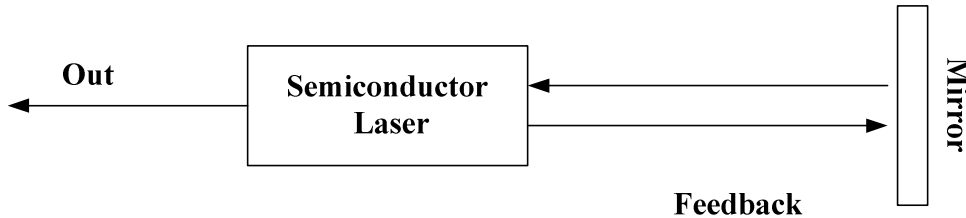


Figure 2.1 Basic schematics of a semiconductor laser exposed to optical feedback

In general, feedback-related physics can be of a highly complicated nature, since the delay time involved caused the system to have an infinite number of degrees of freedom. Theoretical investigations of optical feedback effects are usually based on

the Long-Kobayashi rate equations [57] which have proven to contain all the dominant effects observed experimentally. These rate equations read:

$$\dot{E} = \frac{1}{2}(1 + i\alpha)(\Gamma G(N) - \frac{1}{\tau_p})E(t) + \gamma\tau_{in}E(t - \tau_f)\exp(-i\omega_0\tau_f) \quad (2.1)$$

$$\dot{N} = \frac{I}{q} - \frac{n}{\tau_c} - G(N)|E(t)|^2 \quad (2.2)$$

Describing the temporal behavior of the slowly varying complex amplitude $E(t)$ of the optical field and the carrier number N . The optical feedback is accounted for by two parameters: the delay time τ_f , and the feedback-rate γ . The first has a ‘double’ role in the feedback term: on one hand it appears in the delayed amplitude $E(t - \tau_f)$ and on the other hand it also plays a subtle role via the phase factor $\exp(-i\omega_0\tau_f)$, where ω_0 is the angular frequency of the solitary laser. τ_{in} is roundtrip time of the diode laser cavity, the ratio of the power reflected from the external mirror and the power reflected from the laser facet is given by the feedback level $\gamma\tau_{in}$. Furthermore, α is the line width enhancement factor, Γ is the gain confinement factor, τ_p is photon lifetime, τ_c is the carrier lifetime, I the injection current, q the elementary charge unit. With this model, in terms of external control parameters, the operation of a diode laser exposed to optical feedback is governed by the bias pump current I , the feedback rate γ and the feedback time τ_f . It is often convenient also to regard the phase $\omega_0\tau_f$ as an independent control parameter, because a negligible change in τ_f can have a dramatic effect on the phase.

The first phenomenological experimental classification of the different types of behavior of semiconductor lasers with optical feedback was reported by Tkach and Chraplyvy in 1986 [58]. They used distributed feedback (DFB) lasers operating at $1.5\mu\text{m}$, with a pump current twice the threshold value. By varying the external cavity length and the feedback level they charted the systems behaviors in (γ, τ_f) -space. They distinguish between five regimes of qualitatively different behaviors. It should be noted that although their classification is rather rough, it is widely used in the field of diode lasers with optical feedback. In different regimes, researchers have observed many interesting phenomena, like linewidth reduction [53], mode-hopping [59], coherence collapse [60], several routes to chaos [61], and so on.

Besides the normal optical feedback, i.e. without altering the frequency content of the feedback light, filtered optical feedback has been studied. It offers a potential to control the laser dynamics via two external parameters, the spectral width of the filter and its detuning from the solitary laser frequency. The complex dynamical behavior arising in lasers with feedback is primarily rooted in the undamping of the intrinsic relaxation oscillations in the laser combination with the relatively large phase-modulation property of semiconductor lasers (expressed by the α -parameter). Filters not only provide a mechanism for controlling the influence of relaxation oscillations on the dynamical response, but they also introduce an externally controllable nonlinearity of the device [62].

Studies on diode laser exposed to optical feedback also included modifying the feedback mirror, namely, diode laser exposes to optical phase-conjugate (OPC) feedback. Optical phase conjugation is a technique, involving various possible nonlinear optical effects, for precisely reversing both the direction of propagation and the overall phase factor for each plane wave in a beam of light. OPC can therefore be regarded as a unique ‘mirror’-process: a beam reflected by a phase conjugator retraces its original path, in which many nonlinear effects, like four-wave mixing, are involved. Therefore, semiconductor lasers, in general, display richer chaotic dynamics in case of phase-conjugate feedback than in the case of normal feedback [63].

2.2 Model of unidirectional ring laser with incoherent feedback

In previous studies, Optical feedback (including filtered optical feedback and optical phase-conjugate feedback) means that a portion of the laser output is fed back into the laser cavity. The feedback light propagates through the laser cavity together with the lasing light. These systems can be studied in the framework of Lang-Kobayashi model [51].

In this chapter, we present a unidirectional ring laser with a different form of optical feedback as shown in Figure 2.2. A semiconductor optical amplifier (SOA) acts as the laser gain medium. The system consists of a ring cavity and a feedback arm. The ring cavity contains an arrayed waveguide grating (AWG) [64] that acts as a filter to select lasing wavelength and an optical isolator that allows the light to propagate in only one direction (thus to ensure unidirectional lasing). The mechanical switch in the ring cavity is used to close or open the cavity at demand. A fraction of the lasing light is

coupled out of the ring into the feedback arm by a splitter, which light is reflected back into the SOA through the feedback arm. Note that the feedback light is amplified by the SOA, but it cannot build-up into a lasing state due to the presence of the isolator. The feedback light depletes the nonlinear gain medium and thus influences the lasing light indirectly. Therefore the kind of feedback is called incoherent feedback, in contrast to conventional laser with optical feedback, in which the feedback light becomes a part of the lasing light when feedback into the laser cavity [51].

The output power of the unidirectional ring laser with incoherent feedback shows oscillation as a function of time. We will show that, depending on the control parameters – in particular the feedback strength, the laser exhibits either periodic (limit-cycle type in the context of general nonlinear dynamics [65]) oscillations or irregular (chaotic-type) oscillations. The periodicity of the periodic oscillation is determined by the ratio of the roundtrip times in the feedback arm and the ring cavity.

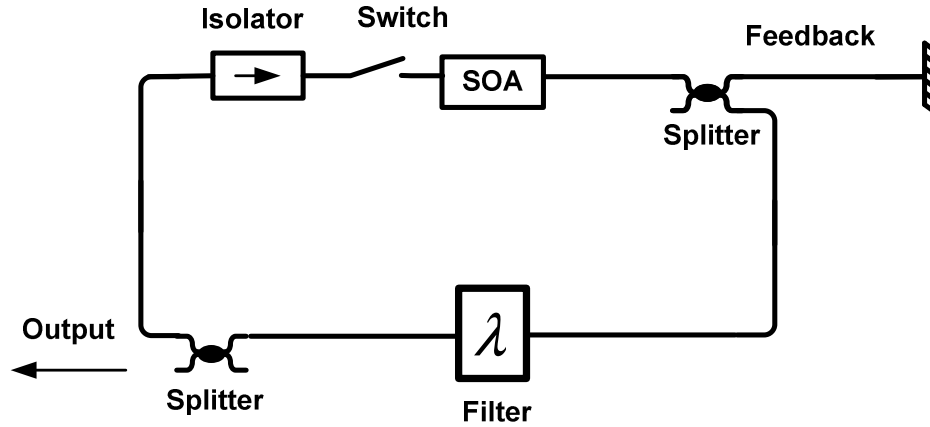


Figure 2.2: a unidirectional ring laser with incoherent feedback.

2.2.1 General model

In Figure 2.3a schematic representation of a ring laser with incoherent feedback is given. We formulate the dynamics of this system in terms of roundtrip time equations instead of rate equations since, in the experimental implementation of this system, the laser are composed out of discrete commercially available fiber pigtailed elements and hence each laser has a very large ring cavity length (~ 10 meters, typical value of the

experimental setup made by fiber-pigtailed components). This means that the roundtrip times of the lasers are large compared to the carrier lifetime.

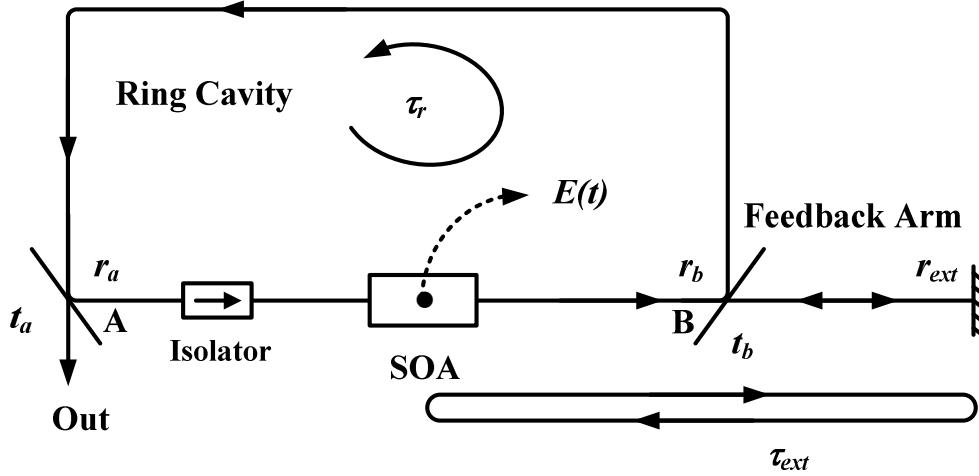


Figure 2.3: Schematic of unidirectional ring laser with incoherent feedback. SOA: semiconductor optical amplifier.

The roundtrip equations for the fields are formulated at a reference point inside the SOA, as indicated in Figure 2.3. The SOA itself is modeled as a point amplifier. The roundtrip equations [66] formulated for the field inside the SOA are used to describe the system as follows:

$$E(t) = t_r \exp(-ik_s L_s - i\omega\tau) E(t - \tau) \quad (2.3)$$

$$E_f(t) = t_f \exp(-ik_s L_s - i\omega\tau_{ext}) E(t - \tau_{ext}) \quad (2.4)$$

Where,

$$t_r = r_a r_b ; t_f = t_b^2 r_{ext} \quad (2.5)$$

In (2.3)-(2.5), $E(t)$ is the complex optical field amplitudes in the ring cavity, $E_f(t)$ is the complex field amplitude of the light that is fed back into the SOA in the counter propagating direction, r_i and t_i ($i \in \{a, b\}$) are the reflections and transmissions through the beam splitters in the system, r_{ext} is the reflectivity of the end-mirror in the

feedback arm, τ_r is the roundtrip times in ring cavity and τ_{ext} is the roundtrip time through the feedback arm. The SOA length is represented by L_s , ω the central optical frequencies of the lasing light in cavity 1. In the roundtrip equations as given above, it is assumed that the amplification of the light propagating through the SOA is wavelength independent. If we introduce the notation, $t_r = |t_r| \exp(i\varphi_r)$, $t_f = |t_f| \exp(i\varphi_f)$, it is found that (2.3) and (2.4) are equivalent with:

$$E(t) = |t_r| \exp(-ik_s L_s - i\omega\tau_r + i\varphi_r) E(t - \tau_r) \quad (2.6)$$

$$E_f(t) = |t_f| \exp(-ik_s L_s - i\omega\tau_{ext} + i\varphi_f) E(t - \tau_{ext}) \quad (2.7)$$

We define the SOA gain by using that the light passing through the SOA is amplified according to:

$$\frac{dE}{dz} = [G_R(N) + iG_I(N)] E \quad (2.8)$$

Where the real and imaginary parts of the gain take confinement into account. If we integrate (2.8) over a SOA length, we obtain:

$$E(L_s) = \exp[G_R(N)L_s + iG_I(N)L_s] \equiv \exp(-ikL_s) \quad (2.9)$$

If we furthermore linearize the real and imaginary parts of the complex gain around the threshold value N_{th} , we find:

$$G_R(N) = G_R(N_{th}) + \frac{\Gamma\xi}{2[1 + \varepsilon S(t)]v_g} (N - N_{th}) \quad (2.10)$$

$$G_I(N) = G_I(N_{th}) + \frac{\Gamma\xi\alpha}{2[1 + \varepsilon S(t)]v_g} (N - N_{th}) \quad (2.11)$$

Where, ξ is the linearized gain coefficient, Γ is the gain confinement factor, ε is the corresponding gain saturation parameter, $S(t) = |E(t)|^2$ is the corresponding photon

number, v_g the group velocity and α the linewidth enhancement factor. If we substitute and (2.9)-(2.11) into (2.6)-(2.7), we find:

$$E(t) = \exp \left\{ (1 + i\alpha) \frac{\Gamma \xi L_s}{2[1 + \varepsilon S(t)]v_g} n(t) \right\} E(t - \tau_r) \quad (2.12)$$

$$E_f(t) = \frac{|t_f|}{|t_r|} \exp \left\{ (1 + i\alpha) \frac{\Gamma \xi L_s}{2[1 + \varepsilon S(t)]v_g} n(t) + i[\varphi_f - \omega \tau_{ext} + G_I(N_{th})L_s] \right\} \times E(t - \tau_{ext}) \quad (2.13)$$

Where it was used that $n = N - N_{th}$ and that the following roundtrip condition has to be satisfied:

$$\varphi_r - \omega \tau_r + G_I(N_{th})L_s = 2n\pi \quad \exp[G_R(N_{th})L_s] = \frac{1}{|t_r|} \quad (2.14)$$

We can further simplify (2.12)-(2.13) by introducing the following notation:

$$\Psi_f = \varphi_f - \frac{2\pi c}{\lambda} \tau_f - \varphi_r + \frac{2\pi c}{\lambda} \tau_r \quad K_f = \frac{|t_f|}{|t_r|} \quad (2.15)$$

Where it is used that $\omega = 2\pi c/\lambda$. If (2.14)-(2.15) are substituted in (2.10)-(2.11) we find:

$$E(t) = \exp \left\{ (1 + i\alpha) \frac{\Gamma \xi L_s}{2[1 + \varepsilon S(t)]v_g} n(t) \right\} E(t - \tau_r) \quad (2.16)$$

$$E_f(t) = K_f \exp \left\{ (1 + i\alpha) \frac{\Gamma \xi L_s}{2[1 + \varepsilon S(t)]v_g} n(t) + i\Psi_f \right\} E(t - \tau_{ext}) \quad (2.17)$$

Finally, the rate equation for the carrier number is:

$$\frac{dn}{dt} = \frac{I}{q} - \frac{I_{th}}{q} - \frac{n(t)}{\tau} - 2v_g G_R(n) \left\{ |E(t)|^2 + |E_f(t)|^2 \right\} \quad (2.18)$$

Where I represents the injection current and q is the elementary charge unit. By using (2.10) and (2.14), we find that (2.18) is equivalent with:

$$\begin{aligned} \frac{dn}{dt} = \frac{I}{q} - \frac{I_{th}}{q} - \frac{n(t)}{\tau} - \left\{ \frac{\xi}{[1 + \varepsilon S(t)]} n(t) - 2v_g \frac{\ln(|t_r|)}{L_s} \right\} \\ \times \left\{ |E(t)|^2 + |E_f(t)|^2 \right\} \end{aligned} \quad (2.19)$$

The model is formed by Equations (2.16) and (2.17) in combination with (2.19).

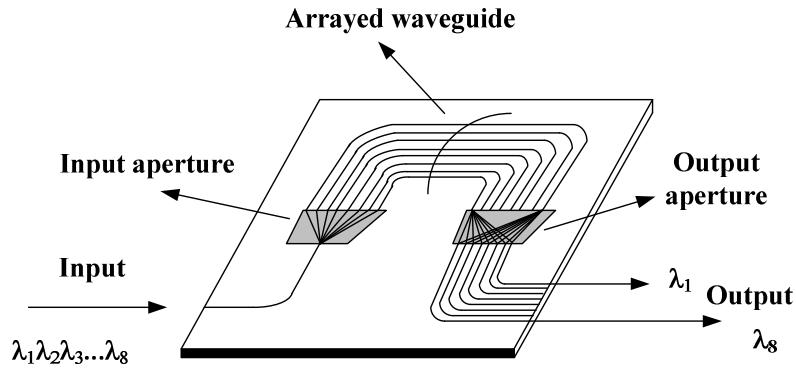
It is shown in this model that the feedback light influences the lasing light indirectly via carrier equation (2.19), which is different as the Long-Kobayashi model in Equation (2.1) and (2.2).

2.2.2 Model with optical filter

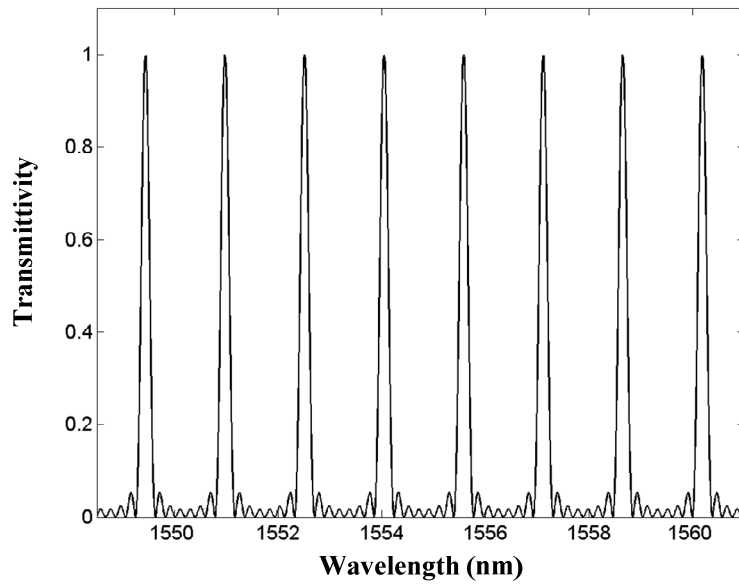
The experimental system was built up with fiber-pigtail components, corresponding to a ring cavity of about 10 meters long. In the case of such a long ring cavity and without a feedback arm, the model predicts irregular intensity fluctuations in the laser field. However, the corresponding experimental results show the lasing light in the long ring cavity to converge to a continuous wave operation. We conjecture that it is the optical filter placed in the ring cavity that suppresses the instability, whose high frequency components are filtered out. Therefore, an optical filter will be included in the model as well [66], and this indeed yields the stable CW operation as observed.

The optical filter used in our experiments is an AWG [64], which is a planar lightwave circuit (PLC) with one input and eight output ports, as shown in Figure 2.3a. It comprises an input aperture, an arrayed waveguide and an output aperture. When multiplexed optical signals are incident on the input aperture, they are spread by diffraction over the arrayed waveguides. Since adjacent waveguides of the array differ in length by a fixed amount ΔL , passing through the arrayed waveguides induces phase differences, in such a way that focusing occurs at the end of the output aperture

at different points depending on the wavelength. Thus signals of distinct wavelengths can be selected by disposing the output waveguides at their respective focal points.



a



b

Figure 2.4: Panel a: Schematic configuration of the AWG filter. Panel b: Amplitude response of the filter (by a simplified model).

The corresponding amplitude response of the filter is shown in Figure 2.3b. Therefore, as a simple model [67], the output optical field $E(t)$ of the AWG filter at a certain wavelength can be expressed as

$$E(t) = \sum_{j=0}^7 r_j E(t - \Delta T - j \times \Delta t) \quad ; \quad (j = 0, 1 \dots 7) \quad (2.20)$$

Where j labels the corresponding waveguide (there are 8 of them), r_j is the filter coefficient for the waveguide, ΔT is the propagation time for the shortest waveguide, Δt is the propagation time interval corresponding to the length difference (ΔL) of two adjacent waveguides.

Including the AWG filter, the roundtrip equations for the laser field formulated at a reference point inside the SOA can now be expressed as:

$$E(t) = \exp \left\{ (1 + i\alpha) \frac{\Gamma \xi L_s}{2[1 + \varepsilon S(t)] v_g} n(t) \right\} E(t - \tau_r) \quad (2.21)$$

$$E(t - \tau_r) = \sum_{j=0}^7 r_j E(t - \tau_r - j\Delta t) \quad ; \quad (j = 0, 1 \dots 7) \quad ; \quad (2.22)$$

$$E_f(t) = K_f \exp \left\{ (1 + i\alpha) \frac{\Gamma \xi L_s}{2[1 + \varepsilon S(t)] v_g} n(t) + i\Psi_f \right\} E(t - \tau_{ext}) \quad (2.23)$$

$$\begin{aligned} \frac{dn}{dt} = & \frac{I}{q} - \frac{I_{th}}{q} - \frac{n(t)}{\tau} \\ & - \left\{ \frac{\xi}{[1 + \varepsilon S(t)]} n(t) - 2v_g \frac{\ln(|t_r|)}{L_s} \right\} (|E(t)|^2 + |E_f(t)|^2) \end{aligned} \quad (2.24)$$

$$\Psi_f = \varphi_f - \frac{2\pi c}{\lambda} \tau_f - \varphi_r + \frac{2\pi c}{\lambda} \tau_r \quad ; \quad K_f = \frac{|t_f|}{|t_r|} \quad . \quad (2.25)$$

2.3 Simulation and experimental results

2.3.1 Origin of oscillation

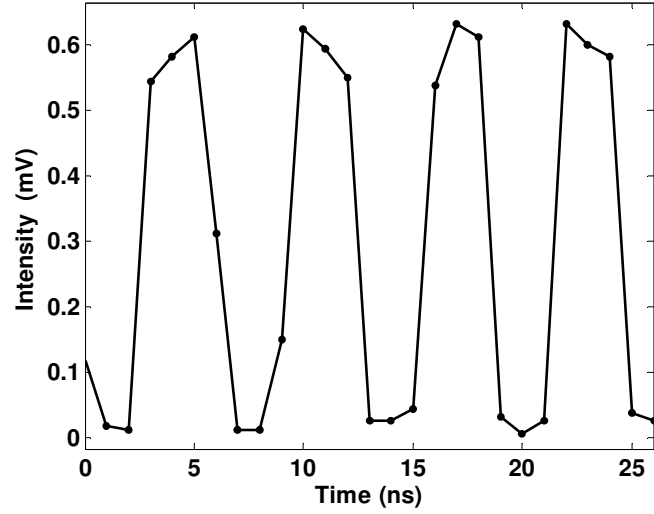
In the system shown in Figure 2.2, the feedback coefficient K_f can be controlled by adjusting the coupling ratio of the splitter connecting the ring cavity and the feedback arm. When K_f is larger than unity, most of the light that outputs the SOA is coupled back into the gain medium with delay via the feedback arm. Gain saturation induced by the delayed feedback light causes the light in the ring cavity to receive a reduced amplification. Consequently, less light is coupled into the feedback arm so that after one roundtrip of the feedback arm the SOA will be less depleted. As the field evolves further, periodic oscillations of the gain build up, accompanied by the oscillating intensity of the light, which then has evolved into a periodic (limit-cycle) oscillation.

Figure 2.5a shows a particular experimental result for which the output power of the system is periodically oscillating². The experimental result is obtained by using a system made out of fiber-pigtailed components, using a strained-bulk SOA with an active region of 800 μm that was pumped with 190 mA of current (the threshold current of the system is 120 mA). The corresponding RF spectrum is shown in Figure 2.5b, indicating that the oscillation frequency is 162.5 MHz (Note that the RF spectrum analyzer used in this testament didn't have a good response at frequency lower than 10MHz). The harmonic frequency 16.2 MHz is the fundamental frequency regarding to the roundtrip of the ring cavity, showing that the ring cavity is 12.3 meters long. The oscillator was stable under normal environmental conditions, like 10-degree room temperature variations, vibrations of standard experimental tables, etc.

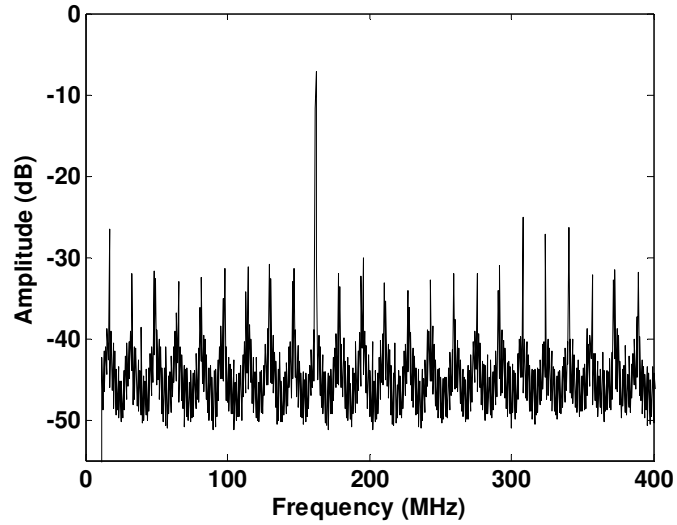
The simulation shown in Figure 2.6 illustrates the evolution process of the oscillation that is visible in Figure 2.5. The value of the parameters used in the model is listed in Table 2.1. The horizontal axis of Figure 2.6 represents the time expressed in ns (lower scale) and in units of cavity roundtrip times (upper scale). The vertical axes of Figure 2.6a and 2.6b represent the power of the lasing light and the feedback light in the SOA, respectively, while the vertical axis of Figure 2.6c represents the net gain in the ring cavity (the amplification of the SOA minus the loss in the ring cavity). In the

² In physics, this kind of oscillatory objects is denoted as self-sustained oscillators. This system in limit-cycle regime can be called a limit-cycle oscillator. It should be note that lasers are traditionally called oscillators, which indicate the oscillation of the electromagnetic field at optical frequency. While the concept of oscillators in this paper means optical systems whose output optical power are not continuous but oscillating.

simulation, we assume that $K_f=2$ (this means that the transmission of the ring cavity is 50% compared to the transmission of feedback arm), τ_r is 50 ns (a typical value for our fiber-pigtail setup) and τ_f is 25 ns.



(a)



(b)

Figure 2.5: Typical output of a single unidirectional ring laser with incoherent feedback. Panel a: the output in time domain; Panel b: the output in RF frequency domain.

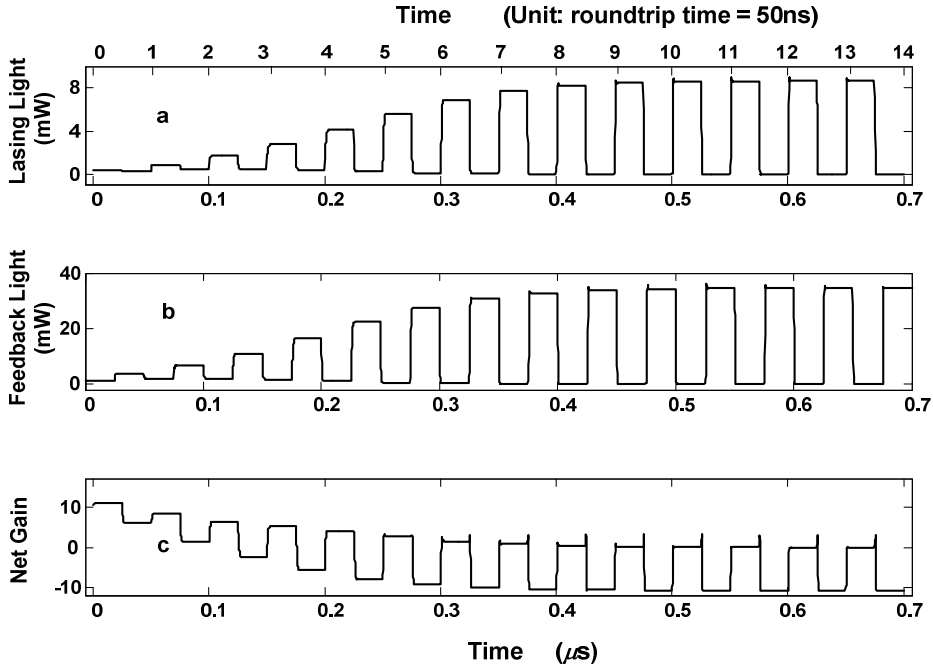


Figure 2.6: Simulation of the evolution of the system. Panel a: Power of the lasing light in the SOA versus time. Panel b: Power of the feedback light in the SOA versus time. Panel c: Net gain for the lasing light versus time.

Suppose that for $t < 0$ while the switch in Figure 2.2 is open, the SOA is electrically pumped, so that the ring-cavity and the feedback arm are filled with spontaneous emission. At $t = 0$, the switch is closed and the system starts to evolve. The initial value is chosen such that the laser initially generates -30 dBm of spontaneous emission around its central frequency.

It follows from Figure 2.6a and 2.6b that the light in the ring cavity and the feedback arm receive the same amplification by the SOA. In the first half-roundtrip time, the SOA amplifies the spontaneous emission in both the ring cavity and the feedback arm. Most of the amplified spontaneous emission in the ring cavity is coupled in the feedback arm during the first half roundtrip time (since $K_f = 2$). The light in the feedback arm is reflected back, and saturates the SOA during the second half roundtrip time. As a consequence, the light in the ring cavity receives less amplification during the second half roundtrip time. During the next two roundtrips,

Table 2.1

Description of value of symbols used in equations

Symbol	Description	Value
τ_r	Roundtrip time of ring cavity	50 ns
τ_f	Roundtrip time of feedback arm	25 ns
Γ	Gain confinement factor	0.14
ξ	Gain coefficient	3000 s^{-1}
v_g	Group velocity in SOA	$8 \times 10^7 \text{ m/s}$
α	Linewidth enhancement factor	3
L_s	Length of SOA	800 μm
ε	Gain saturation parameter	1×10^{-7}
K_f	Feedback coefficient	2
Δt	AWG character time	5 ps
r_j	AWG filter coefficient	0.125
τ_c	Carrier lifetime	500 ps
q	Elementary charge unit	1.6×10^{-19}
I	Injection current	190 mA
I_{th}	Threshold current	120 mA

the system evolves further and the light in the ring cavity always receives a higher gain during the first half roundtrip and less gain in the second half roundtrip. This is due to the fact that the feedback arm has half the length of the ring cavity, and the SOA gain recovery time is small compared to the round-trip time. Thus the power of the light in the ring cavity during each first half-roundtrip time increases with each oscillation period of the roundtrip time τ_r . After several roundtrips, the power of the feedback light has become so strong that the net gain during the second half roundtrip becomes negative. The lasing light only receives amplification at the corresponding first half of each roundtrip time. Eventually, the system evolves into a stable oscillating state and the net gain is modulated to become periodically negative as shown in Figure 2.6c.

In the experiments, we observed that the type of dynamics of the system is determined mainly by two parameters, i.e. the feedback coefficient K_f and the parameter $k = \tau_f / \tau_r$. This is indeed to be expected for a unidirectional ring laser with roundtrip time τ_r , subjected to strong feedback light with delay time τ_f . K_f represents the feedback strength, and the interplay between the feedback time delay and the roundtrip time is represented by k . We will now analyze the dynamics of the system as a function of k , while K_f is kept fixed at the value $K_f = 2$.

2.3.2 Control parameter k

If k is integer, the system will evolve into a state of Continuous Wave (CW). This follows from the fact that for integer k , the length of the feedback arm is an integer times the length of the ring cavity. This means that the net gain in the ring cavity is constant during each roundtrip and oscillations cannot build up. However, if k is not integer, the net gain in the ring cavity fluctuates during each roundtrip due to the imbalance between τ_f and τ_r , which makes the system evolve into an oscillating state. This is illustrated in Figure 2.7 where on the vertical axis k is varied between 0 and 0.5 while on the horizontal axis the time is indicated after 100 roundtrip times (so that the transients have died out). The black areas in Figure 2.7 indicate that the output power of the ring laser is larger than the average value, while the white areas indicate that the power of the lasing light is below that value. It can be seen in Figure 2.7 that the oscillation period is highly sensitive to the value of k , where a small change in value may lead to a dramatic change in the period of oscillation.

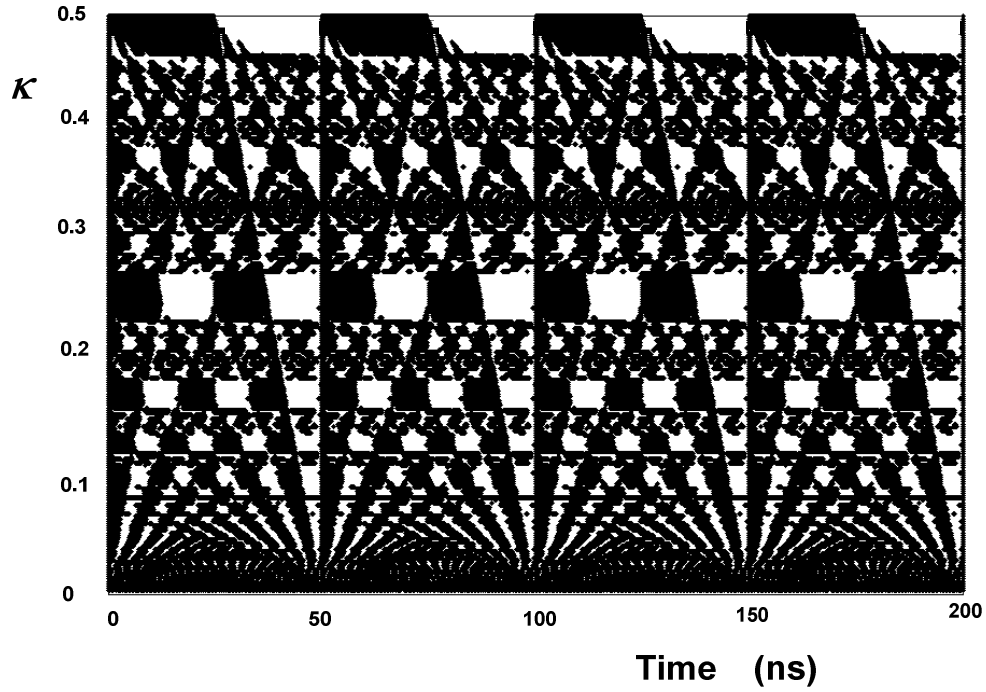


Figure 2.7 Overview of the system dynamics for values of k between 0 and 0.5. For each given value of k the dynamics is indicated horizontally: black areas indicate that the output power of the ring-laser is larger than 2.6 mW, whereas white areas indicate that the power is below that value.

The numerical observation that the oscillation period is highly sensitive to the value of k is confirmed experimentally. A tunable optical fiber delay line, whose length can be adjusted up to a 20-centimeter range, is inserted into the ring cavity in the setup shown in Figure 2.2. The lengths of the ring cavity and the feedback arm are about 10 meters and 2 meters, respectively. The time series of the output light is recorded using oscilloscope. It is shown in Figure 2.8a, where 59 periodicities are recorded within 200 ns. The optical fiber delay line is then prolonged to increase the length of the ring cavity by 5 centimeters, while the remaining setup is kept the same. The time series of the output light with the changed setup is shown in Figure 2.8, where 52 periodicities are observed within 200 ns. It is confirmed in this experiment that oscillation period is sensitive to parameter k . Furthermore, it is also observed in experiments that the

change of the oscillation periodicity is irregular with k in the 20-centimeter tunable range of the ring cavity length.

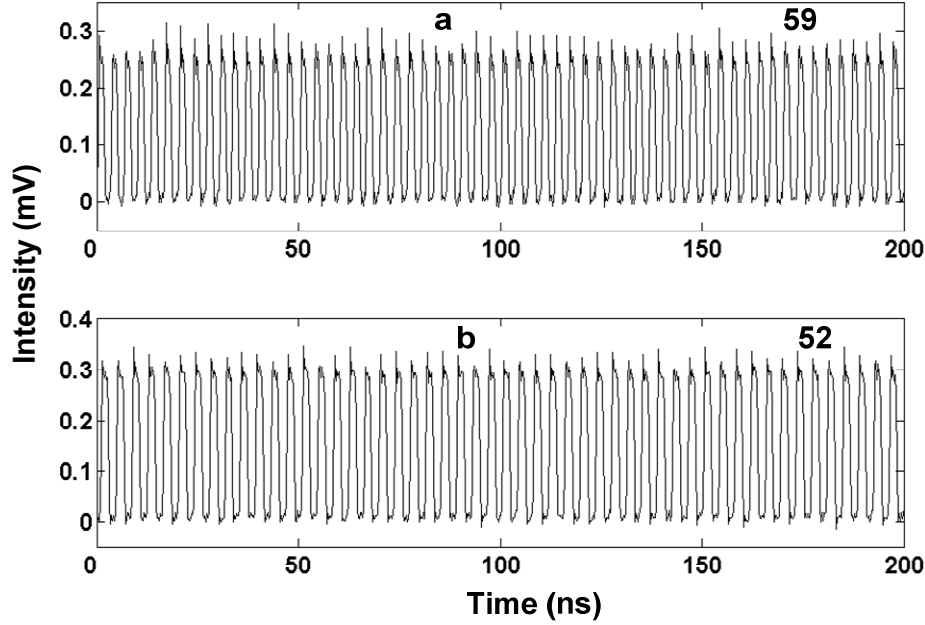


Figure 2.8 The change of oscillation period due to a 5-centimeter change in ring cavity. Panel a: the original oscillation time series (59 periodicities within 200 ns). Panel b: the oscillation time series after the feedback was prolonged 11 centimeter (52 periodicities within 200 ns).

2.3.3 Control parameter K_f

In the dynamical regimes determined by k , the dynamics of the system also critically depends on the feedback coefficient K_f . To illustrate this, Figure 2.9a shows the bifurcation diagram for $S(t)$ as a function of K_f while $k = 0.48$. The bifurcation diagram is computed at each value of K_f by firstly letting the system evolve for 100 roundtrip times so as to get rid of transients. Next, the system evolves for another 10 roundtrip, all the values of the last 10 roundtrips for the optical power (converted from the photon number) at regular intervals are plotted in the plane that the optical power versus K_f .

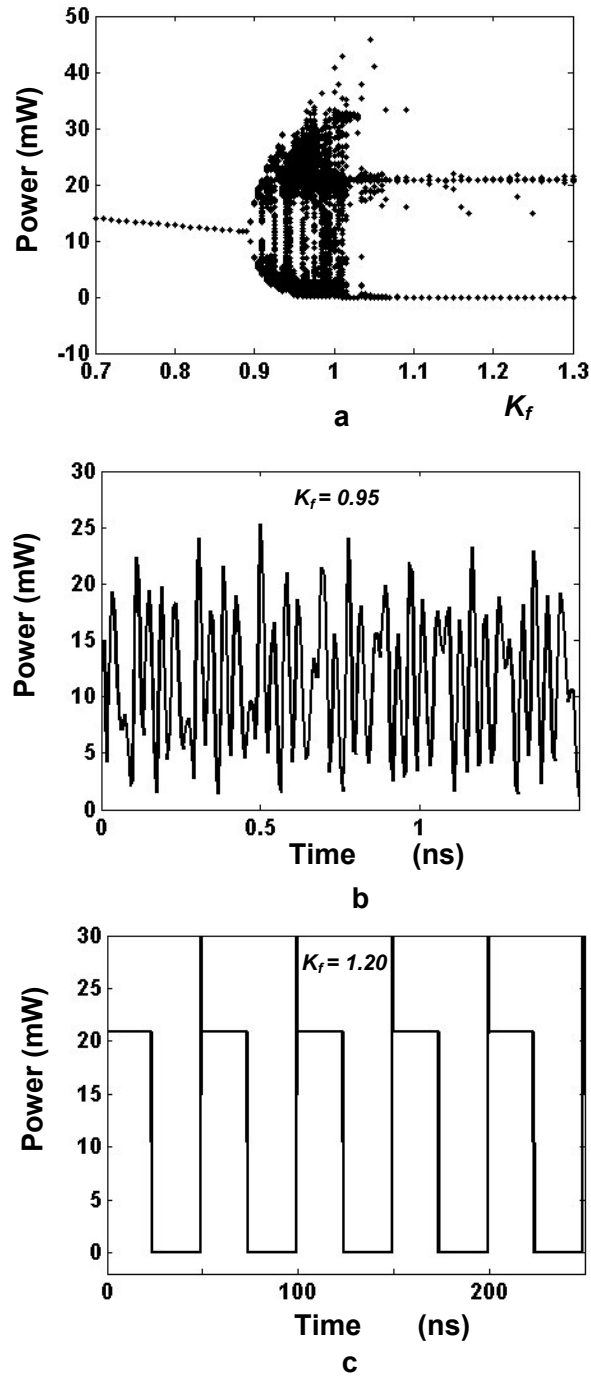


Figure 2.9: System dynamics for $k=0.48$. Panel a: Bifurcation diagram for the laser output power as a function of the K_f . Panel b: Time series for $K_f = 0.88$. Panel c: Time series for $K_f = 1.20$.

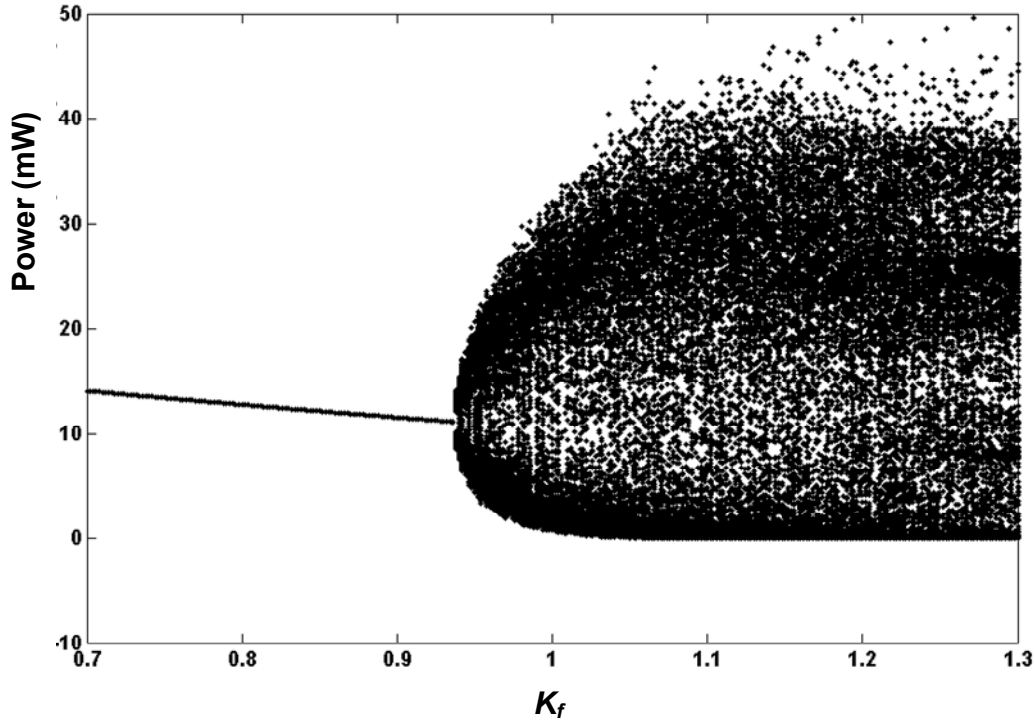


Figure 2.10: Bifurcation diagram for the laser output power as a function of K_f for $k = 0.33$.

For all values of K_f in the interval $[0, 0.88]$, the system evolves into CW operation, although the photon number decreases with increasing K_f due to the enhanced depletion of the SOA. At $K_f = 0.88$, a bifurcation is seen to take place and the system starts to oscillate. When K_f has reached 0.95, the system shows irregular oscillations as shown in Figure 2.9b. If K_f is increased beyond 1.08, the system becomes regular again and finally, it returns to a limit-cycle regime, as shown in Figure 2.9c ($K_f = 1.20$).

It is shown in Figure 2.7 that for some values of k (for example $k = 0.33$), the oscillation frequency increases dramatically. We will now show how K_f determines the dynamic behavior of the system for the case $k = 0.33$. Figure 2.10 shows the corresponding bifurcation diagram as a function of K_f , while $k = 0.33$. It is clear that a bifurcation occurs around $K_f = 0.93$ and the system becomes irregular for K_f greater

than 0.93. This indicates the system cannot evolve into a stationary state with larger K_f .

2.4 Conclusion

In the chapter, we present a unidirectional ring laser with incoherent feedback, namely, the feedback light influence the lasing light indirectly by saturating the active element. This incoherent type of optical feedback is different from the previous studied semiconductor lasers exposed to optical feedback, which can in principle be investigated in the framework of Lang-Kobayashi [57].

It has been shown that the system can exhibit various types of dynamics depending on the combination of two control parameters: the feedback coefficient K_f and the parameter k , which is the ratio between the roundtrip times of the feedback arm and the ring cavity. When K_f is sufficiently large, the system will operate in the limit-cycle regime for most cases, while the periodicity of the corresponding limit-cycle oscillator can be controlled by the parameter k (as shown in Figure 2.7 and Figure 2.8), and the oscillation frequency is high order harmonic of the fundamental frequency regarding to the roundtrip of the ring cavity. Once the limit-cycle oscillator has become stationary, i.e. after the transient has died out, the gain medium is modulated by the corresponding oscillation period (as shown in Figure 2.6c), this feature is essential for the dynamical behaviors of two coupled such oscillators, which will be presented in next chapter.

Chapter 3

Synchronization and bistability of two coupled oscillators based on ring lasers with incoherent feedback

The dynamics of a single unidirectional ring laser with incoherent feedback has been discussed in chapter 2. The laser behaves as an oscillator in the sense that the output power is oscillating as a function of time. It is shown that, depending on the control parameters, in particular the feedback strength, the laser exhibits either limit-cycle type dynamics or chaotic-type oscillations. The periodicity of the limit-cycle oscillator is determined by the ratio between the roundtrip times of the feedback arm and the ring cavity. The question arises what happens if two such oscillators are coupled together through the same active element?

In this chapter¹, we investigate the dynamics of a system that consists of two coupled limit-cycle oscillators sharing the same nonlinear gain medium as well as the same feedback arm. We found that the two oscillators tend to synchronize if their periodicities are close; otherwise the system is bistable.

This chapter is organized as follows: A general introduction to dynamics of coupled oscillators is given in Section 3.1. The model of two coupled ring lasers sharing the same gain medium and the same feedback arm, as well as the simulation results are shown in Section 3.2. The experimental results on synchronization and bistability are presented in Section 3.3. Future experimental investigation on characters of the

¹ This chapter is based on the following papers:

S. Zhang, D. Lenstra, Y. Liu, H. Ju, Z. Li, G.D. Khoe and H.J.S. Dorren, Multi-state optical flip-flop memory based on ring lasers coupled through the same gain medium, *Optics Communications*, accepted.

S. Zhang, Y. Liu, D. Lenstra, M.T. Hill, H. Ju, G.D. Khoe, H.J.S. Dorren, Ring-laser optical flip-flop memory with single active element. *IEEE Journal of Select Topics in Quantum Electronics* 10, 1093 (2004).

synchronization and bistability are shown in Section 3.4. A short summary is given in Section 3.5.

3.1 Introduction to dynamics of coupled oscillators

Coupled oscillators are widely considered to provide insight in collective behavior in physics [68-70], chemistry [71-74], biology [75-79] and even human society [80]. The predominant effect of coupled oscillators is synchronization, which was discovered by Huygens in a system of two coupled pendulum clocks more than three centuries ago [81]. In the 1920s, synchronization was for the first time systematically studied by Appleton and Van der Pol for two triode generators [82, 83], which found their applications in the field of radio communications. From the 1960s to 1980s, Winfree and Kuramoto [84-86] presented models for large numbers of coupled limit-cycle oscillators, based on the assumption that each oscillator weakly and globally (all-to-all) couples with each other. The models predict that some of the oscillators synchronize whereas the others remain unaffected with increasing the coupling strength, and were recently verified in a chemical system [73]. A diversity of synchronizations is observed in circadian rhythms [87], superconducting Josephson junction arrays [68], fireflies [88], and audiences clap in the theater [80]. Applications in engineering are found, for instance, in lasers [69], computer chips [89], and power grids [90].

More sophisticated models for coupled oscillators accounting for amplitude effects show in the case of stronger coupling a phenomenon called amplitude death [91], which means that the oscillators cease oscillating. Rayleigh discovered this phenomenon in an acoustical system in the middle of the nineteenth century [92]. Time delay between the oscillators also can lead to amplitude death [93] and was observed in an electrical circuit [94].

Although all the coupled oscillators investigated before are different as to the disciplines they belong to, their complexities, their ways of coupling and their dynamic behavior, they have one property in common: each of the coupled oscillators has its *own* gain source. A different situation arises if the oscillators are coupled through the *same* gain source and the question arises as to what new physics will be involved in this way of coupling?

In this chapter, the dynamics of a system that consists of two coupled ring cavities sharing the same nonlinear gain medium as well as the same feedback arm is investigated. It will be shown in this chapter that if each individual laser operates in a limit cycle regime and the losses in both cavities are similar, the limit-cycle oscillators coupled through the same gain medium synchronize into the same periodicity if their periodicities are sufficiently close to each other, while otherwise the oscillators show bistability, i.e. one of the lasers will be on, while the other one is suppressed. It should be remarked that this synchronization phenomenon is similar to the synchronization of weakly coupled oscillators that have separated gain mediums [95-98]. However, bistability between two coupled limit-cycle oscillators seems not have been described before. In the remainder of this chapter, these phenomena will be investigated with simulation and experimental results.

3.2 Model of two coupled ring lasers sharing the same nonlinear gain medium as well as the same feedback arm

The schematic in Figure 3.1 shows two ring lasers that share the same gain medium and the same feedback arm. It is a direct extension of the unidirectional ring laser with incoherent feedback as shown in Figure 2.3. Note that a filter is considered in each ring cavity. A model that can describe the coupled system reads:

$$E_m(t) = \exp \left\{ (1 + i\alpha) \frac{\Gamma \xi L_s}{2[1 + \varepsilon S(t)]v_g} n(t) \right\} E_m(t - \tau_m) ; \quad (m = 1, 2); \quad (3.1)$$

$$E_m(t - \tau_m) = \sum_{j=0}^7 r_j E_m(t - \tau_m - j\Delta t) ; \quad (j = 0, 1 \dots 7) ; \quad (3.2)$$

$$E_f(t) = K_f \exp \left\{ (1 + i\alpha) \frac{\Gamma \xi L_s}{2[1 + \varepsilon S(t)]v_g} n(t) \right\} \times [E_1(t - \tau_f) \exp(i\Psi_{f1}) + E_2(t - \tau_f) \exp(i\Psi_{f2})] ; \quad (3.3)$$

$$\begin{aligned} \frac{dn(t)}{dt} = & \frac{I}{q} - \frac{I_{th}}{q} - \frac{n(t)}{\tau_c} - \left\{ \frac{\xi}{[1 + \epsilon S(t)]} n(t) - 2v_g \frac{\ln(t_r)}{L_s} \right\} \\ & \times \left\{ |E_1(t)|^2 + |E_2(t)|^2 + |E_f(t)|^2 \right\} ; \end{aligned} \quad (3.4)$$

$$\Psi_{fm} = \varphi_{fm} - \frac{2\pi c}{\lambda_m} \tau_f - \varphi_m + \frac{2\pi c}{\lambda_m} \tau_m ; \quad K_f = \frac{|t_f|}{|t_r|} . \quad (3.5)$$

This model is a straightforward extension of the model for a unidirectional ring cavity with incoherent feedback presented by Equations (2.21)-(2.25). All the symbols are as same as those in Section 2. The index m indicates the ring laser. It should be noted that there is no index for K_f since it is assumed that the loss in each ring cavity is the same.

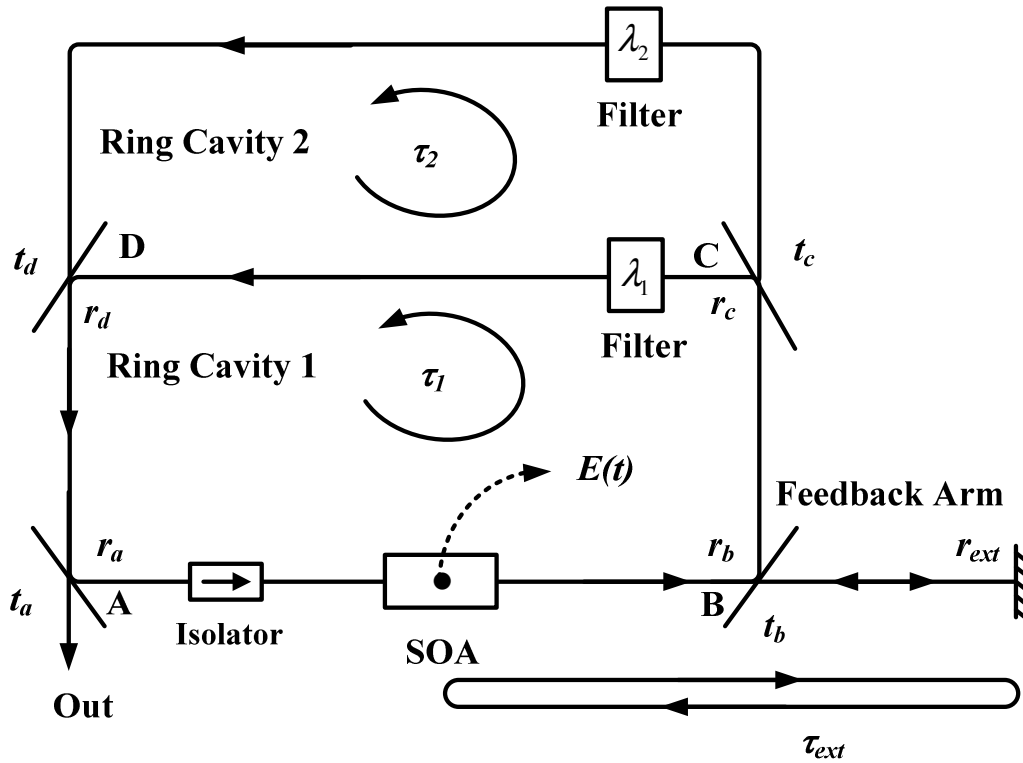


Figure 3.1: Schematic of two ring lasers that share the same SOA and feedback arm.

It has been discussed in chapter 1 that a ring laser with feedback can operate in the limit cycle regime if the feedback strength and the length of the cavities are properly matched. Once the limit-cycle oscillation has built up, the gain medium of the ring cavity is modulated by the corresponding periodically oscillating light. The oscillation periodicity can be controlled by adjusting the parameter k . We will then discuss the situation that two ring lasers are coupled through the same gain medium while sharing the same feedback arm.

Suppose the initial power in one of the cavities, say cavity 1, is larger. If the fields in both cavities evolve in time, the power of cavity 1 grows stronger, and thus forces the gain medium to oscillate in the periodicity of the limit-cycle oscillator of cavity 1. The net gain becomes negative in both cavities when the strong feedback light of cavity 1 passes through the gain medium. If the periodicities of the two limit-cycle oscillators are sufficiently close to each other, they tend to synchronize into the same periodicity. As a consequence, both the two limit-cycle oscillators build up simultaneously. On the other hand, if the periods of the two limit-cycle oscillators are not close enough, the limit-cycle oscillation in cavity 2 cannot build up due to the periodic negative gain produced by the limit-cycle oscillator of cavity 1. Since this reasoning applies as well when cavity 2 would be initially dominant, the system is in fact bistable as demonstrated below.

Figure 3.2 shows a simulation of the time-evolution of the optical power in both cavities. The length of cavity 1 is 10.00 meter, while the length of cavity 2 is 10.80 meter. The length of the feedback arm is 2.70 meter. Figure 3.2a shows the case in which the power (P_1) of cavity 1 is initially set to be larger than the power (P_2) in cavity 2. It is clearly visible that both P_1 and P_2 increase in the first ten roundtrips. P_1 increases faster than P_2 due to the different initial conditions. Hence, P_1 modulates the gain deeper compared to P_2 . The net gain of each cavity (both cavities have the same cavity loss) becomes negative during the time that the gain medium is deeply saturated by the strong feedback of P_1 , (similarly as shown in Figure 3.4c in the previous section). Therefore the limit-cycle oscillator of cavity 2 cannot build up since both oscillators have different oscillation periodicities (see Figure 3.2a). If the power P_2 is initially set to be larger than P_1 , the limit-cycle oscillator of cavity 2 builds up and the limit-cycle oscillator of cavity 1 is eventually suppressed as illustrated in Figure 3.2b.

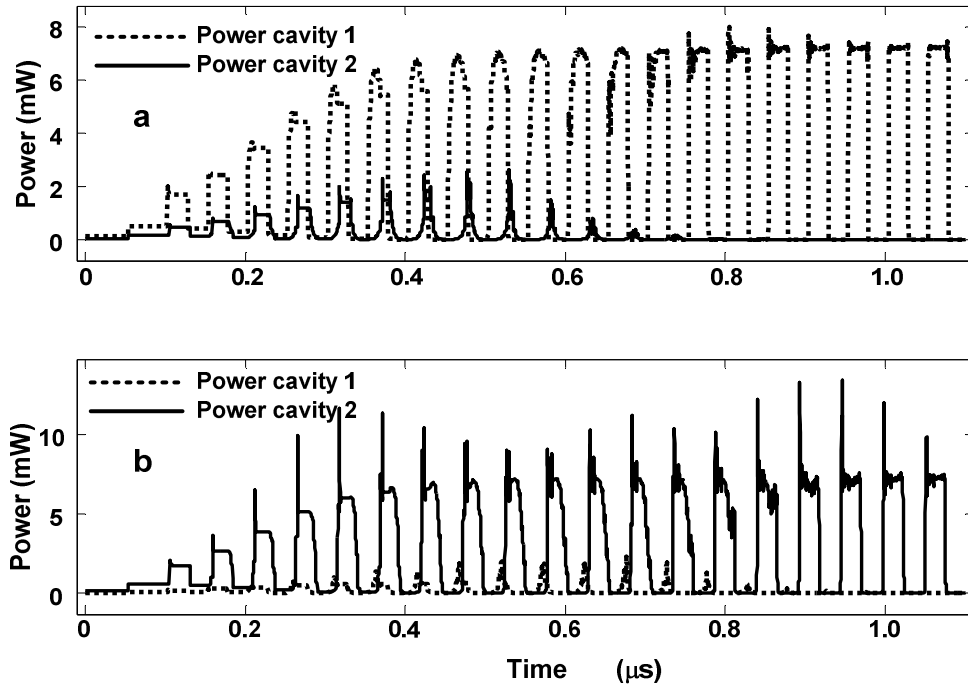


Figure 3.2: Simulation result illustrating bitable behavior of two coupled limit-cycles. The dashed line indicates the power in cavity 1 and the solid line shows the power in cavity 2. In a the initial values are set such that the power in cavity 1 is larger than in cavity 2, while in b the power in cavity 2 is larger than in cavity 1

3.3 Experimental results on synchronization and bistability

This numerical result is verified experimentally by implementing the scheme of Figure 3.1. In our experiment, the filters are AWGs, have a 3dB bandwidth of 0.50 nm. The two cavities have central wavelength of 1549.30 nm and 1558.70 nm, respectively. The laser gain medium is a strained-bulk SOA with an active length of 800 μm that is pumped with 190 mA of current, which corresponds to a small signal roundtrip gain of 25 dB. The two ring lasers have a threshold current of 120 mA. Under these conditions, the system is set in the limit cycle regime ($K_f \approx 2$).

3.3.1 Synchronization

Lasing is established in each individual ring cavity by disconnecting the other. The result is shown in Figure 3.4, where the upper left and center panels show the optical spectra of the individual lasers, and the corresponding time series are shown. It is clearly visible the both individual lasers exhibit limit-cycle behavior. The limit-cycle oscillators have a difference in periodicity of 0.07 ns (2.56%). Next, both ring cavities are connected and the output optical spectrum is shown in Figure 3.4e. The lasers now operate simultaneously with both limit-cycle oscillators synchronized at the same periodicity as demonstrated in the corresponding time series in Figure 3.4f. It demonstrates that synchronization of the coupled limit-cycle oscillators takes place when their periodicities are close to each other.

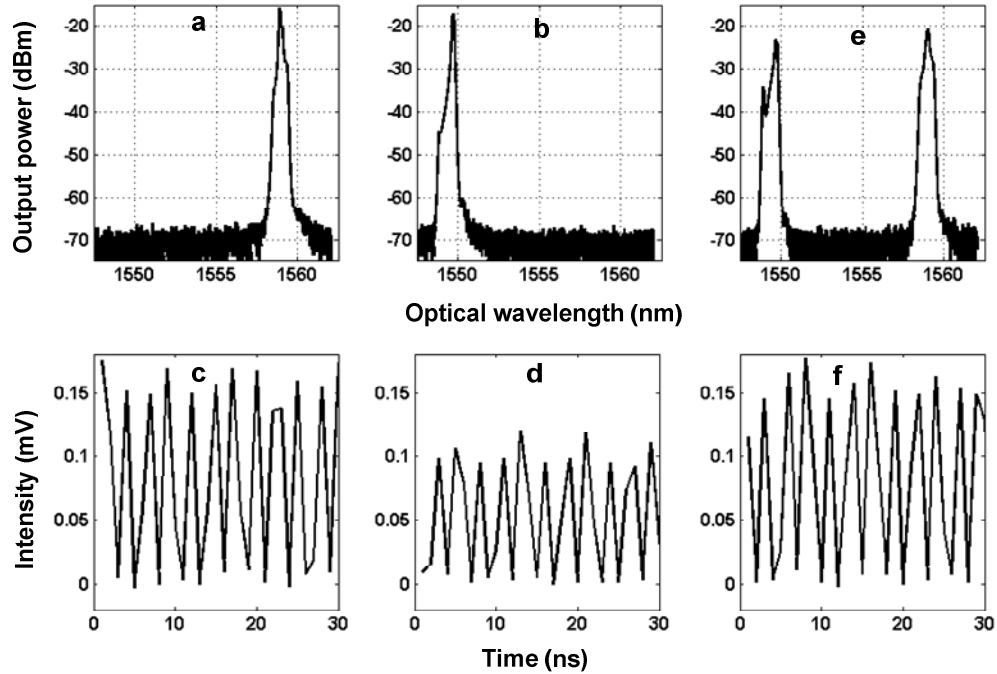


Figure 3.4: Synchronization of two coupled oscillators. Panel a: Output spectrum when only ring cavity of 1558.7 nm was connected; Panel b: Output spectrum when only ring cavity of 1549.3 nm was connected; Panel c, d: Time series corresponding to the limit cycle in Panel a and b, respectively. Panel e: The output spectrum when both ring cavities were connected. Panel f: Time series corresponding to Panel e.

3.3.2 Bistability

Now we turn back to the case in which only one laser is lasing. Suppose this is the laser lasing at the wavelength of 1558.70 nm. If an additional meter of fiber is inserted in its cavity, while keeping the rest of the set-up unchanged, the dynamics of the affected ring laser dramatically changes as shown in Figure 3.5c. The optical spectra of the individual cavities are shown in Figure 3.5a and 5b, similar as the spectra shown in Figure 3.4a and 3.4b. The corresponding time series are shown in Figure 3.5c and 3.d. It is clearly seen that both cavities still show limit-cycle behavior, but the difference in period between the two limit-cycle oscillators has increased to 2.29 ns (85.71%). This is due to the fact that the additional meter of fiber has changed the ratio k between the feedback arm and the ring cavity for the ring laser at the wavelength of 1558.70 nm.

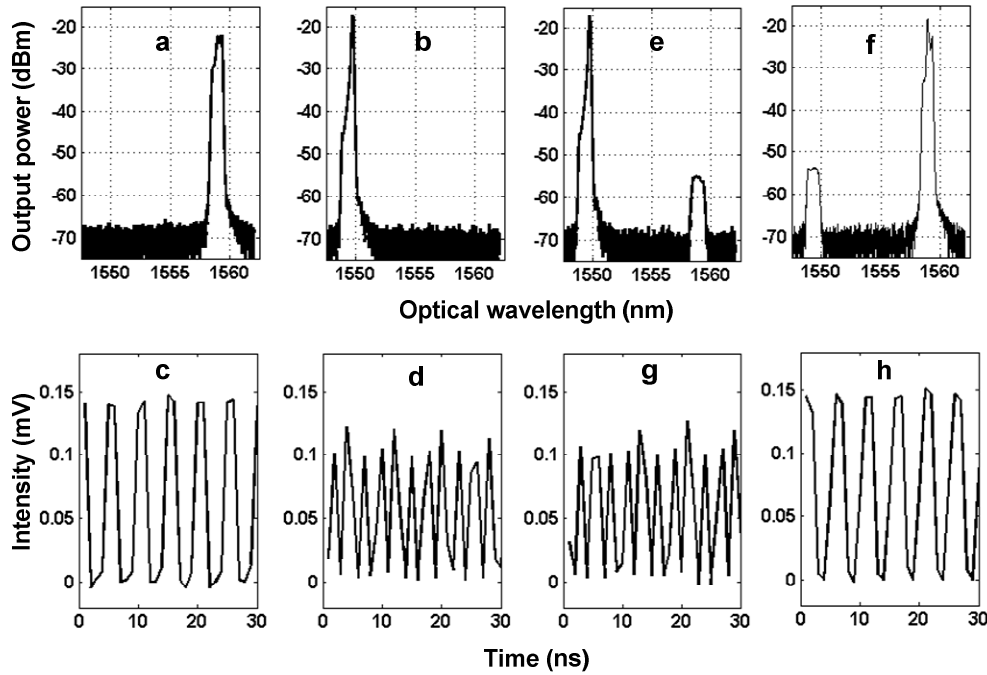


Figure 3.5: Bi-stability of two coupled oscillators. Panel a: Optical spectrum for the case that the ring cavity with a central wavelength of 1558.7 nm was connected (after adding an additional meter fiber into the cavity); Panel b: Output spectrum when only the ring cavity with a central wavelength of 1549.3 nm was connected; Panel c, d: Time series corresponding to Panel a and b, respectively; Panel e: Optical spectrum when both ring cavities were connected, with the ring cavity of 1549.3 nm connected first; Panel f: Same as in e, but now the ring cavity of 1558.7 nm connected first; Panel g, h: Time series corresponding to Panel e and f, respectively.

When both cavities are reconnected and the system is observed to become bistable (Figure 3.5e, f, g, h). In the first state the ring laser at the wavelength of 1549.30 nm is

lasing, while the power in the other cavity is suppressed with 35 dB as shown in Figure 3.5e. The corresponding limit-cycle oscillation is shown in Figure 3.5g. In the second state the ring laser at the wavelength of 1558.70 nm is lasing while the first laser is suppressed as shown in Figure 3.5f. Its corresponding limit-cycle oscillator is shown in Figure 3.5h. It demonstrated that bistability of the coupled limit-cycle oscillators take place when their periodicities are not close to each other.

3.4 Dynamic investigation on synchronization and bistability

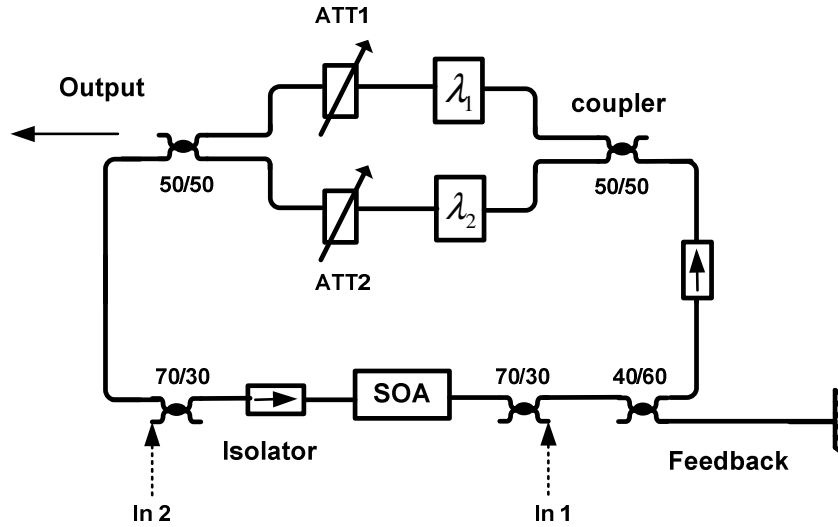


Figure 3.6: Experimental setup of two unidirectional ring lasers with incoherent feedback. The two Filters are implemented by Fabry-Perot filters. ATT: Attenuator.

Synchronization and bistability of the coupled oscillators have been observed in previous sections. It is interesting to investigate how the synchronization of the coupled oscillators builds up, namely the evolution process of the synchronization. The bistability of the coupled oscillator is also very interesting, especially it could have some application in signal processing as one basic logic element. It is important to know the characters of the bistability, like its wavelength dependence, polarization dependence, contrast ratio, switching method, and switching speed. In this section, synchronization and bistability of the coupled oscillators system are investigated in these aspects. The experimental setup is shown in Figure 3.6.

The two ring cavities are realized by using two 50/50 couplers. Each cavity contains a Fabry-Perot Filter (FPF) that acts as a wavelength selective element. The FPFs have 3dB bandwidth of 0.20 nm and free range of 80.0 nm. The central wavelength λ_1 of the FPF in the ring cavity 1 is 1552.52 nm while the central wavelength λ_2 in the ring cavity 2 is 1555.75 nm. The attenuator in each cavity is used to control the cavity loss to balance or unbalance the system. A 40/60 coupler is used to couple light into and from the feedback arm (with 60% port). Two 70/30 couplers are placed in the common laser cavity to couple external light for controlling the system (with 30% port). The SOA injection current is 300 mA and the threshold current is 172 mA. Under these conditions, the system is set in the limit cycle regime. The system is made out of commercially available fiber pigtailed components, which makes that the total cavity length is in the order of 10 meters, similarly as the experiments in previous section.

3.4.1 Evolution process of synchronization

The synchronization process of the two coupled oscillators is estimated at the order of microseconds. Therefore a dynamical method is developed to record such a process. The basic idea is to switch off the oscillating operation periodically using external optical pulse injection (optical clock) and the oscillators build up naturally after the optical pulse is removed. The whole evolution process can thus be recorded if the time interval between two optical pulses is long enough. The experiment based on this idea is done as follows.

The system of coupled oscillators is firstly set in the regime of synchronization. An asymmetrical case is discussed firstly. The loss in cavity 2 (1555.75nm) is set to be larger, namely oscillator 2 is weaker. The output spectrum is shown in Figure 3.7a. Two lasers are lasing simultaneously, which indicates that the corresponding oscillators are synchronized together as shown in Figure 3.4e and 3.4f. The time trace of the optical clock pluses is shown in Figure 3.7b. The optical clock pluses, at the wavelength of 1545.00nm and 3 mW peak power, are generated by external optical modulators and have a period of 100.00 μ s with the duty cycle of 25%. The optical clock pluses are injected into the system via port 1 as shown in Figure 3.6 and deeply saturate the SOA, thus both oscillators are quenched. After the optical clock pulses are removed, both oscillators start building up and coexist as shown in Figure 3.7c and 3.7d. From previous section, it is shown that both oscillators only coexist in case of

synchronization. The oscilloscope used for recording the time series of both oscillators have a resolution of 250 ps, which enable us to see the evolution process of the synchronization by zooming in the time series of both oscillators.

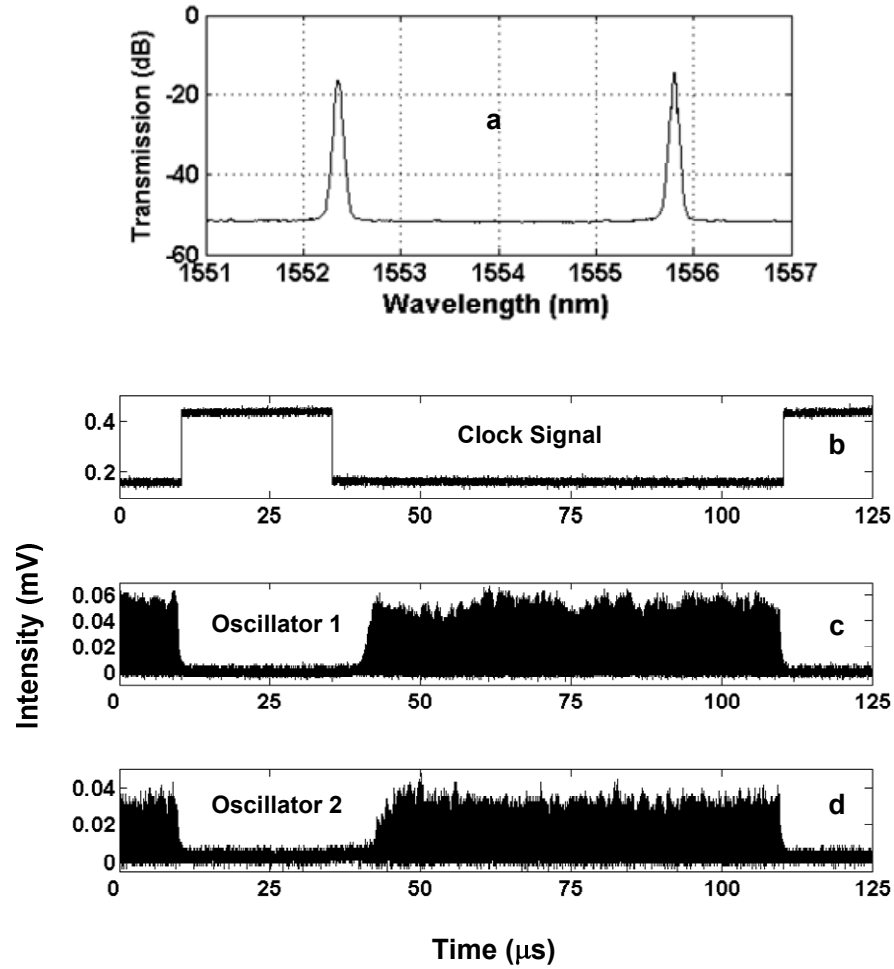
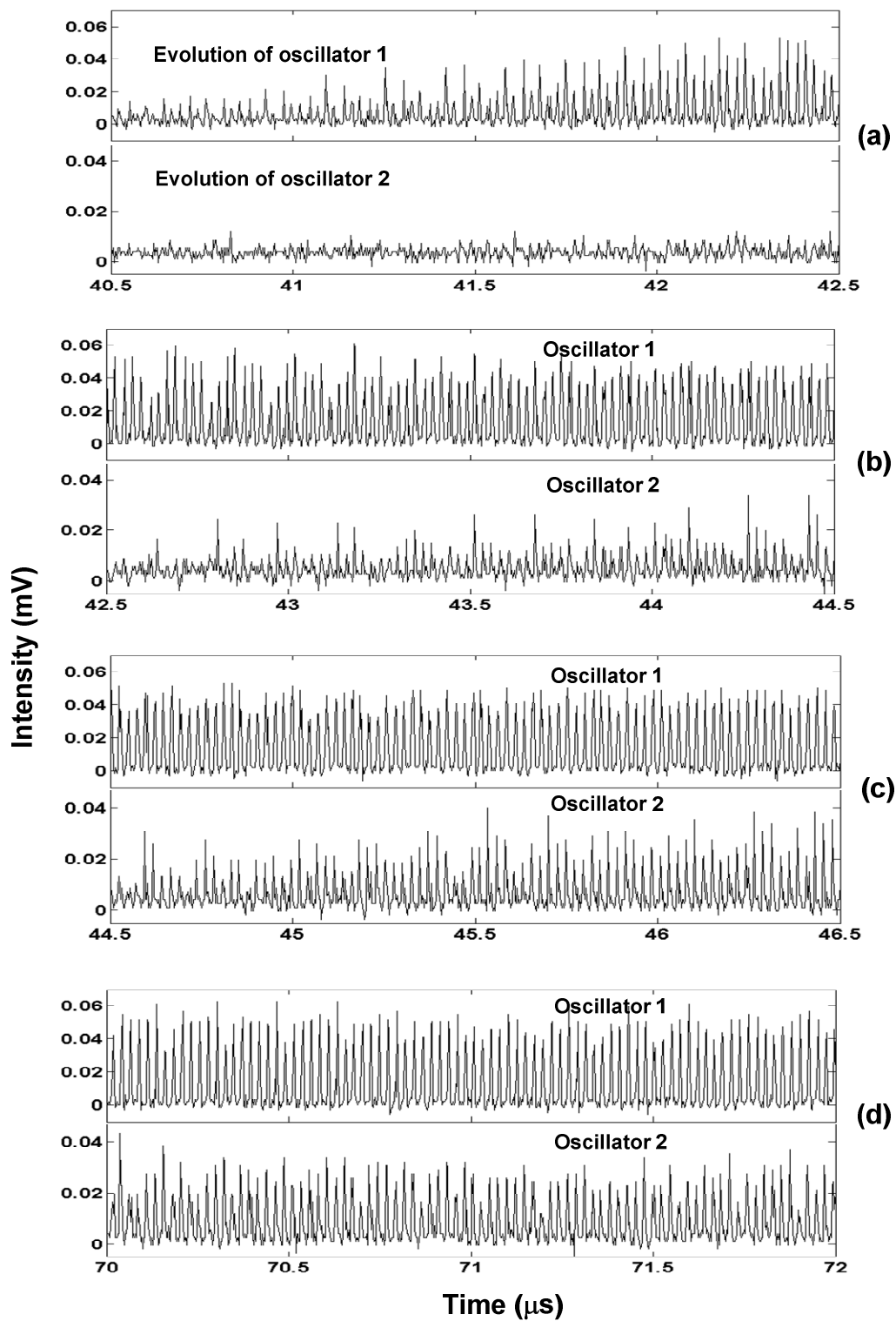


Figure 3.7: Panel a: the output spectrum of the coupled oscillators system showing that both oscillators synchronize together; Panel b: the clock signal that is injected into the system through port 2 to switching off both oscillators; Panel c and d: the time series of oscillator 1 and oscillator 2, respectively, showing that both oscillators synchronize together in absence of clock pulses.



The caption of this figure is in the next page

Figure 3.8: The evolution process of the synchronization of the two coupled oscillators. Panel a: the first $2 \mu\text{s}$ evolution processes of the two oscillators after the clock pulse is removed (upper time series for oscillator 1, while lower time series for oscillator 2); Panel b: the next $2 \mu\text{s}$ evolution processes follow Panel a; Panel c: the next $2 \mu\text{s}$ evolution processes follow Panel b; Panel d: $2 \mu\text{s}$ evolution processes when two oscillators have synchronized together.

Both oscillators start building up from about $40 \mu\text{s}$ when an optical clock is removed, as shown in Figure 3.7. The evolution process of both oscillators starting from $40.50 \mu\text{s}$ is shown in Figure 3.8. The first $2 \mu\text{s}$ evolution processes of the two oscillators is shown in Figure 3.8a (the upper time series for oscillator 1 and the lower time series for oscillator 2). Oscillator 1 firstly builds up due to it has a smaller cavity loss, while oscillator 2 builds up slowly after $1 \mu\text{s}$. In the next $2 \mu\text{s}$, oscillator 1 evolves into a stable oscillation state, while oscillator 2 continues to build up irregularly, but tending to follow the periodicity of oscillator 1, as shown in Figure 3.8b.

In the continuing $2 \mu\text{s}$, oscillator 1 is oscillating stably, while oscillator 2 builds up stronger, following the periodicity of oscillator 1, as shown in Figure 3.8c. As time goes on, the two oscillators synchronize² in terms of oscillation periodicity. The whole synchronization evolution process takes about $8 \mu\text{s}$. The synchronized time series of the two oscillators is shown in Figure 3.8d. The irregularity of the time series is due to the external light injection. Because the ground level of the external optical clock pluses is not zero due to the imperfect modulation, there is still a mount of light injected into the system when the optical pulse is absent, as shown in Figure 3.7b.

In the asymmetrical case, the stronger oscillator (oscillator 1) builds up in $3 \mu\text{s}$, while the weaker oscillator (oscillator 2) builds up slower and has the tendency to follow the periodicity of the stronger 1. When the weaker one evolves into a stable state, the synchronizing process finishes. This is different as the symmetrical case.

The symmetrical state is obtained by reducing the attenuation in cavity 2, namely, both oscillators have similar strength. Using the same method based on optical clock pulse injection, the time series of both oscillators are recorded. Both oscillators build up almost simultaneously. In the beginning of the building up process, both oscillators

² The synchronization in the thesis refers to the case that two oscillators with different individual oscillation periodicities oscillate in a common oscillation periodicity.

show chaotic-type of oscillation. The average intensity of each oscillator keeps constant after 4 μs . But it takes about 20 μs for the two oscillators to synchronize (the time series is too long to be shown here).

In the asymmetrical case, the weak oscillator tends to synchronize with the strong one in the building up process, and it takes about 8 μs for them to synchronize together. In the symmetrical case, the two oscillators have similar strength and can hardly become dominate. They have to compromise with each other to get harmony. Therefore, both oscillators are observed to have some chaotic-type of oscillation in the beginning, and it takes longer time (20 μs) for them to synchronize together.

3.4.2 Wavelength dependence of the bistability

The principle of the bistable behavior has been shown in previous sections. One of oscillators modulates the net gain into periodic negative, which prevents the other oscillator with different oscillation periodicity building up. What matters is the difference between the oscillation periodicities of the coupled oscillators. According to this principle, the bistable behavior should be independent of lasing wavelength as long as the oscillation can exist. The wavelength dependence of the system should be only related with wavelength dependent components, like filter and active element.

The wavelength dependence of the system is investigated by adjusting the central wavelengths in both cavities. It turns out that bistability can be obtained over a spectra range, in which the SOA can provide enough gain to compensate the cavity loss. The wavelength dependence for bistability is evaluated by wavelength difference between the two cavities. The lower limitation of the wavelength difference is 0.1 nm, limited by the bandwidth of the Fabry-Perot filter, as shown in Figure 9a and 9b; whereas the upper limitation of the wavelength difference is 62.87 nm, limited by the optical gain bandwidth of the SOA, as shown in Figure 3.9c and 3.9d. It is shown in Figure 3.9 that the power contrast ratio between the dominant oscillator and suppressed oscillator is more than 30 dB in any case. Moreover, the system is polarization independent, thus no polarization controlling components are needed in the experimental setup as shown in Figure 3.6.

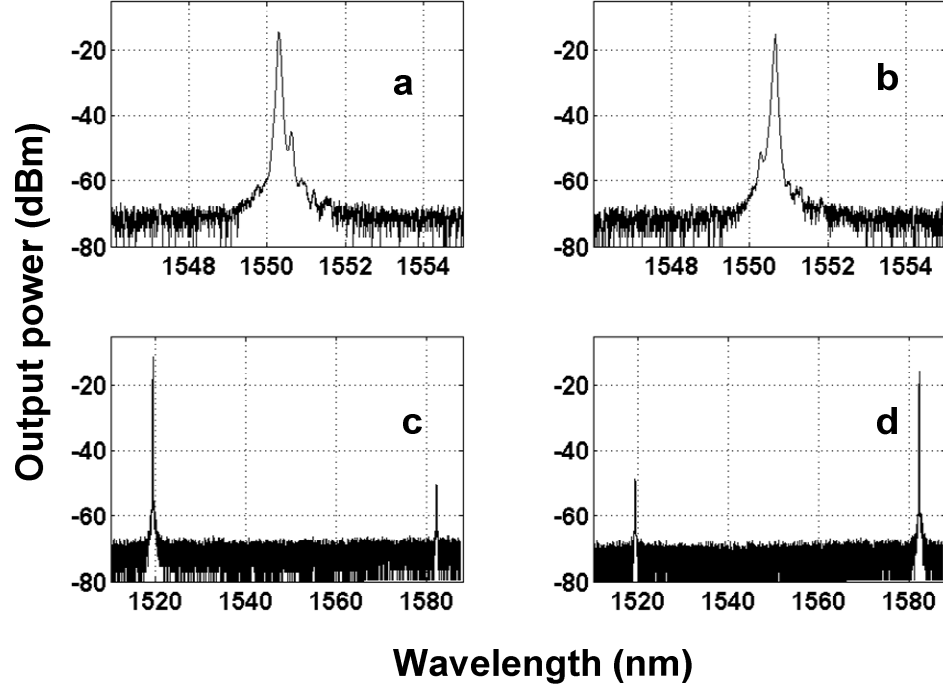


Figure 3.9: Output spectra showing the wavelength dependence of the system. Panel a and Panel b show both states in the case that $\lambda_1 = 1550.32$ nm and $\lambda_2 = 1550.42$ nm. The contrast between both states is about 40 dB. Panel c and panel d show the case that $\lambda_1 = 1519.34$ nm and $\lambda_2 = 1582.21$ nm indicating that the bistability takes place over a large wavelength range.

3.4.3 Switching methods

To induce switching between the bistable states, external light at the same wavelength of the suppressed cavity is injected into the system in two ways. One is to inject external light, co-propagating with the lasing light with a central wavelength of the suppressed cavity, through port ‘In 2’ as shown in Figure 3.6. In this experiment, the central wavelengths of the two cavities are $\lambda_1 = 1550.92$ nm and $\lambda_2 = 1552.52$ nm. The oscillator at λ_1 is initially dominant.

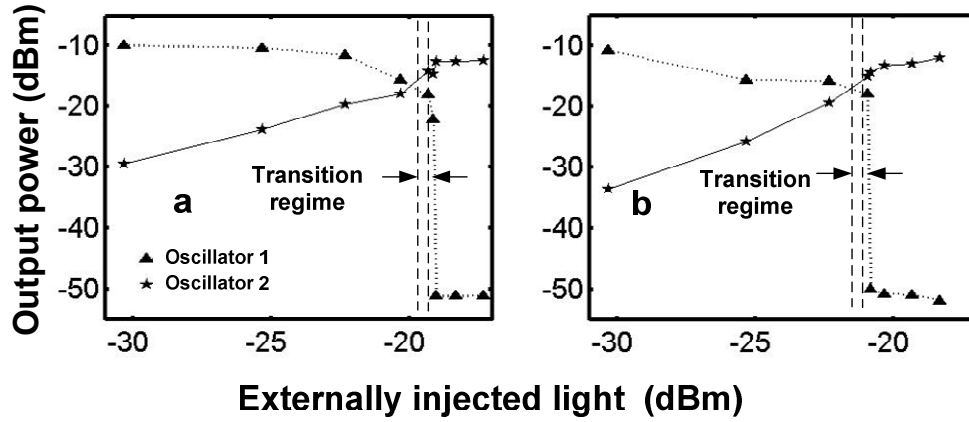


Figure 3.10: The output power of each oscillator versus the power of the externally injected light that co-propagates with the lasing light. Panel a: The switching curve if the attenuator values were 0.50 dB (for attenuator 1) and 0.82 dB (for attenuator 2). Panel b: similar result is shown, but now for the attenuation values of 1.00 dB (attenuator 1) and 1.32 dB (attenuator 2).

The injected light is at λ_2 and can hence propagate through the suppressed ring cavity. It is amplified by the SOA and starts building up an oscillation in the suppressed cavity. The output power of the two cavities is shown in Figure 3.10a. The output power of the suppressed cavity increase proportional to the power of the external light. As a result of this, the injected light disturbs the modulation of the gain caused by the limit-cycle oscillation in the dominant cavity. The output power of the dominant cavity decreases when power of the external light exceeds -22.20 dBm (corrected for 70% of the splitter loss of the coupler).

The system reaches the transition regime where the initially dominant oscillator is no longer stable, when the power of the injected light is increased above -20.50 dBm. The initially suppressed oscillator becomes dominant when the power of the external light increases beyond the transition regime (-20.50 ~ -19.05 dBm). The gain is forced to follow the period of the newly dominant oscillator, while the other oscillator is suppressed. After the system has switched its status, it maintains its state even if the injected light is removed. In this sense, such a configuration can serve as an optical memory, a basic logic unit for optical signal processing. It should be remarked that both oscillators are not stable in the transition regime. This implies that switching is

only guaranteed if the injected power exceeds the transition regime. Hysteretic effect is not observed in the switching.

Figure 3.10b shows a similar result but now in the case of a slightly increased attenuation in both cavities. It follows that in this case the switching power is reduced with 1 dB. This effect is explained by the fact that a higher attenuation in the cavity leads to a reduced number of photons contribute to the oscillations. Hence, switching can be realized by injecting less power in the system.

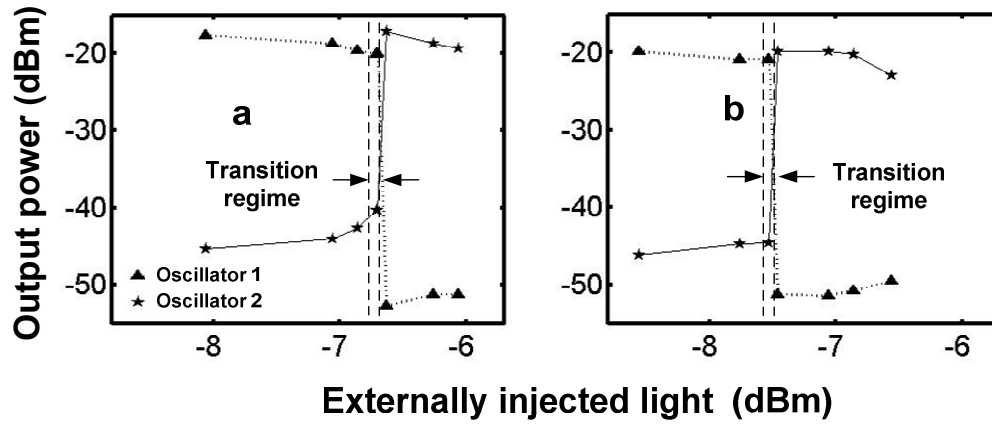


Figure 3.11: The output power of each oscillator versus the power of the externally injected light that is counter-propagates with the lasing light. Panel a: The switching curve if the attenuator values were 0.50 dB (for attenuator 1) and 0.82 dB (for attenuator 2). Panel b: similar result is shown, but now for the attenuation values of 1.00 dB (attenuator 1) and 1.32 dB (attenuator 2).

The other way for switching is to inject external light that counter-propagates with the lasing light with a central wavelength of the suppressed cavity, say λ_2 , through port 'In 1' as shown in Figure 3.6. The external light saturates the SOA, thus decreases the intensity of the dominant oscillator. A small amount of the amplified external light is reflected back into the laser cavity by the SOA facet, which has a typical reflectivity of -40dB. The output power of the two cavities is shown in Figure 3.11a. The output power of the dominate cavity decreases with the power of the external light, while the power of the suppressed cavity is increasing slightly due to the refection of the SOA facet. The reflected amplified external light oscillates in the suppressed cavity. The system reaches the unstable transition regime of the power of the external light

exceeds -6.78 dBm. The initially suppressed oscillator becomes dominant when the power of the external light increases beyond the transition regime (-6.78 dBm \sim -6.63 dBm). After the switching, the system remains lasing at the wavelength λ_2 in spite of the removal of the external light. Figure 3.11b shows the case for which the attenuation in the cavity is enlarged. Similarly as in the case presented in Figure 3.10b, it is visible that the injected switching power reduced. Power is an essential concern in applications. The switching method with co-propagating injection (Via port 'In2') obviously requires much less power to switch. Therefore this method is often chosen to control the system in the rest of this thesis.

The switching speed of the system is investigated experimentally and numerically. Numerical results indicate that it takes approximately thirty round-trip times to switch the state. This was confirmed by experiments. Decreasing the cavity length is essential to realize higher switching speed. Integrating the system in a single chip could greatly increase the switching speed. The size of the integrated version might be limited by the size of three components: the filter, the active element and the isolator. The dimensions AWGs and SOAs are typical at the order of several hundreds of micrometers, while the dimensions of the integrated isolators are at the order of millimeters, with losses proportional to its length [99]. Therefore the dimensions of an integrated version of this system is at the order of centimeters, which leads to a switching speed up to a few hundreds MHz.

3.5 Conclusion

In this chapter, it have been shown that when two (or more) of such ring lasers, operating in the limit-cycle regime, are coupled together while sharing the same active gain element and the same external feedback arm, they either synchronize (if their periodicities are sufficiently close to each other) or show bistability between the limit-cycle oscillators. The reason for the bistability is that the strong feedback light causes modulated depletion of the gain medium and forces the net gain to become periodically negative, which prohibits the fulfillment of the roundtrip condition for the other oscillator.

The characters of the dynamics of the coupled oscillators are investigated experimentally. Synchronization is investigated on the evolution process of the synchronization, which is recorded. Two cases are compared. In one case a weak oscillator is coupled with a strong oscillator (asymmetry), where in another case two

similarly strong oscillators are coupled together (symmetry). Experiments show that it takes shorter time to synchronize for the asymmetrical case. Furthermore, the coupling through the same gain medium is a new category of coupled limit-cycle oscillators. It is worthwhile to further investigate this new category in other fields. For example, what happens if chemical oscillators share the same gain reaction liquid, or if groups of oscillating population abundances of interacting species share the limited available food?

The characters of the bistable behavior of the system are investigated in many aspects. The system is polarization independent. In terms of wavelength dependence, the bistability is only limited by the composed components, like the bandwidth of the gain medium, the bandwidth of the filter. Switching between different states has been realized by injecting external light at the wavelength of the cavity intended to switch on. Switching speed is proportional to the cavity length and is thus limited by the size of the system. Furthermore, it should be in principle allowed to extend this concept to realize multi-stable operation, which will be discussed in next chapter.

Chapter 4

Multi-stable operation of coupled oscillators

The dynamics of a two coupled oscillators based on ring laser with incoherent feedback has been discussed in Chapter 3. It is shown that, depending on their periodicities, they either synchronize their limit-cycle oscillators (if the periodicities are sufficiently close to each other) or show bistability between the limit-cycle oscillators. Periodically negative net gain of the ring cavity, caused by the strong feedback of the firstly built-up oscillator, plays an essential role for the bistable behavior. This principle makes it possible for the bistable system to be extended into multi-state operation by adding more oscillators coupled through the same gain medium.

In this chapter¹, the multi-fold stability of coupled oscillators is investigated. An eight-fold stability of coupled oscillators is demonstrated. Moreover, a sixteen-fold stability is achieved by cascading two sets of four-coupled oscillators. Switching between different states can be done by injecting external light, in this sense, the multi-stable systems act as multi-state optical memories.

This chapter is organized as follows: In Section 1, a system with four-coupled oscillators is discussed, the spectrum and time series of four-fold stability of the coupled oscillators are shown; an eight-stable optical memory is demonstrated. In Section 2, a sixteen-state optical memory is achieved by cascading two four-state optical memories. A discussion about the multi-state optical memory is shown in Section 3.

¹ This chapter is based on the following paper:

S. Zhang, D. Lenstra, Y. Liu, H. Ju, Z. Li, G.D. Khoe and H.J.S. Dorren, Multi-state optical flip-flop memory based on ring lasers coupled through the same gain medium, *Optics Communications*, accepted.

4.1 Multi-fold stability of coupled oscillators

4.1.1 Demonstration of four-fold stability of coupled oscillators

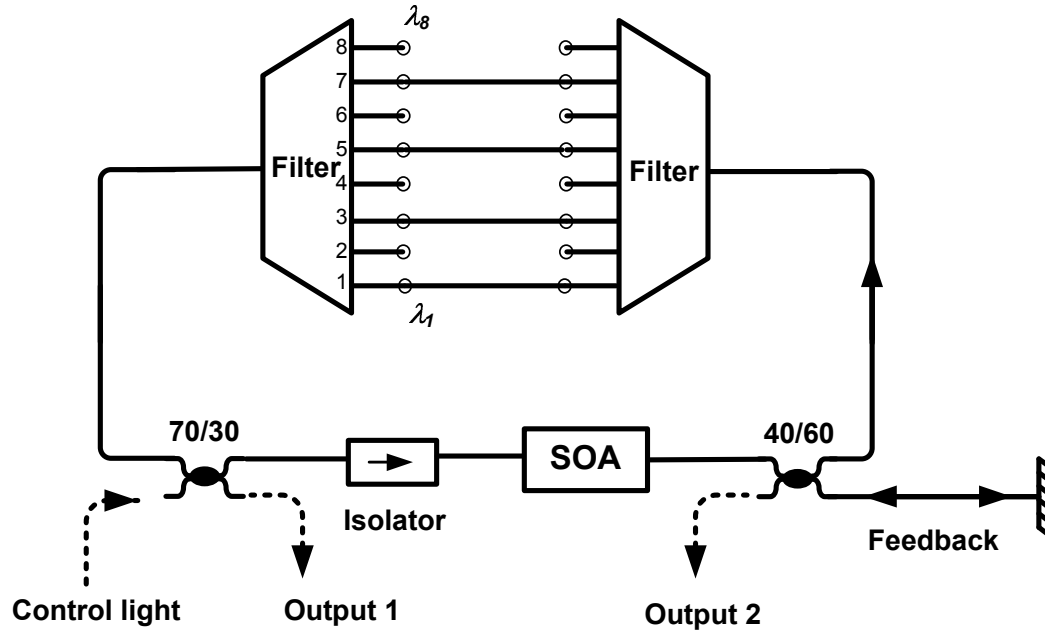


Figure 4.1: Experimental setup of four coupled oscillators based on unidirectional ring lasers with incoherent feedback. The two Filters are implemented by Array Waveguide Gratings

Figure 4.1 shows the experimental setup of four coupled oscillators, each of which is basically a unidirectional ring lasers with incoherent feedback. The filters are AWGs, which act as eight-port filters that are implemented to form the four ring cavities. The AWGs have a 3dB bandwidth of 0.50 nm at each port. The center wavelengths are in a range between 1549.30 nm and 1560.20 nm with a regular interval of 1.40 nm. The four ports used in this experiment are the 1st port (1549.30 nm), the 3rd port (1552.52 nm), the 5th port (1555.75 nm) and the 7th port (1558.91 nm), respectively. They are interconnected with short pieces of optical fiber. Note that these pieces of optical fiber have different length into order to implement different k parameter for each ring laser with feedback, according to the principle of the bistability presented in Chapter 3. A 40/60 coupler is used to couple light into and from the feedback arm (with 60% port),

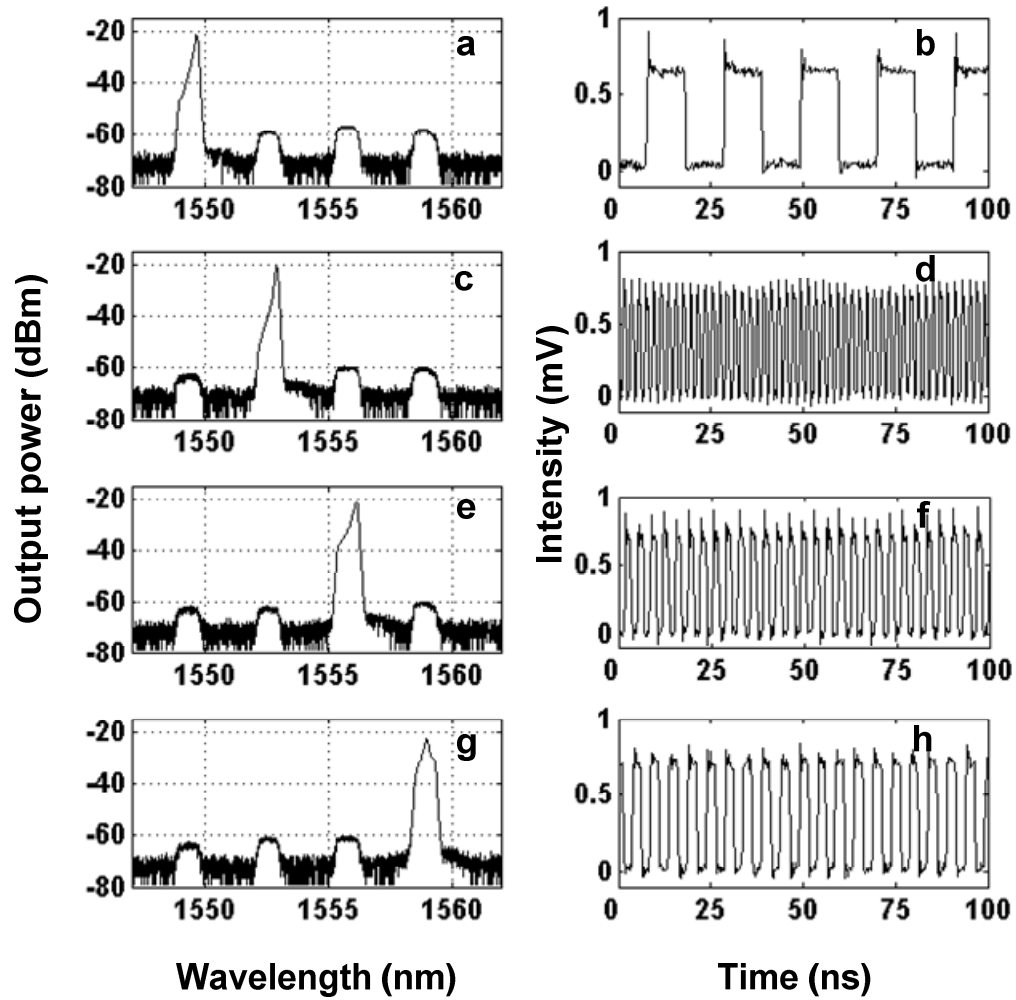


Figure 4.2: The spectrum and time series showing four-fold stability of the four-coupled oscillators. Panel a: Output spectrum showing the oscillator of cavity 1 (1549.30 nm) is dominate, the corresponding time series is shown in Panel b; Panel c and d show the case for the oscillator of cavity 3 (1552.52 nm) is dominate; Panel e and f show the case for the oscillator of cavity 5 (1555.75 nm) is dominate; Panel g and h show the case for the oscillator of cavity 7 (1558.91 nm) is dominate. The switching between these states is realized by injection of external light at the wavelength of the chosen ring cavity.

and the idle port of the coupled is used as one of the outputs. A 70/30 couplers are placed in the common laser cavity to couple external light for controlling the system (with 30% port), and the idle port of the coupled is used as output port as well. The laser gain medium is a strained-bulk SOA with an active length of 800 μm that is pumped with 250 mA of current, which corresponds to a small signal roundtrip gain of 28 dB. The ring lasers have a threshold current of 160 mA. Under these conditions, the system is set in the limit cycle regime ($K_f \approx 2$).

When the four cavities in Figure 4.1 are connected, we realize a system of four ring lasers sharing the same gain medium and the same feedback arm. If all individual ring lasers are prepared to operate in limit-cycle dynamics, the coupled limit-cycle oscillators turn out to behave in a similar fashion as the case of two coupled limit-cycle oscillators. If one limit-cycle oscillator firstly builds up first, all other oscillators either synchronize into the same periodicity or become suppressed. If no combination of two limit-cycle oscillators exists that can synchronize together, the system shows four-fold stability. Figure 4.2 presents the spectrum and time series out of the port ‘Output 1’, showing four-fold stability of the four-coupled oscillators. The contrast ratio between the dominant and the suppressed states is more than 35 dB. The time series of each stable state shown in Figure 4.2 confirm again the principle of the bi (multi-fold) stability again that each oscillator should have different periodicities. Switching between different states is realized by injecting external light at the same central wavelength of the cavity that is chosen to be dominant. The system keeps the new stable state even if the external injection light is removed.

4.1.2 Experimental realization of an eight-state optical memory

When all the eight cavities in Figure 4.1 are connected with different length of pieces of optical fiber, we realize a system of eight ring lasers sharing the same gain medium and the same feedback arm. Similarly, if no combination of two limit-cycle oscillators exists that can synchronize together, The system turns out to be eight-stable in the sense that at one time only one of the oscillators is operating, where the other seven are quenched, as shown in Figure 4.3, where only the output spectrum of each stable state is presented in order to save place. Note that the output spectra are taken from the port ‘Output 2’, whose power is stronger than the port ‘Output 1’, since less loss the feedback light experiences. Similarly as in the four-stable case, injection of the external light at the same wavelength of the chosen suppressed ring cavity is used to switch the state of the system. In this sense, an eight-state optical memory is realized.

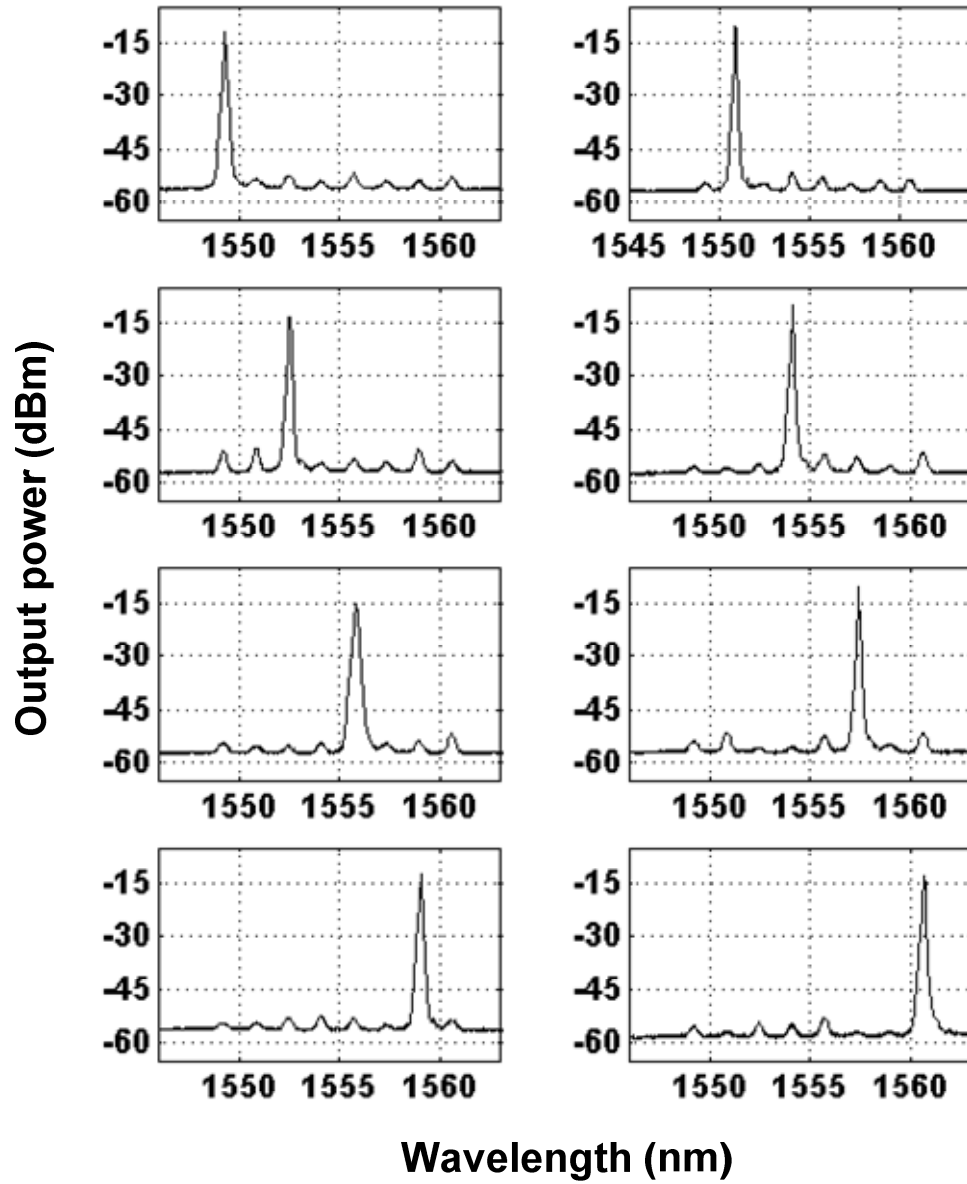


Figure 4.3: Output optical spectra for each of the eight states for the eight-stable system with eight ring cavities.

4.2 Sixteen-state optical memory based on two connected four-state optical memories

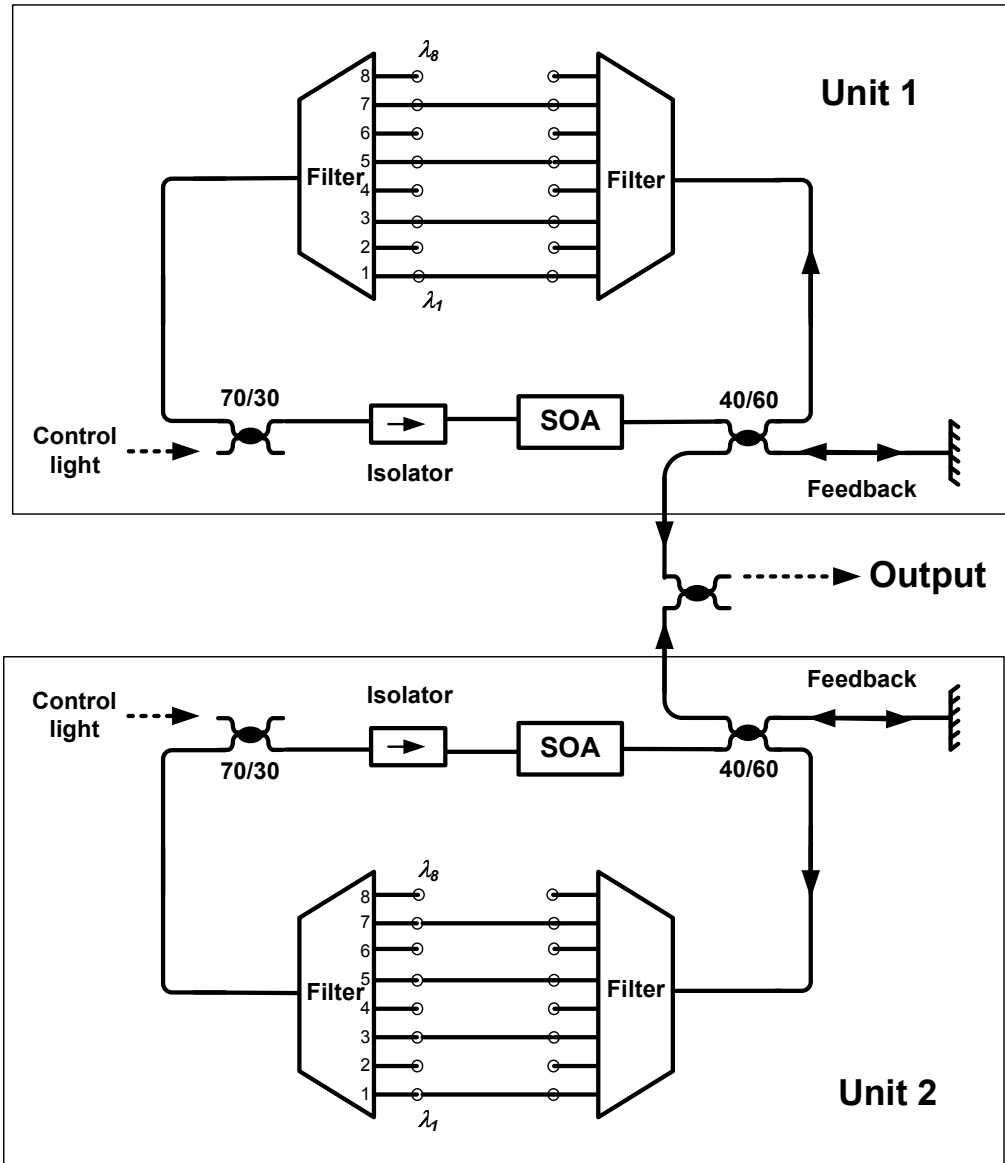


Figure 4.4: Experimental setup of two coupled units, each of them contains four-state optical memories based on unidirectional ring lasers with incoherent feedback.

Another approach to realize more stable state operation is to combine several systems with lower number states together. As an example, a sixteen-state system is realized by connecting two four-state optical memories.

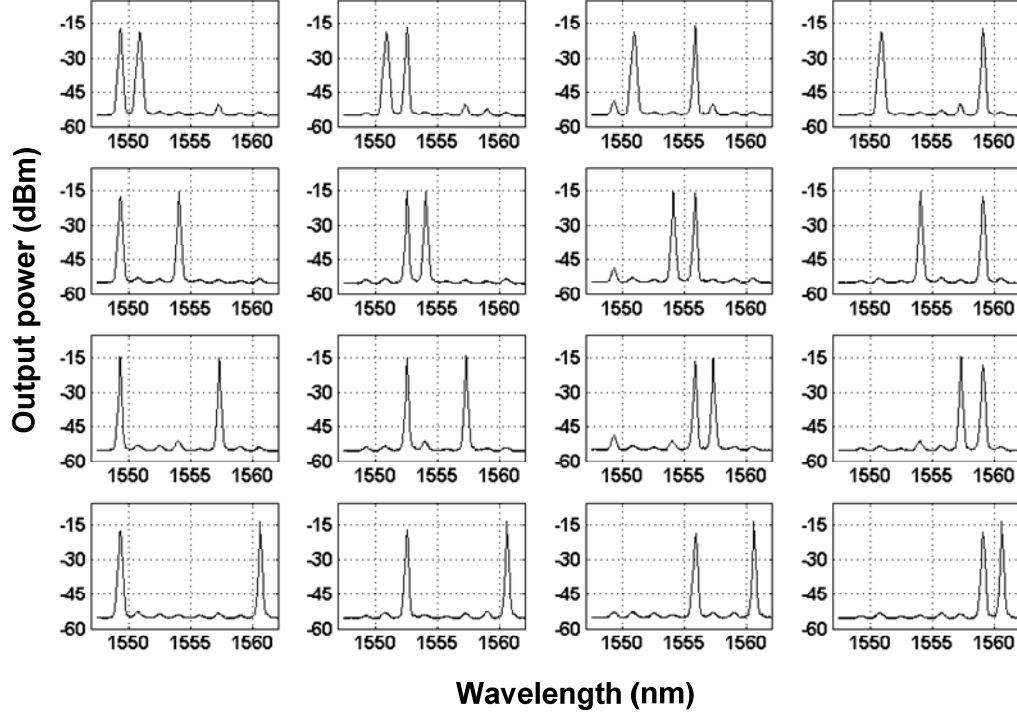


Figure 4.5: Output optical spectra showing sixteen-state memory out of two connected four-state memory

The experimental setup is shown in Figure 4.4, where two units of four-state optical memory are connected. Unit 1 is as same as the four-stable system shown in Figure 4.1, where it contains four lasers at center wavelength of 1549.30 nm, 1552.52 nm, 1555.75 nm and 1558.91 nm, respectively. Unit 2 is basically as same as Unit 1, except that it contains four lasers at different center wavelengths that are 1550.87 nm, 1552.52 nm, 1555.75 nm and 1558.91 nm, respectively. For each unit, only one laser is active, while the others are suppressed. Similarly as previous experiments, injection of the external light at the same wavelength of the chosen suppressed ring cavity is used to switch the state of the each unit. The output of each unit is combined by a 50/50 coupler.

Sixteen different combinations come out of the two sets of four-state system. The corresponding spectra of the system are shown in Figure 4.5. Sixteen bits of information are thus stored. Switching between these states is achieved by injecting external light to both sets. Straightforwardly, 64 bits of information are stored if 3 sets of such four-state optical memory are connected.

4.3 Discussion

In this chapter, the extension of the bistable behavior of the coupled oscillators is investigated. An eight-stable system based on eight coupled oscillators is experimentally demonstrated. A fundamental question is how many stable states can such a system realize? The answer to this question is firstly related to the number of ring lasers that can be coupled together. An AWG, which has 512 channels in the bandwidth of SOAs, has been presented in Ref. [100]. Therefore, it is feasible to couple hundreds of ring cavities. The second factor is the number of oscillation periodicities that the system can enable. It follows from the numerical and experimental results in Chapter 2 that the periodicity of the oscillation is very sensitive on the ratio between the roundtrip times of feedback arm and ring cavity. Yet the irregular sensitivity on the parameter k makes it very difficult to know the number of the oscillation periodicities the system can enable. Furthermore, it is not clear how many of the oscillators avoid synchronization. The irregular sensitivity dependence on the parameter k and the quantitative characterization of the synchronization regimes should be further investigated.

Another approach for extension is to connect several of such system with different operating wavelength. A sixteen-state optical memory made out of two connected four-state optical memories is demonstrated. This approach of extension has a number of advantages. Firstly, it leads to an optical memory with m^n states, where m is the number of the states for each unit, n is the number of units that are connected. This expansion is growing exponentially, which means large number bits of information could be stored by less components. Secondly, it decreases the requirement for the building blocks. For example, if a sixteen-state memory is made of sixteen coupled ring lasers, careful design and adjustment are required to avoid synchronization. Thirdly, it provides a solution to the problem that a single optical memory is hard to be integrated in scale smaller than 1 centimeter as discussed in Chapter 3. Because several connected units can indicate a large amount of information in high density.

For these types of multi-state optical memories, the information is encoded in different wavelengths. It needs further investigation on converting the wavelength encoded data into other formats, like intensity encoded data.

Chapter 5

Multi-stable operation of serially interconnected lasers

A multi-state optical memory based on coupled ring lasers with incoherent feedback has been presented in previous Chapters. However, the output of this optical memory is oscillating in intensity, which can not be applied in the some applications, For instance in optical packet switching network, where a CW output is required.

In this Chapter¹, we present a multi-state optical memory based on gain quenching. The output of this optical memory is CW. The system consists of a large number of serially interconnected lasers. Each laser has a different lasing wavelength. Only one of the lasers can lase at a time. A five-state optical memory is experimental demonstrated. This Chapter is organized as follows. Optical bistability based on gain quenching is shorted introduced in Section 5.1. The system concept of the multi-state optical memory is given in Section 5.2. The experimental results and switching methods are presented in Section 5.3. A short discussion is given in Section 5.4

5.1 Optical flop-flop memories based on gain quenching

The concept of gain quenching has been briefly introduced in Section 1.1.2 in Chapter 1. It refers to the phenomenon that the lasing operation of a laser is ceased because its gain medium is deeply saturated by externally injected light. The experimental observation is shown in Figure 5.1.

¹ This Chapter is based on the paper:

S. Zhang, D. Owens, Y. Liu, M.T. Hill, D. Lenstra, A. Tzanakaki, G.D. Khoe, H.J.S. Dorren, Multi-state optical memory based on serially interconnected lasers. *IEEE Photonics Technology Letters*, 17, pp. 1962-1964 (2005).

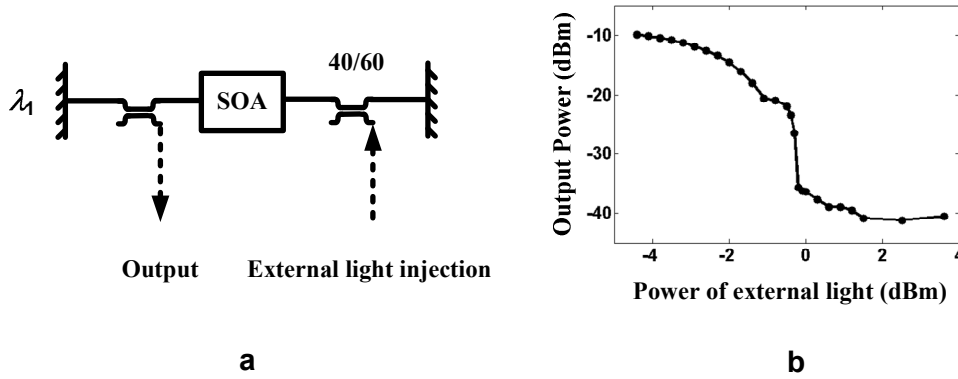


Figure 5.1: Experiment of gain quenching. Panel a: experimental setup; Panel b: power of external light versus output power.

The experiment setup is shown in Figure 5.1a. The laser has a Fabry-Perot cavity, a SOA acts as the active element. Two 40/60 couplers are placed in the cavity to output light and to receive external light injection. The lasing wavelength is determined by the wavelength dependent mirrors, which is a fiber Brag Grating (FBG) with a center wavelength of 1552.52 nm and a bandwidth of 0.5 nm. The employed SOA is commercially available strained bulk SOA that has a typical small gain of 20 dB at 200 mA injection current and a 3dB saturation power of -5 dBm. In this experiment, the SOA is biased with 180 mA injection current. The power-in-versus-power-out curve is shown in Figure 5.1b, where the output power of the laser decreases when the power of the external light increases from -4.2 dBm, due to gain saturation of the SOA. The laser ceases operation when the power of the external light exceeds the threshold value, -0.2 dBm in this experiment as shown in Figure 5.1b.

If the external light is replaced by another identical laser but lasing at a different wavelength, the system is a two-coupled-laser system, as shown Figure 5.2. It has been explained in Section 1.2.2 in Chapter 2 that the system is bistable if the coupling between the two lasers is strong enough [36]. Laser 1 is gain-quenched if Laser 2 is set to be lasing firstly, and vice versa. Switching between the two states can be realized by injecting external light at a different wavelength into the system as shown in Figure 5.2. In the case that Laser 1 is dominant and Laser 2 is suppressed. The external light is injected into the cavity of Laser 1, and makes it gain-quenched, Laser 2 starts lasing since no injection from Laser 1. Once the lasing operation in Laser 2 has generated, Laser 2 keeps Laser 1 gain-quenched. The system is be reset by

injecting external light into the cavity of Laser 2. An optical memory is thus realized. This concept has been integrated in a photonic chip [101].

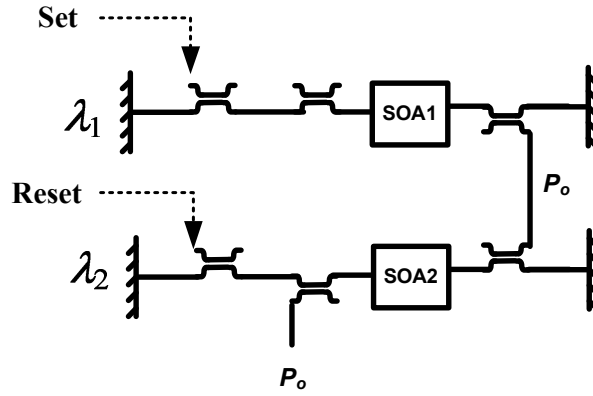


Figure 5.2: Experimental setup of the optical memory based on two coupled lasers. Set and reset refer to switch between the two stable states.

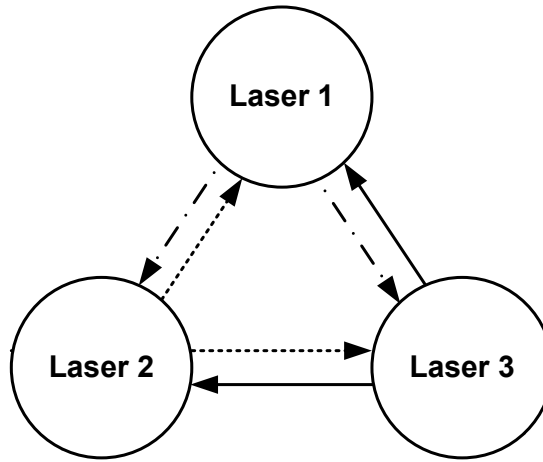


Figure 5.3: Three-state optical memory based on three inter-coupled lasers.

The concept of optical memory based on gain-quenching is extended in Ref. [50] to realize a three-state optical memory, as shown in Figure 5.3. The output of each laser is divided into two parts, which are injected into the cavities of the other two lasers. If any of the three lasers is set to be lasing firstly, the other two lasers are gain-quenched if the injection power exceeds their threshold. Since the power from each laser is

divided into two parts, each laser has to be pumped with high current in order to realize gain-quenching. If more lasers are inter-coupled based on this concept to realize more states optical memory, each laser should operate with even higher output power in order to realize gain-quenching based multi-stability. Therefore the “Power” issue hinders this concept to be extended further.

Since “Power” is the key issue for gain-quenching operation, we have to find an alternative method to make use of the resources efficiently to get enough power for multi-stable operation. This is the contribution from this thesis, as shown in next section.

5.2 Operation principle

We first come back to Figure 5.2, where a bistable setup is presented. In the case that Laser 1 is lasing, Laser 2 is gain-quenched. Although Laser 2 is suppressed because the net gain of the cavity becomes negative, the corresponding active element SOA2 still has the capability of amplification. SOA2 is just deeply saturated by the injected light from Laser 1. The saturated SOA in the suppressed laser can be used to amplify the injected light to compensate for losses. Thus the power of the injected light from Laser 1 can be recovered to be the original power (P_0) at the output of Laser 2, as shown in Figure 5.2. The recovered injected light can continue to gain-quench the next laser cascaded with Laser 2. The saturated SOA in the suppressed laser is therefore a resource that can be used to realize optical memories with multi-state operation.

The schematic configuration of the multi-state optical memory is shown in Figure 5.4. Five identical lasers are interconnected. Each individual laser is as same as the laser shown in Figure 5.2. Suppose Laser 1 is set to become lasing firstly, same as the bistable case previously discussed, Laser 1 suppresses Laser 2, and the injected light from laser 1 still receives amplification from the saturated SOA2. The amount of amplification can compensate for the loss for the injected light passing from port C to port E through SOA2. Therefore the injected power from Laser 1 is recovered at port E of Laser 2, and continues to quench Laser 3. After receiving amplification from SOA 3, the injected light from Laser 1 quenches the rest of the lasers in the same way. Eventually, laser 1 dominates all the other lasers.

If Laser 2 is set lasing first, the output light of Laser 2 quenches Laser 1 and Laser 3 through gain saturation. After receiving amplification from SOA3, the injected light from Laser 2 at port H keeps on quenching the rest of the lasers. Eventually, Laser 2 suppresses all the other lasers. Therefore, any of the five lasers can dominate all the others in a similar way. Since each laser has a different wavelength, fivefold-stability is thus realized.

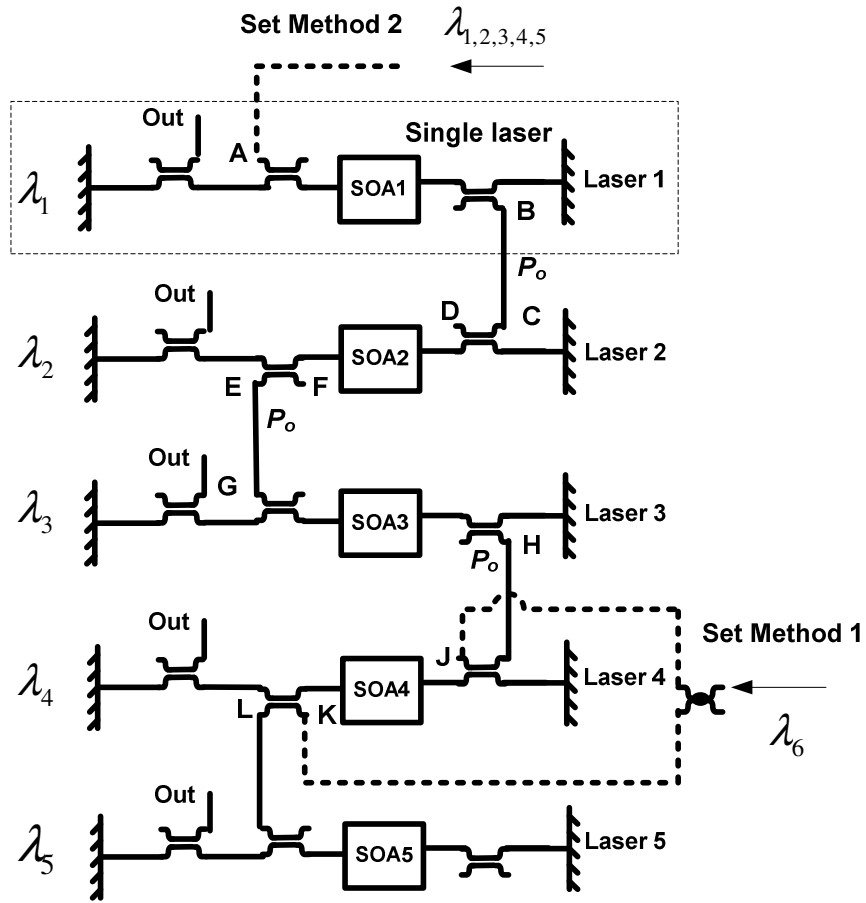


Figure 5.4: Configuration of multi-state optical memory based on serially interconnected lasers.

5.3 Experiment and results

The schematic of Figure 5.4 is implemented by fiber pigtailed components. The wavelength dependent mirrors of laser 1, 2, 3 and 5 are Fiber Bragg Gratings (0.60 nm FWHM) with center wavelengths of 1552.52 nm, 1554.20 nm, 1555.75 nm and 1558.90 nm, respectively. Due to the lack of components, we combine an arrayed waveguide grating (AWG) and one loop mirror to act as a wavelength dependent mirror to form the cavity of laser 4. The AWG serves as a filter (0.80 nm FWHM) with a center wavelength of 1557.40 nm. All the couplers inter-connecting the lasers have a splitting ratio of 40/60. The port with 60% ratio is used to couple with the other lasers. All the couplers used to output light have a ratio of 80/20. 20% of the light is coupled out. The employed SOAs are commercially available strained bulk SOAs that have a typical small gain of 20 dB at 200 mA and a 3dB saturation power of -5 dBm. Different currents are injected into the SOAs to make the system symmetrical in such a way that the output power of each laser is similar.

5.3.1 Five-state optical memory

When the injection currents for SOA 1-5 are 189.4 mA, 177.9 mA, 198.4 mA, 210.7 mA and 192.5 mA, respectively, the power (P_0) of the lasing light coupled to the neighboring lasers is about 0 dBm (1mW) and is recovered by receiving amplification from the saturated SOAs. Since 0 dBm power is sufficient large to quench the neighboring lasers (the threshold injection power is about -3.5 dBm for any single laser), the system turns out to be fivefold-stable. The corresponding spectra are shown in Figure 5.5. Any of the five lasers dominates all the other lasers with a contrast ratio over 30 dB. Note that the spectrum of laser 4 shown in Figure 5.5 has a broader bandwidth because the AWG used as a wavelength dependent element has a wider bandwidth.

If we modify the injection current of any of the five SOAs within a range of about 10 mA, while keeping the injection currents of the other four SOAs unchanged, the five-fold stability still exists. However, the contrast ratio between the states changes, due to the changed amplification by one of the SOAs.

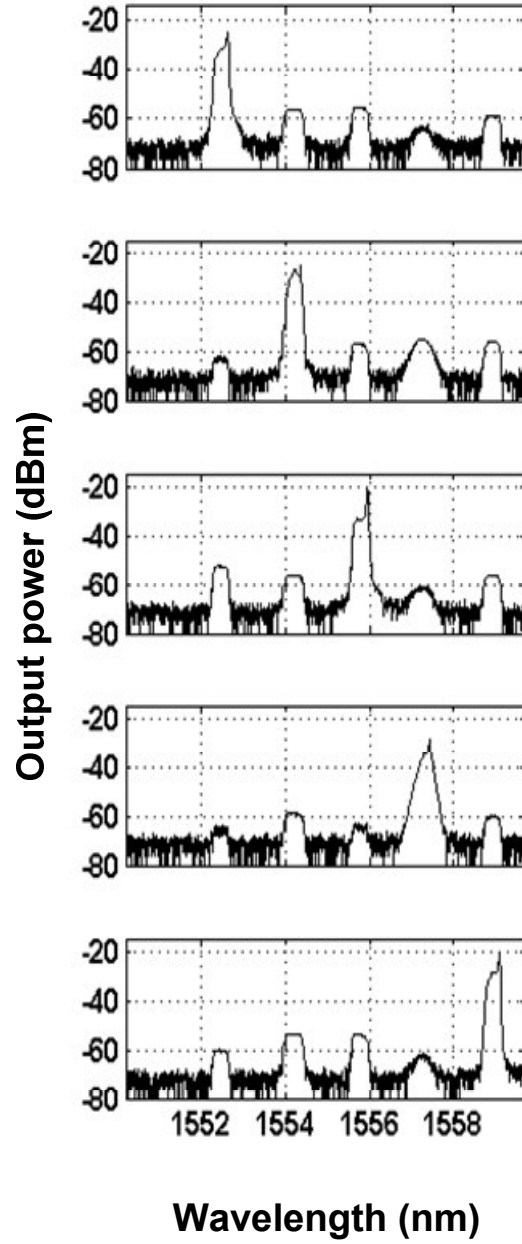


Figure 5.5: Spectra showing the system have five stable states

5.3.2 Two switching methods using external light injection

There are two methods to all-optically select the desired state. One is to inject external light, at a wavelength different from all lasers', into all the lasers except the desired laser [36, 50]. For example, when Laser 2 is lasing, we inject the external light at the wavelength of 1550.00 nm through ports J and K to make Laser 4 lase. The external light is divided into two parts: one part is injected into port K of Laser 4 to quench Laser 5; the other part is injected into port J of Laser 4 to firstly quench Laser 3 and then Laser 2 and 1 through gain saturation. Note that the injected light could not saturate SOA 4 inside Laser 4. Thus Laser 4 became lasing automatically since all the other lasers are gain-quenched. Figure 5.6 shows the output power of Laser 2 (indicated by solid line) and the output power of Laser 4 (indicated by dashed line) versus the power of the externally injected light through port J. Laser 4 becomes lasing and Laser 2 is suppressed when the power of the external light exceeds the threshold value of -3.5 dBm. When the external light is removed, the system remains in the new state.

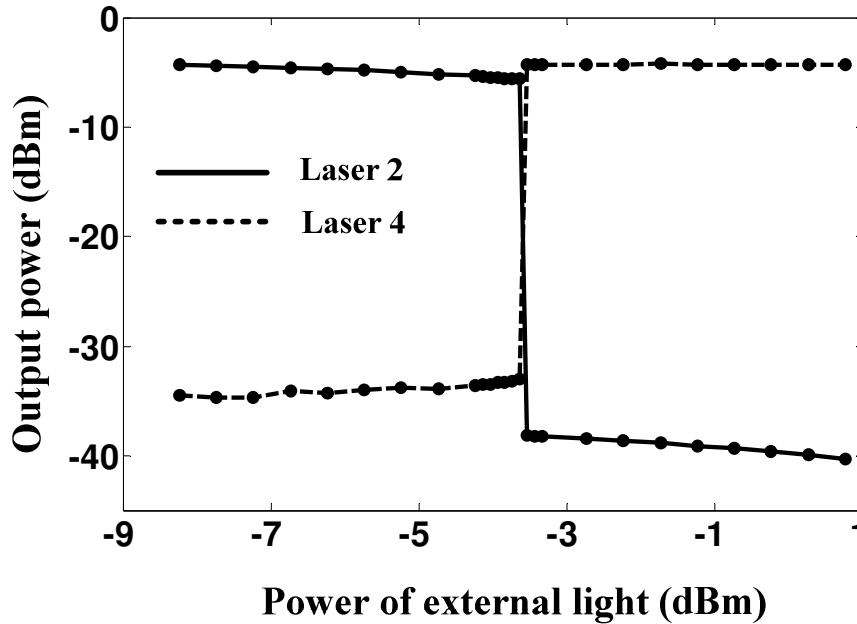


Figure 5.6: Switching from Laser 2 lasing to Laser 4 lasing by injecting external light at 1550.00 nm through ports J and K.

The dynamical operation based on this method is demonstrated in Figure 5.7. The external light at wavelength of 1550.00 nm is modulated by external optical modulator into a regular sequence of optical pulses, which have a period of 25.0 μs with the duty cycle of 0.2. The optical pulses are divided into two parts. One part is injected into the system through the port D and F of Laser 2 to set Laser 2 lasing, as shown in Figure 5.7a. The other part is delayed 10.0 μs , and then is injected into the system through the port J and K of Laser 4 to set Laser 4 lasing, as shown in Figure 5.7b. The toggling between the states of laser 2 lasing and laser 4 lasing as response of the corresponding setting pulses is shown in Figure 5.7c and 5.7d.

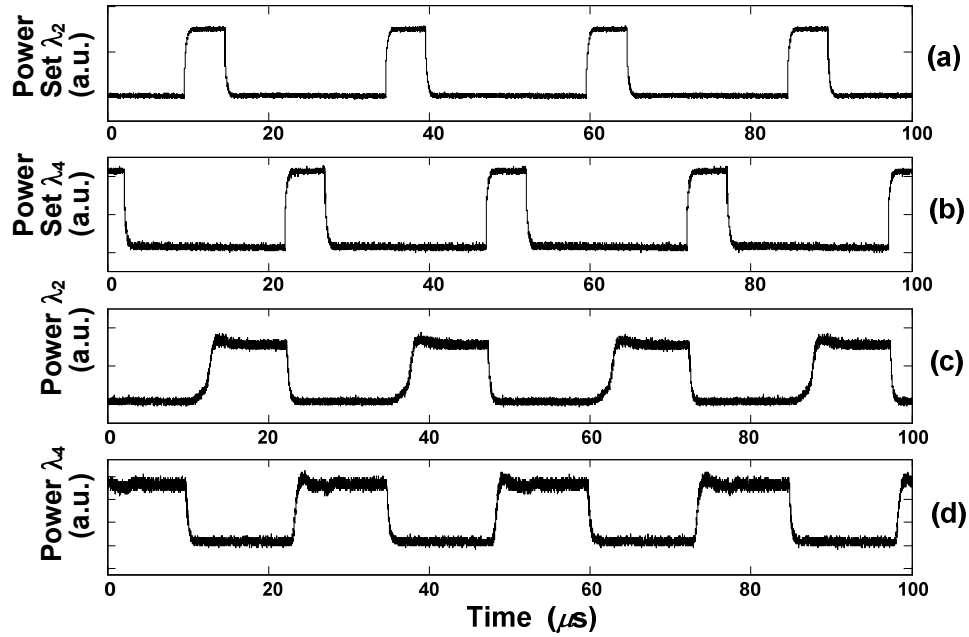


Figure 5.7: Dynamical operation by injecting external light at wavelength 1550.00 nm through different ports. Panels a: Oscilloscope traces of the external injected optical pulses through the port D and F of laser 2, to set laser 2 lasing; Panel b: Oscilloscope traces of the external injected optical pulses through the port J and K of laser 4, to set laser 4 lasing; Panel c and d: The dynamical operation of laser 3 or laser 5 lasing.

The other switching method is to inject external light, at the wavelength of the desired laser, always through port A. For example, when laser 5 is lasing, we inject the

external light at 1555.75 nm, which is the same as the center wavelength of Laser 3, through port A of Laser 1 to make Laser 3 become lasing. The external light first passes through lasers 1-5, saturating the corresponding SOAs. Note that the injected light only resonates in the laser cavity of Laser 3 because it has the same center wavelength. The resonant injected light in the cavity of laser 3 returns to inject into all the other lasers to saturate the corresponding SOAs further, which leads to a weaker power of switching threshold value. It is clearly visible in Figure 5.8 that Laser 5 is suppressed when the power of external light exceeds -13.75 dBm, which is about 10 dB smaller than that of the previous method. Laser 3 simultaneously becomes dominant when laser 5 is suppressed, because the resonant injected light out of laser 3 still keeps the other lasers suppressed. When the external light is removed, the system keeps the new state.

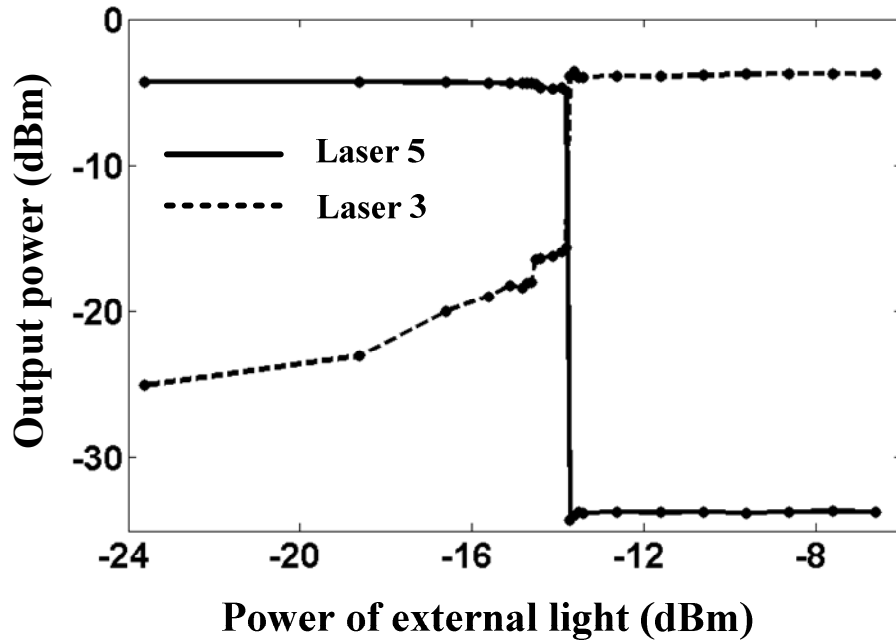


Figure 5.8: Switching from Laser 5 lasing to Laser 3 lasing by injecting external light at 1555.75 nm through port A.

The dynamic operation based on the latter method is demonstrated as well, as shown in Figure 5.9. Two beams of external light are modulated by external optical modulators into two regular sequences of optical pulses, which have a period of 25.00 μ s with the duty cycle of 10%. The sequence of optical pulses setting Laser 3 lasing is

at a wavelength of 1555.75 nm, as shown in Figure 5.9a. The other sequences of optical pulses setting laser 5 lasing is at a wavelength of 1558.90 nm, and has a delay of half period compared to the first sequence of optical pulses, as shown in Figure 5.9b. The toggling between the states of laser 3 lasing and laser 5 lasing as response of the corresponding setting pulses is shown in Figure 5.9c and 5.9d.

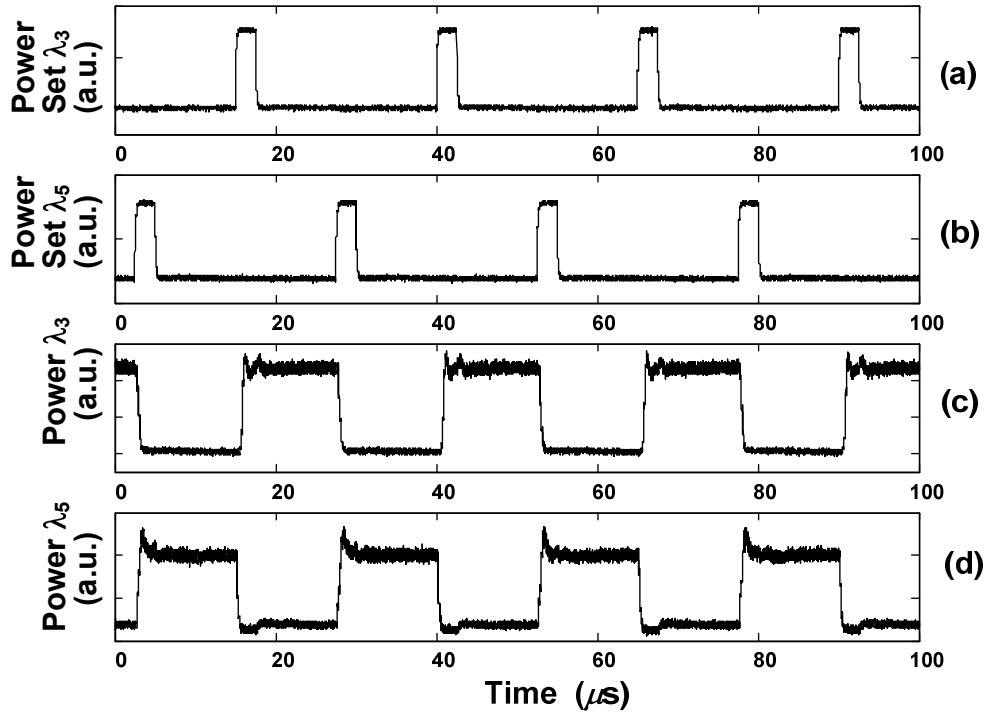


Figure 5.9: Dynamic operation by injecting external light through port A with different wavelength. Panel a: Oscilloscope traces of the externally injected optical pulses at wavelength 1555.75 nm, to set laser 3 lasing; Panel b: Oscilloscope traces of the external injected optical pulses at wavelength 1558.90 nm, to set laser 5 lasing; Panel c and d: The dynamic operation of laser 3 or laser 5 lasing.

5.4 Discussion

A five-state optical memory based on serially interconnected lasers through gain quenching is experimentally demonstrated. The contrast ratio is over 30 dB, which can be further improved by using wavelength dependent components with narrower

bandwidth. Two different switching methods with low power operation are demonstrated.

The switching speed is determined by the size of each laser and the distance between the lasers. Consider, for example, an optical memory with N stable states. The worst case occurs when the laser N is active and the device is switched to laser 1, at the opposite end. The injected pulse must first travel the length of the device to suppress the active laser. The effects will not be felt at laser 1 until the last light from laser N has time to travel the length of the device. Then laser 1 begins lasing. The time for lasing building up is determined by the size of each laser since a certain number of round trips are required. Operation speed can be improved by integration, which is applicable for the configuration shown in Figure 5.4 since no isolators are used. The gain-quenching based multi-state optical memory can be applied in telecommunication networks since its output is CW.

The advantage of the concept here presented is the linear scalability that in principle enables realization of optical memories with large number of states. It should be said, however, that several aspects associated with increasing the number of interconnected lasers need to be investigated further. These are the possibly detrimental effects from SOA-facets and coupler reflections, possible dynamical instabilities induced by the large number of coupled lasers and the influence of the various propagation times between the lasers.

Chapter 6

Optical shift register based on optical memories

Two types of multi-state optical memory have been investigated. It is interesting to further investigate on optical digital systems based on optical memories.

In this Chapter¹, an optical shift register based on optical memories is presented. It is presented in Section 6.1 that a short introduction about the concept of shift registers and optical shifter registers. The system concept of the optical shift register based on optical memories is given in Section 6.2. The experimental results are shown in Section 6.3. Further discussion on extension of this concept is presented in Section 6.4. A short summary of this chapter is given in Section 6.5.

6.1 Introduction to shift registers

In electronics [102], a group of flip-flops can be combined into a *register*. For instance, when an arithmetic calculation takes place in a computer's logic unit, the result must be saved. Each bit of the result is stored in a distinct flip-flop within a group of flip-flops. Since the flip-flops storing the result are all serving a common purpose, they are designated with a name "register". Registers are prevalent in electronic microprocessor and associated peripheral chips.

Shift registers are a certain class of registers. They store data and also allow the data to be shifted through the register, 1-bit at a time. The basic shift register structure is shown in Figure 6.1, where a group of flip-flops connected in a chain so that the output from one flip-flop becomes the input of the next flip-flop, driven by a common

¹ This Chapter is based on the following paper:

S. Zhang, Z. Li, Y. Liu, G.D. Khoe and H.J.S. Dorren, Optical shift register based on an optical flip-flop memory with a single active element, *Optics Express*, 13, pp: 9708-9713 (2005).

clock. The shift register provides a delayed copy of its input as output. If there are n flip-flops in the shift register, the delay will be n times the clock period. With additional outputs, a shifter register can also transfer data in serial fashion (1-bit at a time) or in parallel (multiple bits at a time). Therefore, shift registers are used to generate time delay, to simplify combination logic, to convert serial data into parallel data, and so on [103].

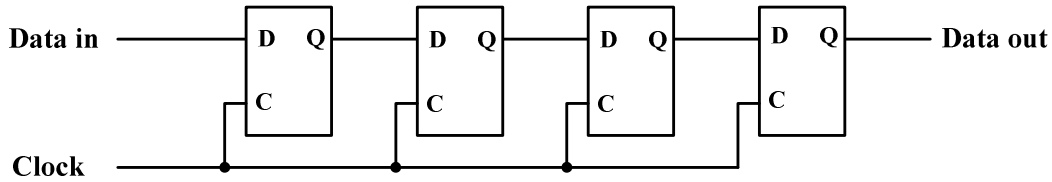


Figure 6.1: schematic configuration of an electronic shift register.

In optics, a large number of publications have been devoted to the realization of single ultrafast optical logic gates [104-107]. It has been shown that SOA based all-optical logic can reach switching time that is below one picosecond [108]. In contrast to the large amount of works to the optical logic gates, only a few publications exist on digital photonic systems based on coupled photonic gates. Optical shift registers have received an increasing attention since they could be potentially applied in optical signal processing. For example they could be used to realize buffering function in the optical packet switching network, where the payload of an optical packet has to be buffered [48]. Several approaches for optical shift registers have been explored. It is shown in Refs. [109, 110] that circulating optical shift registers are realized using either fiber buffers or using Sagnac interferometers. These concepts can not be integrated. Another example, given in Ref. [111], is based on coupled SEEDS (self-electro-optic effect device) driven by changes of the driving voltage.

In this paper, we present an optical shift register based on cascaded optical memories (optical flip-flops) driven by common optical clock pluses. Because only one active element is used in the optical memory investigated in Chapter 2-4, which makes it easily cascaded with each other and controlled by external light. We choose this type of optical memory to be the basic element, and demonstrate an optical shift register at an operation speed of 20 kHz as a proof of concept. The speed is limited by the laser cavities implemented by 10 m long fiber pigtailed components.

6.2 Operation principle

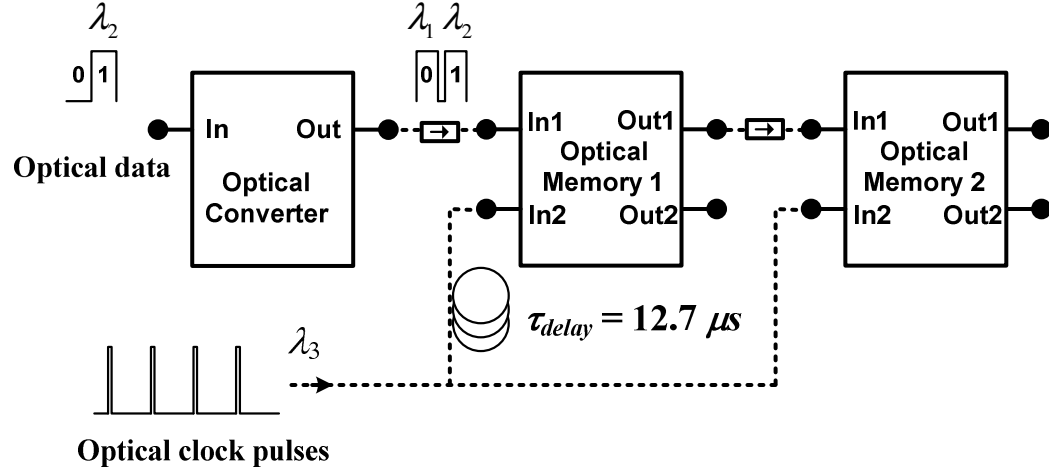


Figure 6.2: Schematic configuration of the optical shift register.

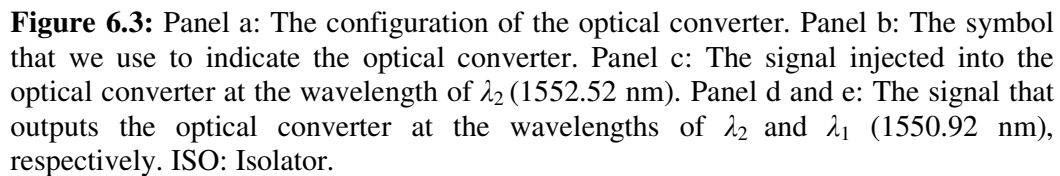
Figure 6.2 shows a block diagram of the optical shift-register, which consists of an optical converter in combination with two cascaded optical memories. The optical memory consists of two coupled ring lasers which are bistable in the sense that in each stable state one of the lasers lases while the other is suppressed, as explained in Chapter 3. The state of the optical memory is thus determined by the wavelength of the dominant laser. Therefore, an optical converter is needed to transform optical data encoded by two binary intensity levels (on and off) into data encoded in two different wavelengths corresponding to the two states of the optical memory. Each optical memory has two input ports and two output ports. The light injected into the port 'In1' can not set a new state unless the optical memory is cleared by a strong external optical pulse injected into the port 'In2'. Two optical memories are cascaded by connecting the port 'Out1' of Optical Memory 1 with the port 'In1' of Optical Memory 2. Port 'Out2' of each optical memory is used to output light for monitoring.

The optical shift register operates in the following fashion. Firstly, the intensity modulated input data are transformed by the optical converter into wavelength encoded data and subsequently injected into the port 'In1' of optical memory1, which is cascaded with Optical Memory 2. The two cascaded optical memories are controlled by optical clock pulses that are required to clear the optical memories. We use an external optical clock signal whose power is divided into two parts. 50% of the

power is delayed while the other 50% of the power is used to clear the state of Optical Memory 2 (by injection via its port 'In2'). The output from Optical Memory 1 then sets the new state of Optical Memory 2. After this operation, the delayed clock pulse is injected into the port 'In2' of Optical Memory 1 and subsequently clears its state. The signal encoded in wavelength that outputs from the optical converter then sets the new state of Optical Memory 1. Thus a complete 'shift' function has been realized.

6.3 Experiment and results

The optical shift register shown in Figure 6.2 is implemented using fiber pigtailed components. The optical converter consists of a unidirectional ring laser as shown in Figure 6.3a. A bulk strained semiconductor optical amplifier (SOA) that acts as the active element has a typical small gain of 20 dB at 200 mA and a 3dB saturation power of -5 dBm. A Fabry-Perot filter (3 dB bandwidth 0.20 nm) with a wavelength of 1550.92 nm (λ_1) is used as a wavelength selective element. An isolator is used to ensure unidirectional lasing. The optical data to be injected into the ring laser are at a wavelength of 1552.52 nm (λ_2) and have an average power of 3 dBm, as shown in Figure 6.3c. If the injected information is a binary '1', 50% of the injected optical power is directly coupled to the output port. The other half of the injected light is coupled into the ring cavity by a 50/50 coupler and suppresses the lasing operation by saturating the SOA, as the gain quenching operation presented in Section 5.1. The light that outputs the optical converter is thus at the wavelength λ_2 , as indicated in Figure 6.3d. If no light is injected into the ring laser (a binary '0'), the ring laser remains lasing at the wavelength λ_1 , as indicated in Figure 3e. In this case, the light that outputs the optical converter is at the wavelength λ_1 . Thus the data encoded in intensities are transformed by the optical converter into the data encoded in wavelengths.



Each optical memory consists of two ring lasers sharing a SOA and a feedback arm as shown in Figure 6.4a. The two ring cavities are formed using two 50/50 couplers. Each ring cavity contains a Fabry-Perot filter acting as a wavelength selective element. A variable attenuator is placed in each ring to balance the cavity losses. The central wavelengths of the Fabry-Perot filter in the ring cavity 1 and 2 are λ_1 and λ_2 , respectively. The SOA is biased with 250 mA injection current. It is shown in Chapter 3 that the roundtrip conditions of the two ring cavities can not be satisfied simultaneously due to the presence of feedback light which leads to a periodic oscillation of the light in the laser cavity. Therefore the system shows bistable

behavior in the sense that only one of the two lasers can lase while the other is suppressed (Figure 6.4c and 6.4d). Switching between the two states takes place by injecting external light, at the same central wavelength of the suppressed laser, to the port ‘In1’. The threshold switching power of the external light is -15.0 dBm in our experiment. The length of the ring cavity is about 10 m employing a fiber pigtailed setup, which leads to a switching time of 5.0 μ s.

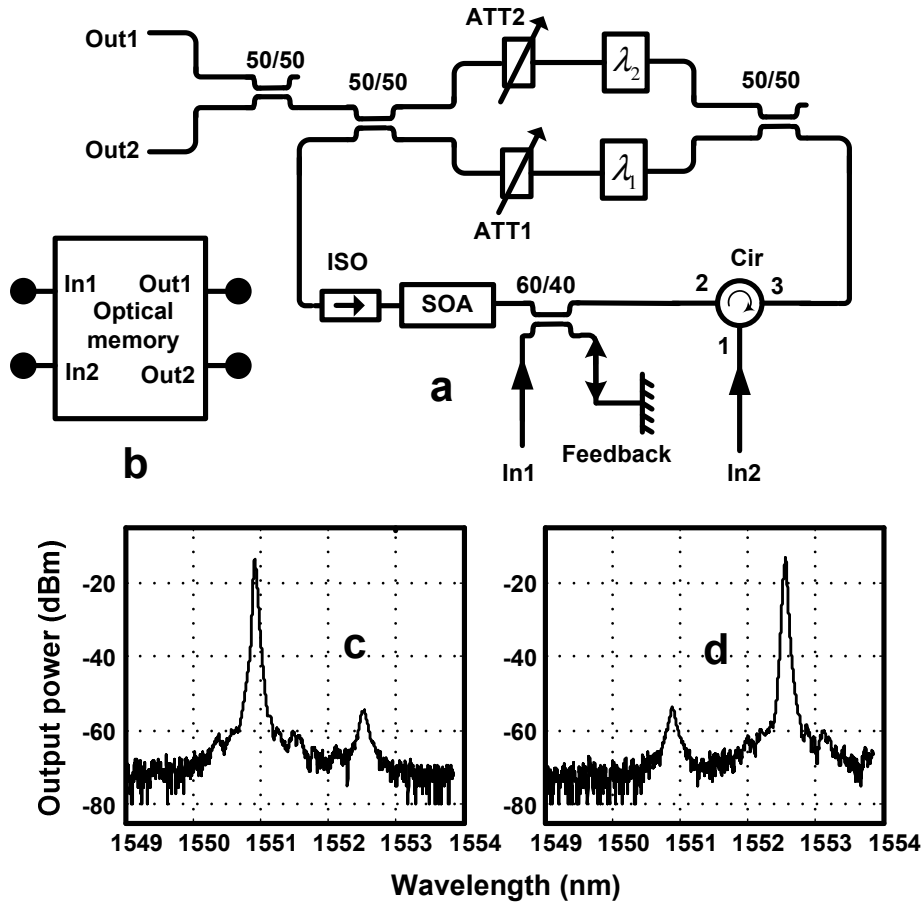


Figure 6.4: Panel a: Schematic configuration of the optical memory. Panel b: The symbol that we use to indicate the optical memory. Panel c and Panel d: Experimental results to show that the system has two stable states. ATT: Attenuator

When the power of the external light is below the threshold value, the system maintains the initial state. In this case, another external light input (with 3 dBm

power) at a central wavelength of 1559.30 nm (λ_3) is injected into the optical memory via the port 'In2. This additional input light deeply saturates the SOA so that both lasers are suppressed. In the remainder of this paper, we refer to this process as clearing of the memory. After clearing the optical memory, the light injection via the port 'In2' is stopped and the light injected via the port 'In1' sets the new state of the memory. Thus the optical memory starts lasing at the wavelength of the light injected via the port 'In1'.

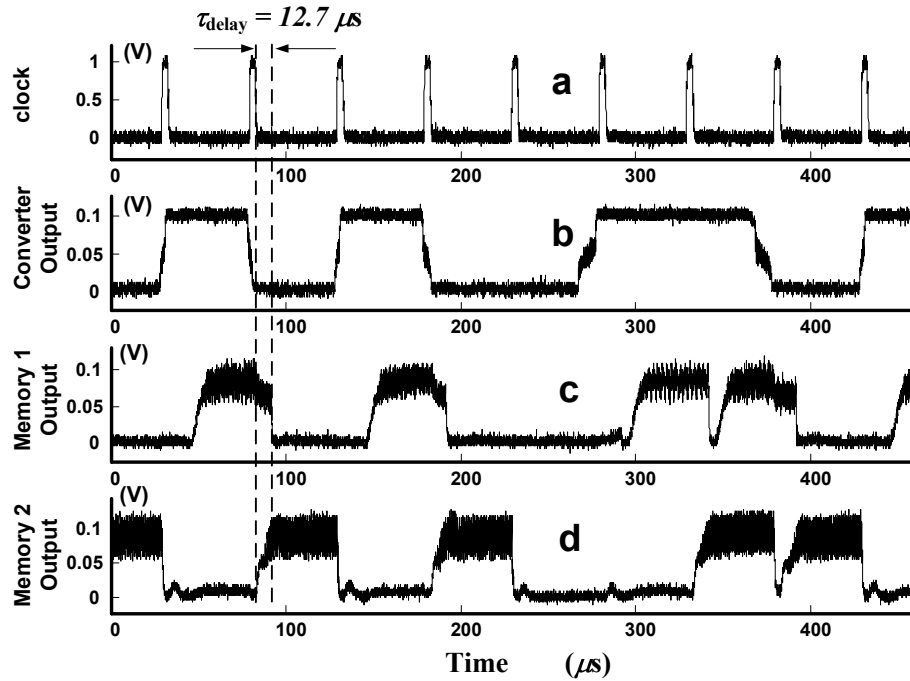


Figure 6.5: Experimental results for shifting of the binary sequence 01010011. Panel a: The 20 kHz clock signal; Panel b: The output of the optical converter; Panel c: The output of Optical Memory 1; Panel d: The output of Optical Memory 2. All the signals in Panel b, c and d are filtered with a center wavelength of λ_2 (1552.92 nm).

The optical converter combined with two cascaded optical memories form the optical shift register. Figure 6.5 shows how the information of a binary 01010011 signal is shifted. As shown in Figure 6.5a, the 20 kHz optical clock pulses are at the wavelength λ_3 and have a pulse-width of 4.0 μ s (Full Width at Half Maximum). The

intensity encoded input signal operates at the same frequency and is synchronized with the clock pulses. The input signal is firstly transformed into wavelength encoded signal by the optical converter, and is then injected into the port 'In1' of Optical Memory 1, which is cascaded with Optical Memory 2. The output of the optical converter, Optical Memory 1 and Optical Memory 2 are shown in Figure 6.5b, 6.5c and 6.5d, respectively. In order to present the experimental results explicitly, the three outputs are filtered using a filter with a central wavelength of λ_2 . Hence, a '0' state in Figure 6.5c and 6.5d correspond to a lasing state at the wavelength λ_1 as shown in Figure 6.4c.

It is shown in Figure 6.5 that both optical memories keep their initial states until they are cleared by the strong clock pulses. This is because the optical power injected into each optical memory via the port 'In1' is below the threshold power and the optical memories can only be cleared by a well-timed clock pulse injected via the port 'In2'. The optical power of the clock signal is split into two parts. 50% of the power is directly injected into the port 'In2' of Optical Memory 2 to clear this memory. After 4 μs (the duration of the clock pulse), the output of Optical Memory 1 sets the new state of Optical Memory 2. This procedure is repeated for Optical Memory 1 using the other 50% of the power of the clock pulse delayed by 12.7 μs . The new state of Optical Memory 1 is then set by the output of the optical converter which leads to the completion of the 'shift' function. All the operations take place within one clock cycle.

As introduced in Section 6.1, a shift register should not only shift data, but also maintain the state in the absence of clock pulses, which is demonstrated as follows. The data to be shifted is a repetitive binary 01010101 signal. The 20 kHz optical clock pulses are modulated in such a way that every six consecutive optical pulses are followed by five consecutive blank cycles as shown in Figure 6.6a. The output of the optical converter, Optical Memory 1 and Optical Memory 2 are shown in Figure 6.6b, 6.6c and 6.6d, respectively. In order to show the experimental results explicitly, the three outputs are filtered using a filter with a central wavelength of λ_2 . Hence, a '0' state in Figure 6.6c and 6.6d corresponds to a lasing state at the wavelength λ_1 as shown in Figure 6.4c. It is shown in Figure 6.6 that both optical memories keep their states in the absence of clock pulses, while the system starts to shift data with an injected optical clock pulse.

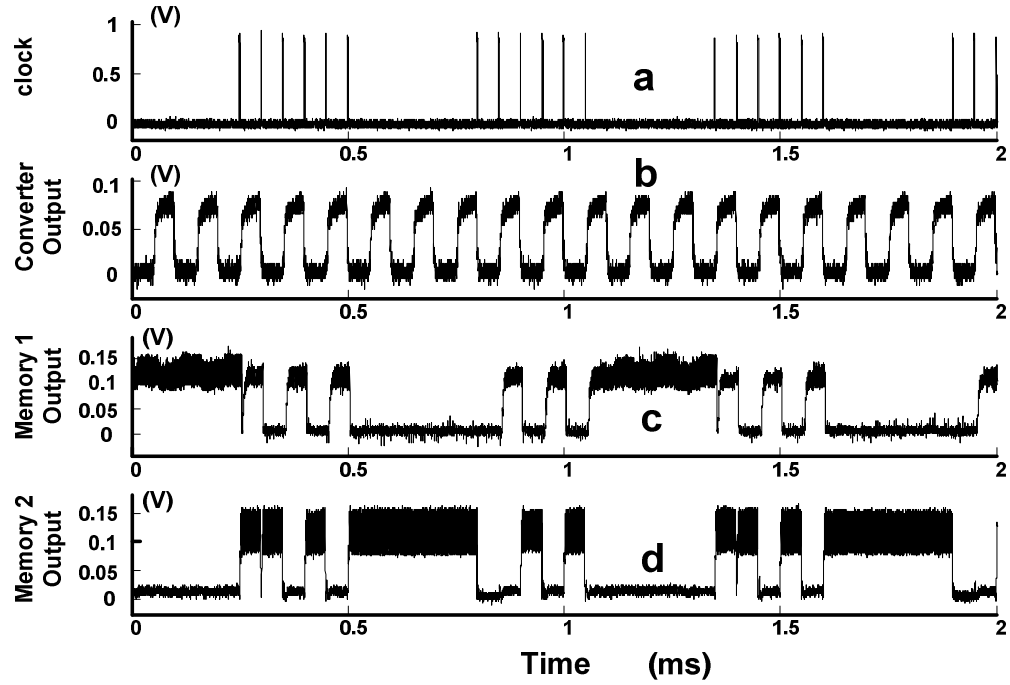


Figure 6.6: Experimental results when the clock signal is modulated such that every six consecutive pluses are followed by five consecutive blank cycles. Panel a: The 20 kHz clock signal; Panel b: The output of the optical converter; Panel c: The output of Optical Memory 1; Panel d: The output of Optical Memory 2. All the signals in Panel b, c and d are filtered by a filter with a center wavelength of λ_2 (1552.92 nm).

6.4 Shift more data

To shift more data, more optical memories need to be cascaded. If the concept shown in Figure 6.2 is extended straight-forwardly for cascading more optical memories, the clock pulse thus has to be divided into more parts with different delays, which increase the complexity. The solution is to introduce some memories to buffer the data inside the shift register as follows.

Figure 6.7 shows a schematic configuration of an optical shift register that can restore and shift 5 bits of data. Any optical memory placed in even number position is connected to a backup optical memory, whose output is injected into the optical memory in the next odd number position. In Figure 6.7, optical memory FFa is inserted between optical memories OM2 and OM3, while optical memory OMb is

inserted between optical memories OM4 and OM5. The clock pulse is divided into three parts no matter how many optical memories are cascaded. The first part is not delayed, the second one is delayed with time τ_d , and the third one is delayed with time $2 \times \tau_d$.

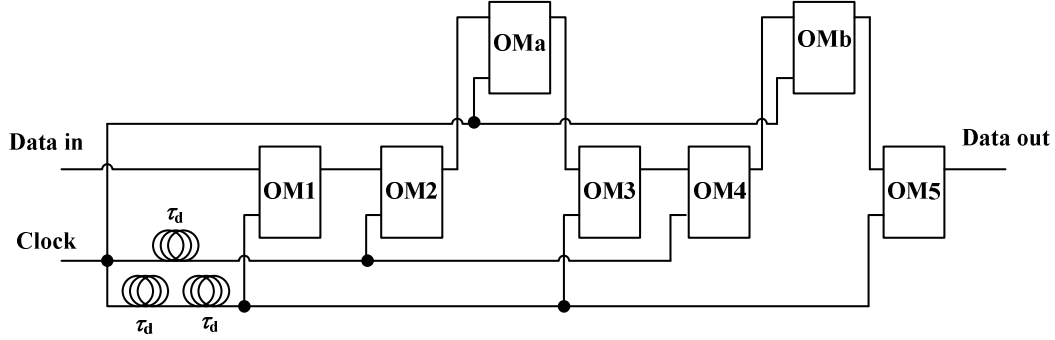


Figure 6.7: Schematic configuration of optical shift register with more cascaded memories.

With the clock pulse that has no delay, the optical memories placed in even number positions shift their states to the corresponding backup optical memories, i.e. OM2 and OM4 shift their states to OMa and OMb, respectively. And then the optical memories placed in odd number positions shift the states to their next optical memories with the clock pulse that is delayed with time τ_d , i.e. OM1 and OM3 shift their states to OM2 and OM4, respectively. Finally, with the clock pulse that is delayed with time $2 \times \tau_d$, the input data and the backup optical memories shift their states to the corresponding memories, i.e. the input, OMa and OMb shift their states to OM1, OM3 and OM5, respectively. As a result, 5 bits of data are shifted.

This concept can be extended to shift more data, while the clock pulses are divided always by three parts. Moreover, more data can be processed if each optical memory operates in multiple states.

6.5 Conclusion

An optical shift register based on serially connected optical memories is experimentally demonstrated at an operation speed of 20 kHz as a proof of concept.

The operation speed is limited by the slow switching speed of the optical memory due to 10 m long ring cavity made by fiber pigtailed components. Photonic integration would decrease the dimensions of the building blocks and increases the operation speed of the shift register. In principle, the concept can be applied using different optical memory concepts, which can be integrated in small scale [45, 101].

Such an optical register has the ability to control data at a bit-level, which has great potential in optical data buffers and optical serial-to-parallel converters. Furthermore, the optical shift register demonstrates that cascaded optical memories can perform sophisticated digital optical signal processing functions.

Chapter 7

Optical pseudorandom number generator based on optical memories

An optical shift register based on cascaded optical memories has been demonstrated in Chapter 6. Since shift registers act as intermediate units between basic logical elements like optical memories and more complicated logic system, we investigate optical digital systems further to realize an optical pseudorandom number generator, which is basically made by an optical shift register cascaded with an optical XOR gate.

This chapter is organized as follows. A short introduction of PRBS generator is given in Section 7.1. The operation principle of the optical PRBS generator is presented in Section 7.2. The experimental implementation is described and the experimental results are shown in Figure 7.3. This chapter is concluded with a short summary in Section 7.4.

7.1 Introduction to the pseudorandom number generator

A binary sequence (BS) is a sequence of N bits,

$$a_j \text{ for } j = 0, 1, \dots, N - 1,$$

i.e. m ones and $N - m$ zeros. A BS is pseudo-random binary sequence (PRBS) if its autocorrelation function $C(v) = \sum_{j=0}^{N-1} a_j a_{j+v}$ has only two values [112]:

$$\begin{aligned} C(v) &= m & \text{if } v \equiv 0 \pmod{N} \\ C(v) &= mc & \text{if } v \not\equiv 0 \pmod{N} \end{aligned}$$

Where $c = (m - 1)/(N - 1)$ is called the duty cycle of the PRBS.

A PRBS is random in a sense that the value of an a_j element is independent of the values of any of the other elements, similar to real random sequences. It is 'pseudo' because it is deterministic and after N ($N = 2^k - 1$) elements it starts to repeat itself, unlike real random sequences, such as sequences generated by radioactive decay or by white noise. PRBS's are used in telecommunication, encryption, simulation, correlation technique etc. A PRBS generator is to produce PRBS data and can be implemented by a linear shift register combined with an exclusive-or (XOR) gate.

An optical PRBS generator has been realized using SOA based interferometer switching gates [113]. In this chapter, we present a photonic pseudo random bit sequence (PRBS) generator based on cascaded optical memories. Our optical PRBS consists of an optical shift register made by two cascaded optical memories and an optical XOR gate. Since the optical shift register based on cascaded optical memories has been demonstrated in Chapter 6, the essential issue is to design the optical XOR gate such that it can handle low-power wavelength encoded input signals, which is different from the conventional optical logic gates [114, 115]. We demonstrate the operation of an optical PRBS generator with a 3 bit pattern length at an operation speed of 10 kHz. The speed is limited by the 10 meter long laser cavities formed by the fiber pigtailed components. It should be noted however, that the concept is generic and can in principle use ultra-compact photonic integrated optical memories.

7.2 Operation principle

The schematic configuration of the optical PRBS generator is shown in Figure 7.1. It consists of an optical XOR gate based on coupled lasers and an optical shift register based on coupled optical memories. The optical memories that we use are described in Chapter 3. A schematic of the optical memory is shown in Figure 6.4a. Each optical memory consists of two ring lasers sharing the same SOA as the gain medium. Both cavities also share a feed-back-arm to saturate the laser gain medium with delayed lasing light. It has been shown that such a system shows bi-stable behavior in the sense that for each stable state, lasing takes place in only one of the cavities, while lasing in the other cavity is suppressed. The state of the optical memory is thus determined by the wavelength of the dominant cavity (see Figure 6.4c and 6.4d).

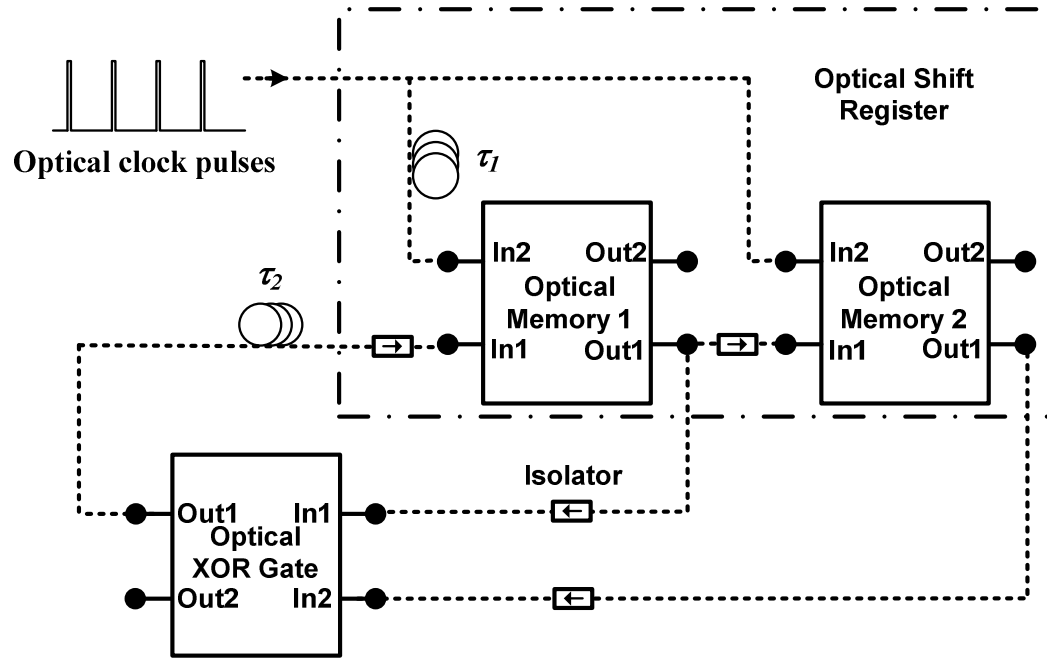


Figure 7.1: Schematic configuration of optical PRBS

It has been shown in Chapter 6 that by cascading a chain of two optical memories, both driven by an external clock signal, a simple optical shift register can be realized. The shift register is shown in the dashed box in Figure 7.1. The optical memories that are used have two input ports and two output ports (see Figure 6.4b). Port ‘Out1’ of each optical memory is connected to port ‘In1’ of the next optical memory in the chain. The system is designed such that a signal injected via port ‘In1’ cannot change the optical memory state alone. Switching the optical memory state is only possible if simultaneously with the signal injected into port ‘In1’, also a strong external clock pulse is injected via port ‘In2’. This additional input light deeply saturates the SOA so that both lasers are suppressed, in the remainder of this paper we refer to this process as clearing of the optical memory. After this operation, the low power signal injected via port ‘In1’ sets the new state. Details about the operation can be found in Chapter 6.

Figure 7.1 also indicates that the output of each optical memory is fed into the input of the optical XOR gate. It should be noted that the optical memories operate in the

wavelength domain. This implies that the optical XOR gate is also required to processes data encoded in different wavelengths. The schematic configuration of our optical XOR gate is shown in Figure 7.2.

The optical XOR gate is made of three coupled ring lasers, which only lase in the counter clockwise direction. Thus externally injected light in the clockwise direction can quench the lasing state, even if the lasing light and the injected light have the same wavelengths. The light that outputs Optical Memory 1 and Optical Memory 2 is injected into the XOR gate via port ‘In1’ and port ‘In2’, respectively. A 50/50 coupler splits the injected light into two arms, in which two Fabry-Perot filters with center wavelengths λ_1 and λ_2 are placed to ensure that only light with wavelength λ_1 can be injected into Laser 1, while only light with wavelength λ_2 can be injected into Laser 2. Both Laser 1 and Laser 2 operate at wavelength λ_1 . The output light of Laser 1 and Laser 2 is combined and coupled into Laser 3 that operates at wavelength λ_2 .

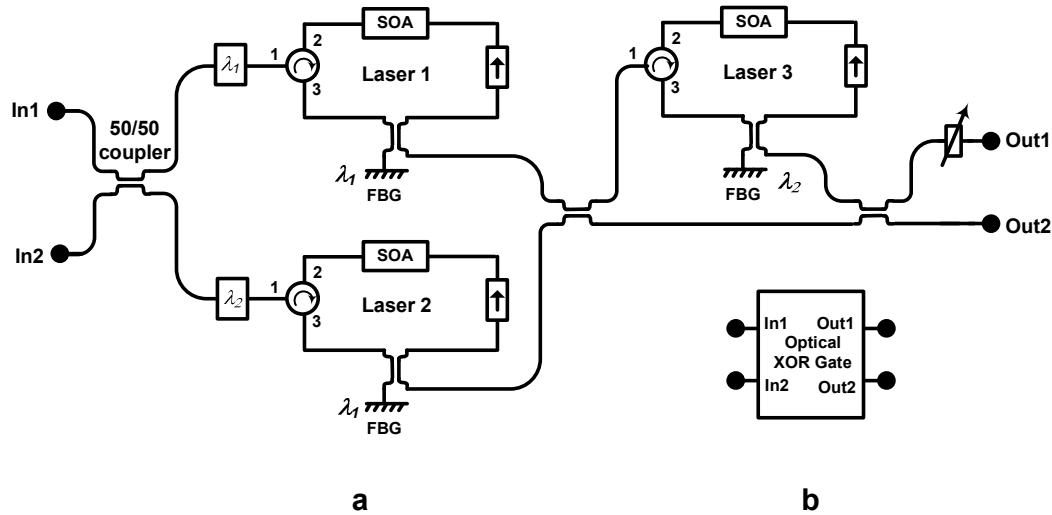


Figure 7.2: Panel a: Schematic configuration of optical XOR gate. Panel b: The symbol that indicates the optical XOR gate.

The XOR gate operates as follows. In the first case we assume that at input port ‘In1’ and ‘In2’ light with different wavelengths is input, both lasing operation in Laser 1 and Laser 2 are suppressed. If Laser 1 and Laser 2 are suppressed, no light is injected

into Laser 3, thus the XOR gate outputs light at wavelength λ_2 (*i.e.* a logic “1”). In the second case, we assume that the light at both import ports have the same wavelengths. Depending of the wavelength of the light at the input, either Laser 1 is suppressed but Laser 2 is still lasing, or Laser 2 is suppressed while Laser 1 is still lasing. Hence, lasing operation of Laser 3 is quenched by injection of external light generated by either Laser 2 or Laser 1. In this case, the XOR gate outputs light at wavelength λ_1 (*i.e.* a logic “0”). If no light is injected, both Laser 1 and Laser 2 quench Laser 3, and thus the system outputs light with wavelength λ_1 . The truth table is shown in Table 7.1 and confirms that the system exhibits XOR operation.

Table 7.1: The true table of the optical wavelength encoded XOR gate.

XOR True Table

In1	In2	XOR
1 (λ_2)	0 (λ_1)	1 (λ_2)
0 (λ_1)	1 (λ_2)	1 (λ_2)
1 (λ_2)	1 (λ_2)	0 (λ_1)
0 (λ_1)	0 (λ_1)	0 (λ_1)

The optical PRBS generator consists of the combined XOR-gate and optical shift register operates in the following fashion: Suppose that before the first clock pulse arrives, Optical Memory 1 is lasing at wavelength λ_1 (*i.e.* a logic “0”) and Optical Memory 2 is lasing at wavelength λ_2 (*i.e.* A logic “1”). From the truth table, it follows that in this case the XOR gate outputs a logic “1” (*i.e.* continuous wave light at wavelength λ_2). When the clock pulse is injected into the shift register, firstly its power is divided into two parts. 50% of the power is delayed with τ_1 before being fed into Optical Memory 1, while the other 50% of the power is used to clear the state of Optical Memory 2. The output from Optical Memory 1 then shifts to set the new state of Optical Memory 2 to be a logic “0”. After this operation, the delayed clock pulse is

injected into port ‘In2’ of Optical Memory 1, to subsequently clear its state. The logic “1” that outputs the XOR gate then defines the new state of Optical Memory 1. Note after the first clock-pulse has passed by, the input states of the XOR gate remain the same, thus the XOR gate continues outputting a logic “1”.

During the second clock cycle, firstly the state of Optical Memory 1 is shifted to Optical Memory 2. This means that the new state of Optical Memory 2 is a logic “1”. Afterwards, Optical Memory 1 will be cleared, and its new state will be the output state of the XOR gate (i.e. a logic “1”). Moreover, the new input states of the XOR gates are both logic “1s”, which makes that the XOR gate outputs a logic “0” (continuous wavelength at light at wavelength λ_1).

During the third clock cycle this procedure repeats. Firstly the state of Optical Memory 1 shifts to Optical Memory 2, making the new state of Optical Memory 2 to be a logic “1”. Moreover, the new state of Optical Memory 1 will be the output state of the XOR, i.e. a logic “0”. Hence, the new output state of the XOR is a logic “1”. If this process is continued, it follows that the system outputs a signal corresponding to the bit-pattern “101101101...”. Thus, we have realized an optical PRBS generator based on two cascaded optical memories and an optical XOR gate. The PRBS generator outputs a Pseudo Random Bit Sequence with a periodicity of 3.

7.3 Experiment and results

The optical PRBS generator shown in Figure 7.1 is implemented using fiber pigtailed components. The experimental setup of the optical memory is the same as the one shown in Figure 6.4a, except that the central wavelengths of the Fabry-Perot filter in the ring cavity 1 and 2 are 1552.52 nm (λ_1) and 1558.90nm (λ_2), respectively. Similarly, switching between the two states takes place by injection of external light, to port ‘In1’. The wavelength of the injected light must have the same central wavelength as that of the suppressed laser cavity. The threshold value for the power of the external light that is required for switching is -15.0 dBm. The switching time between two states is approximately 5.0 μ s, since the length of the ring cavity is implemented by employing commercially available fiber pigtailed components. This makes that the total cavity length is approximately 10 meters.

When the power of the external light is below the threshold value, the system does not change state. In this case, switching can be forced by clearing the optical memory state by injection of 3 dBm of external light, at a central wavelength of 1550.00 nm

(λ_3), into port 'In2'. After clearing the optical memory, light injection via port 'In2' is stopped and the low power input at port 'In1' sets the new state of the optical memory. Thus the optical memory starts lasing at the wavelength of the light injected via port 'In1'.

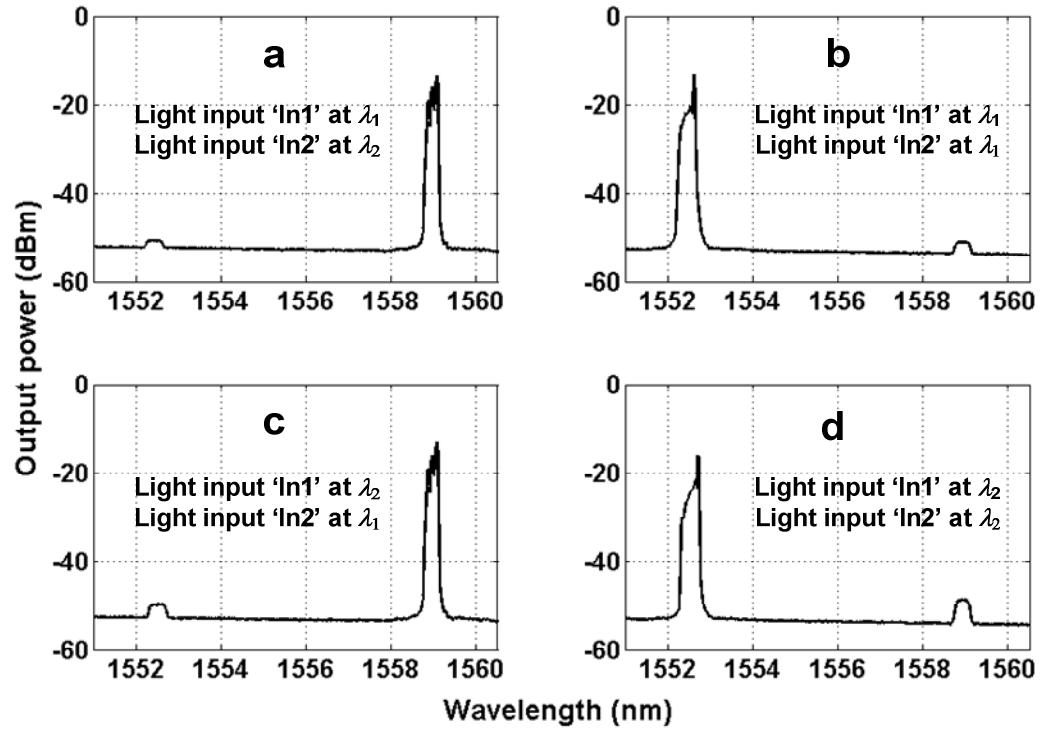


Figure 7.3: The output optical spectra of the optical XOR gate based on three cascaded lasers.

The XOR gate shown in Figure 7.2 is also implemented using fiber pigtailed components. Fiber-Bragg Gratings (3 dB bandwidth 0.40 nm) are used as wavelength selective elements. An isolator is used to ensure unidirectional lasing in counter clockwise direction. External light is input in the lasers in clockwise direction via an optical circulator. Optical spectra indicating the operation of the optical XOR gate are shown in Figure 7.3. When the input light from Optical Memory 1 and Optical Memory 2 are at different wavelengths, the output of the XOR gate is at wavelength λ_2 (i.e. a logic "1") as shown in Figure 7.3a and 7.3c. While the output of Optical Memory 1 and Optical Memory 2 are at the same wavelength, the output of the XOR

gate is at wavelength λ_1 (i.e. a logic “0”) as shown in Figure 7.3b and 7.3d. Therefore an XOR function is realized according to the true table shown in Table 7.1.

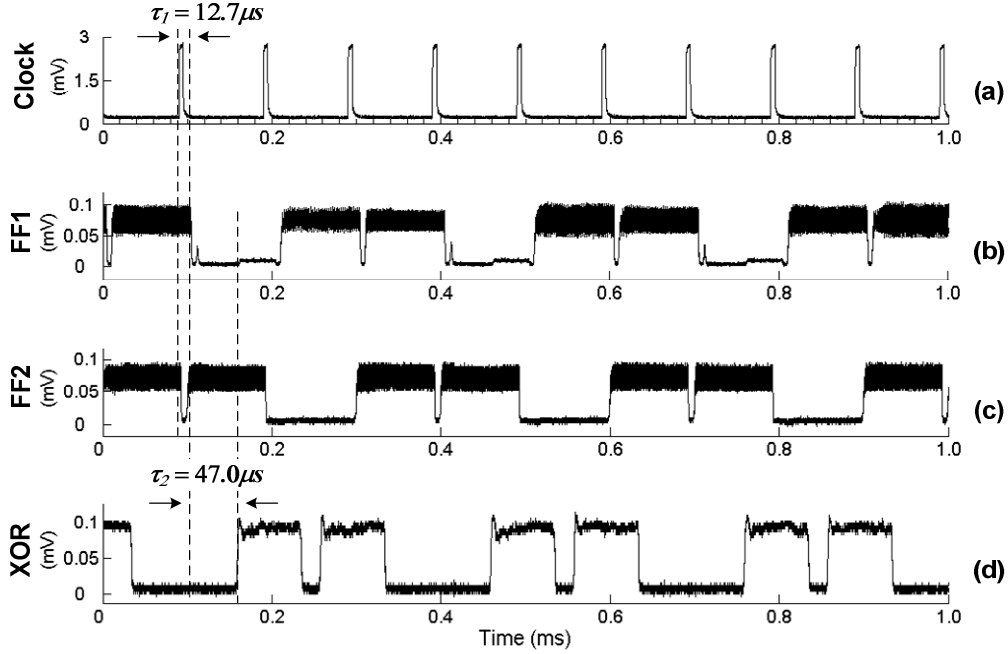


Figure 7.4: Experimental demonstration of PRBS generator. Panel a: The 10 kHz clock signal. Panel b: The output of Optical Memory 1. Panel c: The output of Optical Memory 2. Panel d: The light injected to Optical Memory 1 from optical XOR gate. All the signals in panel b, c and d are filtered by a filter with a center wavelength of λ_2 (1558.92 nm).

The optical XOR gate combined with two cascaded optical memories form the optical PRBS generator. Figure 7.4a shows the optical clock signal. It consists of a repetitive series of optical pulses, each with a pulse-width of $4.0 \mu\text{s}$ (Full Width at Half Maximum). The repetition rate of the clock signal is 10 kHz and the wavelength is λ_3 (1550.00 nm). Figure 4b, 4c and 4d show the output of Optical Memory 1, Optical Memory 2 and the XOR gate as a function of time. In order to make the operation of the PRBS generator visible, the output signals are filtered using a filter with a central wavelength of 1558.90nm (λ_2). Hence, a ‘0’ state in Figure 4b, 4c and 4d corresponds to a lasing state at wavelength λ_1 .

It can be observed from Figure 7.4 that before the first clock pulse arrives both memories store logic “1s”. Hence, the output of the XOR is a logic “0”. Both optical memories keep their initial states until they are cleared by the strong clock pulse. As explained above, the clock pulse is firstly divided into two parts, one part is delayed by τ_1 (12.7 μs), the other part is directly injected into Optical Memory 2. After 4 μs (the duration of the clock pulse), the output of Optical Memory 1 sets the new state of Optical Memory 2, thus Optical Memory 2 stores a logic “1”. This procedure is repeated for Optical Memory 1 using the delayed pulse. The new state of Optical Memory 1 is then set by the injected light from the XOR gate. Note that the injected light from XOR gate is delayed by τ_2 (47 μs) before being shifted to Optical Memory 1. The delay time τ_2 roughly corresponds to the time in between two clock pulses. This means that the input state of Optical Memory 1 corresponds to the state of the XOR gate before the clock pulse arrives. After memories have switched state, the output of both memories set the new state of the XOR gate. Note that during the transition time, the output of the XOR gate is not stable, but this instability doesn’t influence the operation of the system due to the delay time τ_2 (47 μs). With next clock pulse, the procedure repeats. Since two optical memories are cascaded, a Pseudo Random Bit Sequence with a 3-bit periodicity is realized. As a result, a “101101101...” bit-sequence is generated, as shown in Figure 7.4d.

Note that the noisy output from the memories shown in Figure 7.4b and 7.4c is due to the feedback induced oscillation of the intensity of the lasing light [Chapter 2, 3]. This oscillation frequency is typically in the order of a few hundreds of MHz, which is fast compared to the 10 KHz operation speed of the clock signal. The optical XOR gate also acts as a threshold device, which suppresses the intensity fluctuations of the optical memory outputs.

7.4 Conclusion

An optical PRBS generator based on cascaded optical memories and an optical XOR gate are experimentally demonstrated at an operation speed of 10 kHz as a proof of concept. The operation speed is limited by the slow switching speed of the optical memory due to the laser cavities implemented by 10 meters long fiber pigtailed components. Photonic integration would decrease the dimensions of the building blocks and increases the operation speed. In principle, the concept can also be applied using different optical memory concepts with ultra-fast operation speed.

It is shown in the optical shift register and the optical PRBS generator that cascaded optical memories can perform more sophisticated digital optical signal processing functions. The cascaded optical memories are controlled by clock signals that have to be delayed with proper time, since each optical memory needs a certain time to read and write data as a response to the power level of the clock signal. To simplify the optical digital systems further, an optical memory, which operates in an edge-sensitive manner, should be investigated. Furthermore, algorithm based on multi-state operation should be investigated to fulfill the advantage of multi-state optical memories in signal processing.

Chapter 8

Conclusion

In this Chapter, we conclude the physical features of the two optical multi-stable systems based on coupled lasers and their potential in optical signal processing, and give recommendations for further research.

The first type of optical multi-stable system is based on coupled unidirectional ring lasers with incoherent optical feedback. It is shown in Chapter 2 that a single unidirectional ring laser with incoherent optical feedback operates in the limit-cycle regime with proper control parameters. The net gain of the ring cavity becomes periodically negative due to the feedback light. The periodicity of the corresponding limit-cycle oscillator can be controlled by the ratio between the roundtrip times of the feedback arm and the ring cavity. When two such unidirectional ring lasers (limit-cycle oscillators) are coupled together by sharing the same active element and the same feedback arm, the two limit-cycle oscillators either synchronize in oscillation periodicity or show bistable behavior, depending on the differences of their oscillation periodicities, as presented in Chapter 3. The principle of the bistability is that the roundtrip condition of the weaker oscillator cannot be satisfied because the net gain of the ring cavity is modulated into periodically negative by the stronger oscillator, which has a very different oscillation periodicity. Switching between the two states can be realized by injection external light. As an extension of this principle, an eight-state optical memory is demonstrated in Chapter 4.

Models about a single unidirectional ring laser with incoherent optical feedback and two coupled such lasers are derived. The model is established to simulate the experimental setup that the ring cavity length is about ten meters. The numerical results and the experimental results are well coped with each other, except that the synchronization of two coupled oscillator shown in experimental are not observed numerically. The reason might be that the SOA in the model is treated as a point amplifier due to the long cavity.

The recommendations for investigation on this system are as follows:

1. A thorough bifurcation analysis for a single unidirectional ring laser with incoherent feedback is required. This can lead to an understanding of why the oscillation periodicity is so sensitive on the ratio between the roundtrip times of the feedback arm and the ring cavity.
2. The SOA is treated as a point amplifier in the model. To investigate the dynamics inside the SOA, it would be necessary to modify the model in such a way that the SOA is sliced into a number of small sections [116]. The modified model should take into account longitudinal variations of carrier-induced refractive index, photon density, carrier density, and amplified spontaneous emission noise, and the rate-mapping equations are solved at each small section. This is also an important step to simulate the system in a small scale, which is essential for applications.
3. The synchronization behavior needs further investigation in the context of general coupled oscillators. The system is special not only in the either-synchronization-or-bistability behavior, but also in the way with which the oscillators are coupled together, namely, the oscillators are equally and globally coupled through the same nonlinear gain medium. Moreover, Understanding synchronization is important to further extend the system to realize more stable states operation.
4. Isolators in the experimental setup are used to enable unidirectional lasing operation and realize incoherent optical feedback. The difficulty of fabricating isolators in scale smaller than one millimeter is an obstacle to shrink the size of the system further. It's worth investigating how to implement this bistable principle in an alternative manner without isolator.

The second type of optical multi-stable system is based on the extension of gain-quenching bistability. A group of lasers are cascaded in such a way that the active elements in the gain-quenched lasers are used to amplify the injected light to compensate for losses, so that the dominant laser quenches all the other lasers as a chain reaction. A five-state optical memory based on this principle is experimentally demonstrated in Chapter 5. Two switching methods are realized. The memory outputs at CW and can be integrated in a chip enabling GHz switching speed. The advantage of the concept is the linear scalability that in principle enables realization of optical

memories with large number of states. This type of optical memory is suitable for applications in optical telecommunication networks.

This system should be further investigated in the following aspects.

1. The possibly detrimental effects from SOA-facets and coupler reflections. This could be avoided when the system is integrated in a single chip.
2. The essence of the type of multi-state operation is that the active elements in the gain-quenched lasers are used to amplify the injected light to compensate for losses. When a large number of lasers are coupled, the coupling ratio should be carefully designed to avoid possible dynamical instabilities.
3. Investigate the influence of various propagation times between the lasers on the switching speed of the system when a large number of lasers are cascaded.
4. Modify the interconnection among the lasers to improve the switching time of the system. A possible modification of the configuration is using matrix structure, instead of the line type structure.

Another approach for extension of the multi-state operation is presented in Chapter 4. It is to connect several multi-state systems together. A sixteen-state optical memory made out of two connected four-state optical memories is demonstrated. This approach allows multi-state optical memories, which can not be made in ultra small dimensions, to process a large amount of information at high density. The data write-in and read-out technologies should be further investigated.

We also investigate optical digital systems based on optical memories. An optical shift register and an optical pseudorandom number generator based on cascaded optical memories are demonstrated. It is also discussed how to extend this concept to realize optical digital systems by cascading more optical memories.

Recommendations for further investigation on optical digital systems based on optical memories are as follows:

1. Since each optical flip-flop memory needs a certain time to read and write data as a response to the power level of the clock signal, the clock signal has to be

delayed with proper time to control the cascaded optical memories. To simplify the optical digital systems further, an optical memory, which operates in an edge-sensitive manner, should be investigated.

2. These digital systems are two mimics of their electronic counterparts. To fulfill the advantages of the optical multi-state memory, further investigations are required on multi-state optical signal processing.
3. For both types of multi-state optical memory, the information is encoded in different wavelengths. It needs further investigation on converting the wavelength-encoded information into other formats, like intensity-encoded information.

In this thesis, we present two types of optical memory that can operate in multiple states, which are differentiated by different wavelengths. Realizing a multi-state operation in wavelength domain is the intrinsic advantage of Optics¹. We also investigate further extension of the multi-state operations by connecting several multi-state optical memories together. Moreover, we explore optical digital systems based on cascaded optical memories. Further investigations should be conducted to process optical digital information in wavelength domain and in a multi-state manner.

¹ It is not practical to explore electronic memories in wavelength domain, since the operating wavelength limits the dimensions of the devices (optical wavelength is several orders shorter).

References

- [1] H.M. Gibbs, "Optical bistability: controlling light with light", Academic Press, London (1985).
- [2] M Schubert and B. Wilhelmi, "Nonlinear optics and quantum electronics", Chichester : Wiley-Interscience (1986).
- [3] H.H. Lee, E. Roueff, G.P. des Forets, O.M. Shalabiea, R. Terzieva, and E. Herbst, "Bistability in large chemical networks: a global view", *Astronomy and Astrophysics*, 334, pp.1047-1055 (1998).
- [4] J.C. Cheery and F.R. Adler, "How to make a Biological Switch", *Journal of Theoretical Biology*, 203, pp.117-133 (2000).
- [5] G. Nicolile and I. Prigogine, "Self-organization in non-equilibrium systems", Wiley, New York (1977).
- [6] R. Bonifacio and L. A. Lugiato, "Theory of optical bistability", in R. Bonifacio (Ed.), "Dissipative systems in quantum optics", Springer, Berlin (1982).
- [7] T.H. Maiman, "Stimulated Optical Radiation in Ruby", *Nature*, 187, pp.493-494 (1960).
- [8] R.W. Boyd, "Nonlinear optics", 2nd Edition, Academic press, Amsterdam (2003).
- [9] G.J. Lasher, "Analysis of a proposed bistable injection laser", *Solid-state Electronics*, 7, pp. 707-716 (1964).
- [10] M.I. Nathan, J.C. Marinace, R. F. Rutz, A. E. Michel, and G. J. Lasher, "GaAs injection laser with novel mode control and switching properties", *Journal of Applied Physics*, 23, pp. 473-479 (1965) .
- [11] S.L. McCall, "Instabilities in continuous-wave light propagation in absorbing media", *Physical Review A*, 9, pp. 1515-1523 (1974).

-
- [12] H.M. Gibbs, S.L. McCall, and T.N.C. Venkatesan, "Differential Gain and Bistability Using a Sodium-Filled Fabry-Perot Interferometer", *Physical Review Letters*, 36, pp. 1135-1138 (1976).
 - [13] G.P. Agrawal, "Fiber-optic communication systems", 3rd edition Chichester : Wiley-Interscience (2002).
 - [14] H. Kawaguchi, "Bistabilities and Nonlinearities in Laser Diodes", Artech House, Boston, London (1994).
 - [15] C.L. Tang, A. Schremer, and T. Fjitia, "Bistability in two-mode semiconductor lasers via gain saturation", *Applied Physics Letters*, 51, pp. 1392-1394 (1987).
 - [16] M.T. Hill, H. de Waardt, G.D. Khoe, and H.J.S. Dorren, All-optical flip-flop based on coupled laser diodes", *IEEE Journal of Quantum Electronics*, QE-37, pp. 405-413 (2001).
 - [17] H. Kawaguchi, "Optical input and output characteristics for bistable semiconductor lasers", *Applied Physics Letters*, 41, pp. 702-704 (1982).
 - [18] U. Keller, K.J. Weingarten, F.X. Kartner, D. Kopf, B. Braun, I.D. Jung, R. Fluck, C. Honninger, N. Matuschek, and J. Aus der Au, "Semiconductor saturable absorber mirrors (SESAM's) for femtosecond to nanosecond pulse generation in solid-state lasers", *IEEE Journal of Select Topics in Quantum Electronics*, 2, pp. 435-453 (1996).
 - [19] J.A. Goldstone and E.M. Garmire, "Macroscopic manifestations of microscopic optical bistability", *Journal of optical society of America B*, 1, pp. 466 (1984).
 - [20] H. A. Haus, "Theory of mode locking with a slow saturable absorber", *Journal of applied physics*, 46, pp. 3049-3058 (1975).
 - [21] H. A. Haus, "theory of mode locking with a fast saturable absorber", *Journal of applied physics*, 51, pp. 4042-4049 (1980).
 - [22] H. Kawaguchi, "Optical Bistability and chaos in a semiconductor laser with a saturable absorber", *Applied Physics Letters*, 45, pp. 1264-1266 (1984).
 - [23] C.O. Weiss and R. Vilaseca, "Dynamics of Lasers", Weinheim: VCH Verlagsgesellschaft mbH (1991).

-
- [24] H. Seidel, "Bistable optical circuit using saturable absorber within a resonant cavity", U.S. patent 3,610,731, filed May 19, 1969, granted October 5, 1971.
 - [25] A. Szöke, V. Daneu, J. Goldhar, and S.D. Smith, "Bistable optical element and its applications", *Applied Physics Letters*, 15, pp. 376-379 (1969).
 - [26] E. Spiller, "Saturable optical resonator", *Journal of applied physics*, 43, pp. 1673-1681 (1972).
 - [27] J.W. Austin, "Laser saturable resonators and criteria for their bistable operation", PhD Thesis, University of Southern California (1972).
 - [28] K. Otsuka and H. Iwamura, "Analysis of a multistable semiconductor light amplifier", *IEEE Journal of Quantum Electronics*, QE-19, pp. 1184-1186 (1983).
 - [29] M.J. Adams, "Physics and applications of optical bistability in semiconductor laser amplifiers", *Solidstate Electron.* 30, pp. 43-51(1987).
 - [30] C. Henry, "Theory of the linewidth of semiconductor lasers", *IEEE Journal of Quantum Electronics*, QE-18, pp. 259-264 (1982).
 - [31] E. Hecht, "Optics", 4th ed., Addison Wesley, Amsterdam (2002).
 - [32] Y.C. Chen and J.M. Liu, "Polarization bistability in semiconductor lasers", *Applied Physics Letters*, 46, pp. 16-18 (1985).
 - [33] H. Kawaguchi and L.S. Hidayat, "Gigahertz all-optical flip-flop operation of polarization-bistable vertical surface emitting lasers", *IEEE Electronics Letters*, 31, pp. 1550-1551 (1995).
 - [34] L. Xu, B.C. Wang, V. Baby, I. Glesk, and P.R. Proucnal, "Optical spectrum bistability in a semiconductor fiber ring laser through gain saturation in a SOA", *IEEE Photonics Technology Letters*, 14, pp. 149-151 (2002).
 - [35] G.J. Lasher and A.B. Fowler, "Mutually quenched injection lasers as bistable devices", *IBM Journal of Research and Development*, 8, pp. 471-475 (1964).

-
- [36] J.L. Oudar and R. Kuszelewicz, "Demonstration of optical bistability with intensity-coupled high gain lasers", *Applied Physics Letters*, 45, pp. 831-833 (1984).
- [37] M.T. Hill, H. de Waardt, G.D. Khoe, and H.J.S. Dorren, "Fast optical flip-flop by use of Mach-Zehnder interferometers", *Microwave and Optical Technology Letters*, 31, pp. 411-415 (2001).
- [38] Y. Liu, M.T. Hill, H. de Waardt, G.D. Khoe, and H.J.S. Dorren, "All-optical flip-flop memory based on two coupled polarization switches". *IEE Electronics Letters*, 38, pp. 904-906 (2002).
- [39] L.A. Lugiato, "Theory of optical bistability", *Progress in Optic*, XXI, E. Wolf, edition (North-Holland, Amsterdam), pp. 64 (1984).
- [40] D. Lenstra, "On the theory of polarization effects in gas lasers", Section 6, *Physics Reports*, 59, pp. 300-373 (1980).
- [41] H. Kawaguchi, "Bistable laser diodes and their applications: state of the art", *IEEE Journal of Select Topics in Quantum Electronics*, 3, pp. 1254-1270 (1997).
- [42] M.T. Hill, H.J.S. Dorren, T. de Vries, X.J.M. Leijtens, J.H. den Besten, B. Smalbrugge, Y.S. Oei, H. Binsma, G.D. Khoe, and M.K. Smit, "A fast low-power optical memory based on coupled micro-ring lasers", *Nature*, 432, pp. 206-209 (2004).
- [43] H.G. Weber, S. Ferber, M. Kroh, C. Schmidt-Langhorst, R. Ludwig, V. Marembert, C. Boerner, and C. Schubert, "Single Channel 1.28 Tbit/s and 2.56 Tbit/s DQPSK Transmission", in *Proceedings of 31st European Conference on Optical Communication 2005*, Vol. 6, pp. 3-4, 2005.
- [44] K. Fukuchi, T. Kasamatsu, M. Morie, R. Ohhira, T. Ito, k. Sekiya, D. Ogasahara, and T. Ono, "10.92 Tbit/s (273×40Gbit/s) triple-band/ultra-dense WDM optical repeated transmission experiment", in *Proceedings Optical Fiber Communications 2001*, VOL. 4, pp. PD24.1-24.3, Anaheim-USA, 2001.

-
- [45] M.T. Hill, A. Srivatsa, N. Calabretta, Y. Liu, H. de Waardt, G.D. Khoe, and H.J.S. Dorren, "1×2 optical packet switch using all-optical header processing", *IEE Electronics Letters*, 37, pp. 774-775 (2001).
 - [46] D.L. Danielsen, P.B. Hansen, and K.E. Stubkjaer, "Wavelength conversion in optical packet switching", *Journal of Lightwave Technology*, JT-16, pp. 2095-2108 (1998).
 - [47] H.J.S. Dorren, M.T. Hill, Y.Liu, N. Calabretta, A Srivatsa, F. M. Huijskens, H. de Waardt, and G.D. Khoe, "Optical packet switching and buffering by using all-optical signal processing methods", *Journal of Lightwave Technology*, JT-21, pp. 2-12 (2003).
 - [48] Y. Liu, "All-optical buffering based on nonlinear optical processing with semiconductor optical amplifier", *Thesis Eindhoven University of Technology* (2004).
 - [49] C.F. Lin and P.C. Ku, "Analysis of stability in two-mode laser systems", *IEEE Journal of Quantum Electronics*, 32, pp. 1377-1382 (1996).
 - [50] Y. Liu, M.T. Hill, N. Calabretta, H. de Waardt, G.D. Khoe, and H.J.S. Dorren, "Three-state all-optical memory based on coupled ring lasers", *IEEE Photonics Technology Letters*, 15, pp. 1461-1463 (2003).
 - [51] G.H.M. van Tartwijk and D. Lenstra, "Semiconductor lasers with optical injection and feedback", *Journal of optics B. Quantum and Semiclassical optics*, Opt, 7, pp. 87-143 (1995).
 - [52] B. Krauskopf and D. Lenstra, "Fundamental issues of nonlinear laser dynamics". *AIP conference proceedings 548*, American Institute of Physics. AIP, Melville, New York. (2000).
 - [53] G.P. Agrawal, "Line narrowing in a single-mode injection laser due to external optical feedback", *IEEE Journal of Quantum Electronics*, QE-20, pp. 468-471 (1984).
 - [54] H. Haken, "Analogy between higher instabilities in fluids and lasers", *Physics Letters*, 53A, pp. 77-78 (1975).

-
- [55] E.N. Lorenz, "Deterministic Non-periodic Flow, *Journal of the Atmospheric sciences*", 20, pp. 130-141 (1963).
- [56] C.O. Weiss and R. Vilaseca, "Dynamics of lasers", Weinheim: VCH (1991).
- [57] R. Lang and K. Kobayashi, "External optical feedback effects on semiconductor injection laser properties", *IEEE Journal of Quantum Electronics*, QE-16, pp.347-355 (1980).
- [58] R.W. Tkach and A.R. Chraplyvy, "Regimes of feedback effects in 1.5- μ m distributed feedback lasers", *Journal of Lightwave Technology*, LT-4, pp. 1655-1661 (1986).
- [59] K. Petermann, "External Optical feedback phenomena in semiconductor lasers", *IEEE Journal of Select Topics in Quantum Electronics*, 1, pp.480-488 (1995).
- [60] D. Lenstra, B.H. Verbeek, and A.J. Den Boef, "Coherence collapse in single-mode semiconductor laser due to optical feedback", *IEEE Journal of Quantum Electronics*, QE-21, pp.674-679 (1985).
- [61] J. Mork, B. Tromborg, and J. Mark, "Chaos in semiconductor lasers with optical feedback: theory and experiment", *IEEE Journal of Quantum Electronics*, QE-28, pp.93-108. (1992).
- [62] M. Yousefi and D. Lenstra, "Dynamical behavior of a semiconductor laser with filtered external optical feedback", *IEEE Journal of Quantum Electronics*, QE-35, pp. 970-976 (1999).
- [63] G.R. Gray, D. Huang, and G.P. Agrawal, "Chaotic dynamics of semiconductor lasers with phase-conjugate feedback", *Physics Review A*, 49, pp. 2096-2105 (1994).
- [64] M.K. Smit and C. van Dam, "PHASAR-Based WDM-Devices: Principles, Design and Applications", *IEEE Journal of Select Topics in Quantum Electronics*, 2, pp. 236-250 (1996).

-
- [65] S.H. Strogatz, *Nonlinear dynamics and chaos: with applications to physics, biology, chemistry, and engineering*, Addison-Wesley, Amsterdam (1994).
 - [66] S. Zhang, Y. Liu, D. Lenstra, M.T. Hill, H. Ju, G.D. Khoe, and H.J.S. Dorren, "Ring-laser optical flip-flop memory with single active element", *IEEE Journal of Select Topics in Quantum Electronics*, 10, pp. 1093-1100 (2004).
 - [67] G. Toptchiyski, S. Kindt, K. Petermann, E. Hilliger, S. Diez, and H.G. Weber, "Time-domain modeling of semiconductor optical amplifiers for OTDM applications", *Journal of Lightwave Technology*, 17, pp. 2577- 2583 (1999).
 - [68] P. Hadley and M.R. Beasley, "Phase locking of Josephson junction arrays", *Applied Physics Letters*, 52, pp. 1619-1621 (1988).
 - [69] R.A. Oliva and S.H. Strogatz, "Dynamics of a large array of globally coupled lasers with distributed frequencies", *International Journal of Bifurcation and Chaos*, 11, pp. 2359–2374 (2001).
 - [70] J. Benford, H. Sze, W. Woo, R.R. Smith, and B. Harteneck, "Phase locking of relativistic magnetrons", *Physical Review Letters*, 62, pp. 969-971 (1989).
 - [71] K. Nakajima and Y. Sawada, "Experimental studies on the weak coupling of oscillatory chemical reaction systems", *Journal of Chemical Physics*, 72, pp. 2231- 2234 (1980).
 - [72] M.F. Crowley and I.R. Epstein, "Experimental and theoretical studies of a coupled chemical oscillator: phase death, multistability, and in-phase and out-of-phase entrainment", *Journal of Physical Chemistry*, 93, pp. 2496-2502 (1989).
 - [73] I.Z. Kiss, Y. Zhai, and J.L. Hudson, "Emerging coherence in a population of chemical oscillators", *Science*, 296, pp. 1676-1678 (2002).
 - [74] Y. Zhai, I.Z. Kiss, and J.L. Hudson, "Amplitude death through a Hopf bifurcation in coupled electrochemical oscillators: experiments and simulations", *Physical Review E*, 69, 026208 (2004).
 - [75] A.T. Winfree, "The Geometry of Biological Time", Springer-Verlag, New York, Berlin, Heidelberg (1980).

-
- [76] R.E. Mirollo and S.H. Strogatz, "Synchronization of pulse-coupled biological oscillators", *Journal of Applied Mathematics*, 50, pp. 1645-1662 (1990).
 - [77] C. Schafer, M.G. Rosenblum, and J. Jurths, "'Heartbeat synchronized with ventilation", *Nature*, 392, pp. 239-240 (1998).
 - [78] B. Blasius, A. Huppert, and L. Stone, "Complex dynamics and phase synchronization in spatially extended ecological systems", *Nature*, 399, pp. 354-359 (1999).
 - [79] M. Dhamala, V.K. Jirsa, and M. Ding, "Enhancement of neural synchrony by time delay", *Physical Review Letters*, 92, 074104 (2004).
 - [80] Z. Neda, E. Ravasz, Y. Berchet, T. Vicsek, and A.L. Barabasi, "The sound of many hands clapping", *Nature*, 403, pp. 849-850 (2000).
 - [81] Ch. Huygens (Hugenii), "Horologium Oscillatorium, Apud F. Muguet, Parisiis, France (1673)" [English translation: 1986, The Pendulum Clock (Smes: Iowa State University Press)].
 - [82] E.V. Appleton, "The automatic synchronization of triode oscillator", *Proceedings of the Cambridge Philosophical Society (Mathematical and Physical Society)*, 21, pp. 231-248 (1922).
 - [83] B. Van der Pol, "Forced oscillations in a circuit with non-linear resistance (Reception with reactive triode)", *Philosophical Magazine*, 3, pp. 64-80 (1927).
 - [84] A.T. Winfree, "Biological rhythms and the behavior of populations of coupled oscillators", *Journal of Theoretical Biology*, 16, pp. 15-42 (1967).
 - [85] Y. Kuramoto, "Cooperative dynamics of oscillator community", *Progress of Theoretical Physics Supplement*, 79, pp. 223-240 (1984).
 - [86] S.H. Strogatz, "From Kuramoto to Crawford: exploring the onset of synchronization in populations of coupled oscillators", *Physica D* 143, 1-20 (2000).
 - [87] C.A. Czeisler, J.S. Allan, S.H. Strogatz, J.M. Ronda, R. Sanchez, C.D. Rios, W.O. Freitag, G.S. Richardson, and R.E. Kronauer, "Bright light resets the human circadian pacemaker independent of the timing of the sleep-wake cycle", *Science* 233, pp. 667-671 (1986).

-
- [88] J. Buck and E. Buck, "Mechanism of rhythmic synchronous flashing of fireflies", *Science* 159, pp. 1319-1327 (1968).
- [89] I.E. Sutherland and J. Ebergen, "Computers without Clocks", *Scientific American*, 287, pp. 62-69 (2002).
- [90] T.J. Overbye, "Reengineering the electric grid", *American Scientist*, 88, pp. 220-229 (2000).
- [91] R.E. Mirollo and S.H. Strogatz, "Amplitude death in an array of limit-cycle oscillators", *Journal of Statistical Physics*, 60, pp. 245-262 (1990).
- [92] J. Reyleigh, "The theory of Sound", Dover Publ, New York (1945).
- [93] D.V. Ramana Reddy, A. Sen, and G.L. Johnston, "Time delay induced death in coupled limit cycle oscillators", *Physical Review Letters*, 80, pp. 5109-592 (1998).
- [94] D.V. Ramana Reddy, A. Sen, and G.L. Johnston, "Experimental evidence of time-delay-induced death in coupled limit-cycle oscillators", *Physical Review Letters*, 85, pp. 3381-3384 (2000).
- [95] P.C. Matthews, R.E. Mirollo, and S.H. Strogatz, "Dynamics of a large system of coupled nonlinear oscillators", *Physica D*, 52, pp. 293-331 (1991).
- [96] L.M. Pecora, "Synchronization conditions and desynchronizing patterns in coupled limit-cycle and chaotic systems", *Physical Review E*, 58, pp. 347-360 (1998).
- [97] M. Rosenblum, A. Pikovsky, "Synchronization: from pendulum clocks to chaotic lasers and chemical oscillators", *Contemporary Physics*, 44, pp. 401-416 (2003).
- [98] A.S. Pikovsky, M.G. Rosenblum, G.V. Osipov, and J. Kurths, "Phase synchronization of chaotic oscillators by external driving", *Physica D*, 104, pp. 219-238 (1997).
- [99] H. Shimizu and Y. Nakano, "Fabrication and characterization of an InGaAsP/InP active waveguide optical isolator with 14.7 dB/mm TE mode nonreciprocal attenuation", *Journal of Lightwave Technology*, 24, pp. 38-43 (2006).

-
- [100] K. Takada, M. Abe, M. Shibata, M. Ishii, K. Okamoto, "Low-crosstalk 10-GHz-spaced 512-channel arrayed-waveguide grating multi/demultiplexer fabricated on a 4-in wafer", *IEEE Photonics Technology Letters*, 13, pp. 1182-1184 (2001).
- [101] M.T. Hill, T. de Vries, H.J.S. Dorren, X.J.M. Leijtens, J.H.C. van Zantvoort, J.H. den Besten, E. Smalbrugge, Y.S. Oei, J.J.M. Binsma, G.D. Khoe, and M.K. Smit, "Integrated two-state AWG-based Multiwavelength laser", *IEEE Photonics Technology Letters*, 17, pp. 956-958 (2005).
- [102] R.J. Prestopnik, "Digital Electronics: Concepts and Applications for Digital Design", Saunders College Publishing, Philadelphia (1990).
- [103] S.A. Ward and R.H. Halstead, Jr., "Computation Structures", McGraw-Hill Book Company, New York (1989).
- [104] K.E. Stubkjaer, "Semiconductor optical amplifier-based all optical gates for high-speed optical processing", *IEEE Journal of Select Topics in Quantum Electronics*, 6, pp. 1428-1435 (2000).
- [105] H.J.S. Dorren, X. Yang, A.K. Mishra, Z. Li, H. Ju, H. de Waardt, G.D. Khoe, T. Simoyama, H. Ishikawa, H. Kawashma, and T. Hasama, "All-optical logic based on ultrafast gain and index dynamics in a semiconductor optical amplifier", *IEEE Journal of Select Topics in Quantum Electronics*, 10, pp. 1079-1092 (2004).
- [106] A. Bogoni, L. Poti, R. Proietti, G. Meloni, F. Ponzini, and P. Ghelfi, "Regenerative and reconfigurable all-optical logic gates for ultra-fast applications", *IEE Electronics Letters*, 41, pp. 435-436 (2005).
- [107] Z. Li, Y. Liu, S. Zhang, H. Ju, H. de Waardt, G.D. Khoe, H.J.S. Dorren, and D. Lenstra, "All-optical logic gates using a semiconductor optical amplifier assisted by an optical filter", *IEE Electronics Letters*, 41, pp. 1397-1399 (2005).
- [108] H. Ju, S. Zhang, D. Lenstra, H. De Waardt, E. Tangdiongga, G.D. Khoe and H.J.S. Dorren, "SOA-based all-optical switch with subpicosecond full recovery", *Optics Express*, 13, pp. 942-947 (2005).

-
- [109] N.A. Whitaker, Jr., M.C. Gabriel, H. Avramopoulos, and A. Huang, "All-optical, All-fiber circulating shift register with an inverter", *Optics Letters*, 16, pp. 1999-2001 (1991).
- [110] A.J. Poustie, R.J. Manning, and K.J. Blow, "All-optical circulating shift register using a semiconductor optical amplifier in a fiber", *IEEE Electronics Letters*, 32, pp. 1215-1216 (1996).
- [111] B. Tian, W.V. Etten, and W. Beuwer, "Ultrafast all-optical shift register and its perspective application for optical packet switching", *IEEE Journal of Select Topics in Quantum Electronics*, 8, pp. 722-728 (2002).
- [112] P. Horowitz, W. Hill, and P. Hayes, "The art of electronics", 2nd edition, Cambridge University Press, Cambridge (1989).
- [113] A.J. Poustie, K.J. Blow, and R.J. Manning, A.E. Kelly, "All-optical pseudorandom number generator", *Optics Communications*, 159, pp. 208-214 (1999).
- [114] R.P. Webb, R.J. Manning, G.D. Maxwell, and A.J. Poustie, "40 Gbit/s all-optical XOR gate based on hybrid-integrated Mach-Zehnder interferometer", *Electronic Letters*, 39, pp. 79-81 (2003).
- [115] Q. Wang, G. Zhu, H. Chen, J. Jaques, J. Leuthold, A.B. Piccirilli, and N.K. Dutta, "Study of all-optical XOR using Mach-Zehnder interferometer and differential scheme", *IEEE Journal of Quantum Electronics*, QE-40, pp. 703-710 (2004).
- [116] Z. Li, X. Yang, E. Tangdionga, H. Ju, G.D. Khoe, H.J.S. Dorren, and D. Lenstra, "Simulation of model-locking by nonlinear polarization rotation in a semiconductor optical amplifier", *IEEE Journal of Quantum Electronics*, QE-41, pp. 808-816 (2005).

Appendix A

List of abbreviations

ATT	ATTenuator
AWG	Arrayed Waveguide Grating
BS	Binary Sequence
CW	Continuous Wave
dB	Decibel
dBm	Decibel milliwatt
ISO	ISOlator
LD	Laser Diode
PRBS	Pseudorandom Binary Sequence
SOA	Semiconductor Optical Amplifier
WDM	Wavelength Division Multiplexing
XOR	Exclusive-or

Appendix B

List of publications

Journal papers

- [B1] S. Zhang, D. Lenstra, Y. Liu, H. Ju, Z. Li, G.D. Khoe and H.J.S. Dorren, Multi-state optical flip-flop memory based on ring lasers coupled through the same gain medium, *Optics Communications*, accepted.
- [B2] S. Zhang, Z. Li, Y. Liu, G.D. Khoe, and H.J.S. Dorren, “Optical shift register based on an optical flip-flop memory with a single active element”, *Optics Express* 13, pp: 9708-9713 (2005).
- [B3] S. Zhang, D. Owens, Y. Liu, M.T. Hill, D. Lenstra, A. Tzanakaki, G.D. Khoe, and H.J.S. Dorren, “Multi-state Optical Memory Based on Serially Interconnected Lasers”, *IEEE Photonics Technology Letters* 17, pp. 1962-1964 (2005).
- [B4] S. Zhang, Y. Liu, D. Lenstra, M.T. Hill, H. Ju, G.D. Khoe, and H.J.S. Dorren, “Ring-laser optical flip-flop memory with single active element”, *IEEE Journal of Selected Topics in Quantum Electronics* 10, pp. 1093-1100 (2004).
- [B5] H. Ju, S. Zhang, D. Lenstra, H. De Waardt, E. Tangdiongga, G.D. Khoe, and H.J.S. Dorren, “SOA-based all-optical switch with subpicosecond full recovery”, *Optics Express* 13, pp. 942-947 (2005).
- [B6] Y. Liu, E. Tangdiongga, Z. Li, S. Zhang, H. De Waardt, G.D. Khoe, and H.J.S. Dorren, “80 Gbit/s wavelength conversion using a semiconductor optical amplifier and an optical bandpass filter”, *IEE Electronics Letters* 41, pp. 487-489 (2005).

- [B7] Z. Li, Y. Liu, S. Zhang, H. Ju, H. de Waardt, G.D. Khoe, and D. Lenstra, "All-optical logic gates using a semiconductor optical amplifier assisted by an optical filter", *IEE Electronics Letters* 41, pp. 1397-1398 (2005).
- [B8] Y. Liu, E. Tangdionga, Z. Li, S. Zhang, H. De Waardt, G.D. Khoe, and H.J.S. Dorren, "Error-free all-optical wavelength conversion at 160 Gbit/s using a semiconductor optical amplifier and an optical bandpass filter". *IEEE/OSA Journal of Lightwave Technology* 24, pp. 230-236 (2006).

International conference papers

- [B9] S. Zhang, D. Lenstra, Y. Liu, H. Ju, Z. Li, G.D. Khoe, and H.J.S. Dorren, "Eight State Optical Flip-flop Based on Coupled Unidirectional Ring Lasers with Optical Feedback", *Proceedings of CLEO/QELS* (2006).
- [B10] S. Zhang, D. Owens, Y. Liu, M.T. Hill, D. Lenstra, A. Tzanakaki, G.D. Khoe, and H.J.S. Dorren, "Multi-state Optical Memory Based on Serially Interconnected Lasers", *Proceedings of 31th European Conference on Optical Communication* (2005).
- [B11] S. Zhang, Z.Li, Y. Liu, R. Geldenhuys, D. Lenstra, Ju. H, M. T. Hill, H. Ju, G. D. Khoe, and H. J. S. Dorren, "Optical shift register based on flip-flop memory consisting of one active element", *Proceedings of 31th European Conference on Optical Communication* (2005).
- [B12] S. Zhang, D. Lenstra, Y. Liu, Ju. H, Z.Li, H. Ju, G. D. Khoe, and H. J. S. Dorren, "Laser dynamics of a bistable ring system with optical feedback", *Proceedings of 5th Europe Nonlinear Dynamics Conference (ENOC)* (2005).
- [B13] S. Zhang, Y. Liu, D. Lenstra, M. T. Hill, H. Ju, G. D. Khoe, and H. J. S. Dorren, "Optical flip-flop memory based on two-cavity ring laser with feedback", *Proceedings of 30th European Conference on Optical Communication* (2004).
- [B14] Y. Liu, E. Tangdionga, Z. Li, S. Zhang, H. De Waardt, G.D. Khoe, and H.J.S. Dorren, "160 Gb/s SOA-based wavelength converter assisted by an optical bandpass filter", *Proceedings of Optical Fiber Communication Conference* (Post deadline paper 17) (2005).
- [B15] Z. Li, Y. Liu, S. Zhang, H. Ju, H. de Waardt, G.D. Khoe, and D. Lenstra, "All-optical logic gates based on a SOA and an optical filter", *Proceedings of 31th European Conference on Optical Communication* (2005).

- [B16] Y. Liu, E. Tangdionga, Z. Li, S. Zhang, H. De Waardt, G.D. Khoe, and H.J.S. Dorren, “160 Gbit/s wavelength conversion using ultra-fast dynamics in a SOA”, *Proceedings of 31th European Conference on Optical Communication* (2005).
- [B17] Y. Liu, M.T. Hill, N. Calabretta, E. Tangdionga, R. Geldenhuys, S. Zhang, Z. Li, H. De Warrdt, G.D. Khoe, and H.J.S. Dorren, “All-optical signal processing for optical packet switching networks”, *Proceedings of SPIE* (2005).
- [B18] H. Ju, S. Zhang, H. de. Waardt, G. D. Khoe, and H. J. S. Dorren, “Ultrafast all-optical switching by pulsed-induced birefringence in a multi-quantum well semiconductor optical amplifier”, *proc. CLEO/IQEC* (2004).
- [B19] X. Yang, E. Tangdionga, S. Zhang, Z. Li, M.T. Hill, D. Lenstra, G.D. Khoe, and H.J.S. Dorren, “Mode-locked ring lasers and their application in an all-optical flip-flop memory”, *Proceedings of ICTON* (2004).
- [B20] H.J.S. Dorren, X. Yang, E. Tangdionga, S. Zhang, A. Mishra, Z. Li, H. Ju, D. Lenstra, and G.D. Khoe, “All-optical logic based on ultra-fast nonlinearities in a semiconductor optical amplifier”, *Proceedings of MOC* (2004).
- [B21] H.J.S. Dorren, X. Yang, E. Tangdionga, S. Zhang, A. Mishra, Z. Li, H. Ju, D. Lenstra, and G.D. Khoe, “All-optical signal processing based on ultrafast nonlinearities in semiconductor optical amplifiers”, *Proceedings of SSDM* (2004).
- [B22] H.J.S. Dorren, R. Geldenhuys, D. Lenstra, G.D. Khoe, X. Yang, E. Tangdionga, S. Zhang, Z. Li, M.T. Hill, H. Ju, A.K. Mishra, and Y. Liu, “All-optical header processing and optical buffering for optical packet switching network”, *Proceedings of AOC04-APOC04* (2004).

Regional conference papers

- [B23] S. Zhang, D. Owens, Y. Liu, M.T. Hill, D. Lenstra, G.D. Khoe, H.J.S. Dorren, Multi-state Optical Flip-flop Memory Based on Cascaded Lasers, *Proceedings of 10th Annual Symposium of The IEEE/LEOS Benelux Chapter* (2005).

-
- [B24] S. Zhang, Z. Li, Y. Liu, R. Geldenhuys, D. Lenstra, Ju. H, M. T. Hill, H. Ju, G. D. Khoe, H. J. S. Dorren, Optical shift register based on flip-flop memory consisting of one active element, Proceedings of 9th Annual Symposium of The IEEE/LEOS Benelux Chapter (2004).
- [B25] S. Zhang, Y. Liu, D. Lenstra, M.T. Hill, H. Ju, G.D. Khoe, H.J.S. Dorren, Optical flip-flop based on a multiple cavity ring laser with feedback. Proceedings of 8th Annual Symposium of The IEEE/LEOS Benelux Chapter (2003).
- [B26] Z. Li, Y. Liu, S. Zhang, G.D. Khoe, H.J.S. Dorren, D. Lenstra, Towards Tbps wavelength conversion with a bulk semiconductor optical amplifier. Proceedings of 10th Annual Symposium of The IEEE/LEOS Benelux Chapter (2005).
- [B27] Y. Liu, J.P. Turkiewicz, S. Zhang, E. Tangdionga, E.J.M. Verdurmen, H. de Waardt, D. Lenstra, G.D. Khoe and H.J.S. Dorren, 40 Gbit/s SOA-based wavelength conversion assisted by a narrow optical bandpass filter. Proceedings of 9th Annual Symposium of The IEEE/LEOS Benelux Chapter, 251-254 (2004).
- [B28] X. Yang, E. Tangdionga, S. Zhang, Z. Li, D. Lenstra, G.D. Khoe and H.J.S. Dorren, Mode-locked ring lasers and their application in a coupled all-optical flip-flop. Proceedings of 9th Annual Symposium of The IEEE/LEOS Benelux Chapter, 53-56 (2004).

Samenvatting

Optische geheugens zijn bi(multi) stabiele systemen, waarvan de toestanden volledig optisch kunnen worden geschakeld. Als elementaire bouwsteen voor digitale optische signaalbewerking staan zij in hoge mate in de belangstelling. Veel verschillende soorten optische heugens zijn onderzocht, met als gemeenschappelijk kenmerk dat het optische opslag elementen zijn met twee discrete toestanden. Multi-stabiele optische logische bouwstenen zijn interessant voor telecommunicatiesystemen, aangezien zij in beginsel in staat zijn om een groot aantal golfengete kanalen in parallel verband te bewerken.

In dit proefschrift stellen wij twee soorten meervoudig-stabiel werkende systemen voor, gebaseerd op gekoppelde lasers. Het eerste systeem is gebaseerd op twee gekoppelde ringlasers met één gemeenschappelijk actief element en één extra arm, waarmee optische terugkoppeling wordt geïntroduceerd. Een enkele ring laser met optische terugkoppeling kan beschouwd worden als een oscillator, aangezien de lichtintensiteit in de lasertrilholte periodiek varieert. Wanneer men twee van deze structuren koppelt, die beide hetzelfde actieve element en de terugkoppelarm gemeen hebben, dan zullen zij zich synchroniseren op een gemeenschappelijke oscillatie frequentie, mits hun eigenfrequenties dichtbij elkaar liggen; in het andere geval zal een bistabiel gedrag optreden tussen de twee oscillatoren. Schakelen tussen de twee stabiele toestanden kan worden bewerkstelligd door extern licht te injecteren, hetgeen betekent dat een dergelijk systeem zich gedraagt als een optisch geheugen. Aangezien maar één actief element benodigd is, laat het systeem zich opschalen door meerdere ringstructuren te koppelen waardoor meerdere stabiele toestanden kunnen worden gerealiseerd. Op deze wijze is een optisch geheugen met acht stabiele toestanden gedemonstreerd.

Het tweede type multi-stabiel werkende systeem is gebaseerd op serieel doorverbonden lasers. Het werkingsprincipe berust op het mechanisme van het uitdoven van de optische versterking door externe injectie van licht. Het licht van de dominerende laser onderdrukt zijn nabuurlasers door versterkingsverzadiging, echter het licht ondervindt nog steeds versterking in het actieve element van de onderdrukte lasers, waardoor de koppelverliezen tussen de lasers worden gecompenseerd. Het licht van de dominante laser passeert vervolgens de actieve gebieden van alle opvolgende lasers, terwijl het daarbij de andere lasers onderdrukt maar zelf versterkt wordt. Door dit mechanisme zijn al de andere lasers onderdrukt. Echter, er kan maar één laser tegelijkertijd actief zijn, hierdoor is de toestand van het geheugen bepaald

door de golflengte van de dominante laser. Gebaseerd op dit concept is een optisch heugen gedemonstreerd met een vijftal toestanden.

Met de optische heugenelementen als fundamentele logische bouwstenen is een aanzet gegeven tot de realisatie van meer complexe logische operaties. In dit proefschrift wordt een optische schuifregister gepresenteerd opgebouwd uit twee serieel doorverbonden optische geheugens, aangestuurd met dezelfde serie klokpulsen. De conceptuele werking is aangetoond bij een snelheid van 20 kHz. Deze beperkte snelheid wordt veroorzaakt door de zeer lange trilholtjes (10m) gevormd door de lange pigtails aan de commercieel verworven halfgeleider versterkers. Vervolgens is het schuifregister gecascadeerd met een optische XOR poort, waarmee de functionaliteit is aangetoond van een volledig optische PseudoRandom Generator gebaseerd op optische geheugens.

Acknowledgements

This PhD thesis is accumulated throughout of my four-year academic work in Eindhoven University of Technology (TU/e), where I have been working with a number of distinguished researchers and living with many genuine friends. I am happy to have this opportunity to thank all of them.

I would like to thank all my colleagues from the Electro-Optical Communications (ECO) group in TU/e. First of all, I would like to thank my promoters Prof. Giok-Djan Khoe and Prof. Daan Lenstra, and my daily supervisor Dr. Harm Dorren, who together gave me a patient and sincere guidance so that I came to be an independent researcher who can explore new field confidently. I am grateful to the STW organization for financially supporting me to carry out my research work.

I am in great debt to Dr. Yong Liu, who gave me numerous valuable help covering all aspects of my staying here. I would like to thank Prof. Ton Koonen for his kind work on providing a wonderful group environment. I am very grateful to Dr. Huug de Waardt for his nice coordinating of equipments in our group and his kind help on translating my abstract into Dutch. I would like to thank Mr. Zhonggui Li, Dr. Hongkyu Ju, Dr. Javier Molina Vazquez, Prof. Alexander V. Uskov, Mr. Christos Tsekekos, Dr. Mirvais Yousefi and Dr. Hyun-Do Jung, with whom I had so many interesting and enjoyable discussions. I am very grateful to Dr. Xuelin Yang, Dr. Martin Hill, Dr. Eduward Tangdionga, Dr. Yongpeng Zhao, Mr. Frans Huijskens, Mr. Peter van Bennekom and Mr. Johan van Zantvoort for their kind help on my experiments.

I would like to thank our group secretary Mrs. Susan de Leeuw and Mrs. Els Gerritsen-Lecluse and scientific staff Ir. Henrie van den Boom and Dr. Idelfonso Tafur Monroy for their efforts to keep our group running smoothly. I am grateful to have the opportunity to work in a group with so many talents: Mr. Juan Jose Vegas Olmos, Mr. Jaroslaw Turkiewicz, Mr. Jianming Zeng, Mr. Jia Yang, Ms. Ni Yan, Mr. Xinkai Li, Mr. Georgi Petkov, Ir. Erwin Verdurmen, Ms. Maria Garcia Larrode, Ir. Rene Kramer, Mr. Alejandro Lopez Domenech, Ir. Bas Huiszoon, Ir. Archi Delphinanto and Dr. Anthony Ng'oma.

I would like to express my gratitude to the core committee for my PhD thesis: Prof. Thomas Erneux, Prof. Paul Koenraad, and Prof. Ian White. I am very grateful to their reviewing of my thesis.

I would like to give special thanks to the Chinese community in Eindhoven. I had a wonderful life with many genuine friends. There are so many of them that I couldn't list all their names here. I am so lucky to get to know all of them.

Finally, I wish to thank the love from my family who sincerely give me their most enduring and cherish support. I share the happiness of writing down this PhD thesis with them.

Curriculum Vitae

Shaoxian Zhang was born in Lingyuan County, Liaoning Province, P.R. China, in May 1977.

In 1995, he began studying in major of Optoelectronic Technology at University of Electronic Science and Technology of China (UESTC), where he got Bachelor degree with thesis on Measurement of Extinction between TE_0 and TM_0 modes in Proton Exchanged $LiNbO_3$ Optical Waveguide, which received Excellent Undergraduate Thesis Award, in 1999.

From 1999-2002, he continued to stay at UESTC to carry out his Master research, under the supervision of Prof. Yongzhi Liu. His thesis work concerned the Integrated Optical Waveguide Gyroscope based on Ring Resonator and M-Z interference.

In 2002, he moved to the Netherlands where he was appointed trainee research assistant (AIO) to the Electro-Optical Communications group of Eindhoven University of Technology, under the supervisions of Prof. G.D. Khoe, Prof. D. Lenstra and Dr. H.J.S. Dorren. He researches on Optical Multi-state Flip-flop Memories and their applications in All Optical Signal Processing.

